Heating the Sun's corona

P. G. Judge
High Altitude Observatory,
National Center for Atmospheric Research,
Boulder, Colorado 80307-3000, USA

Preface

The addition of this book to the extensive literature concerning the solar corona requires justification, especially since the heating problem is as yet unsolved. With the explosion in the number of research papers which has accompanied both recent space missions and the increased power of computers, it was felt that a new, relatively short guide to the essential physics of coronal heating might be a valuable contribution. The approach is to emphasize, from a physical point of view, those elements of fluid and plasma physics which appear to be essential components of a meaningful theory as determined from observations and measurements. Brevity and physical insight are emphasized over completeness and mathematical development.

Resistive magnetohydrodynamics (RMHD) arguably represents the minimal theoretical framework needed to address the coronal heating problem. Well known non-linearities in the equations for the magneto-fluid in highly non-dissipative regimes lead to a series of practical problems. For example, unique solutions to boundary value problems may not exist even though the Sun knows how to find them; the corona must contain very small structures as are needed for significant energy dissipation; Parker has argued that coronal magnetostatic equilibrium problems will contain mathematical discontinuities coresponding to physical "current sheets". In essence we cannot "build" a credible model corona from ab-initio calculations. Remotely sensed data always have limited spatial resolution and often line-of-sight integration paths which involve enormous spatial scales. The issue of "comparison of theory to observations" is thus of central importance for this particular problem – it is not surprising that after 60+ years of research there is no concensus as to the primary dissipation mechanisms. The book attempts to address this difficulty throughout.

Aimed at graduate students, the book begins with a brief introduction, defining the coronal heating problem, highlighting the gulf between theory and observation. Subsequent chapters introduce step-by-step additional physical complexities guided carefully by specific seemingly robust observational results determined by spectroscopic techniques. SI units are used throughout. The book ends with a discussion of the ideas introduced in the text as applied to some laboratory plasma experiments.

Olivier: “I came to you for answers. Very specific answers”
Gersonides: “So you keep telling me. And I will repeat
the only answer I know. I have none. Not that I haven’t spent
the last forty years looking, but I find answers are as rare as
golden eggs or unicorns. All I can do is help you
look for yourself.”

–Iain Pears, *The Dream of Scipio*

Contents

List of Figures

List of Tables

Acknowledgments

This work is the product of an enforced period of rest in which the author was seriously ill. He is indebted to many people, especially his family and friends, for their unconditional love and support, during this period. He especially would like to thank Dr. Robert Rifkin, of Rocky Mountain Cancer Center at Midtown, Denver. Without Dr. Rifkin's dedication and expertise, and sister Claire Judge's stem cells, he would have never lived to enjoy the loving care and nursing of his wife, Terri, to whom this small book is dedicated, with love.

Figure 1.4 was obtained using the 1 meter Swedish Solar Telescope, which is operated on the island of La Palma by the Institute for Solar Physics of the Royal Swedish Academy of Sciences in the Spanish Observatorio del Roque de los Muchachos of the Instituto de Astrofsica de Canarias. We have used images from the Transition Region and Coronal Explorer, TRACE, which is a mission of the Stanford-Lockheed Institute for Space Research, and part of the NASA Small Explorer program, and from the Solar and Heliospheric Observatory (*SOHO*)

Chapter 1

Introduction

1.1 Background

Visual observations of total eclipses from antiquity, documented by Philostratus and Plutarch, clearly describe the extended glow around the lunar disk which we recognize today as the "corona". Observations in the 19th century revealed that its form changed between eclipses (differences between eclipses of 1871 and 1878 were noted at the time), it sometimes showed curved ray-like structures which reminded several visual observers of lines of magnetic force studied in laboratory magnets (Bigelow 1889, see Figures 1.1 and 1.2 for examples), and by 1871 gross coronal features were suspected to correlate with sunspots. Its origin was unknown. It was not until a famous eclipse of 1869 that it was finally given a solar, as opposed to lunar, optical or terrestrial, origin, as it was self luminous in a certain bright line in the green region, and the moon was known to have no detectable atmosphere. Any remaining doubts were removed by photographic triangulation methods employed during the eclipses of 1870 and 1871, revealing that the corona showed

> "...precisely the same details of coronal form and structure, and are, by themselves, sufficient to demonstrate that the main features of the phenomenon are independent of our terrestrial atmosphere and the accidents of the lunar surface." – Young (1892), p. 225.

Janssen (1879) drew similar conclusions from the stability of the corona seen during the 1871 eclipse. Spectroscopic work in this period revealed unique, unidentified emission lines in the coronal spectrum. Two lines were particularly strong: the "Green line" at 530 nm and the "Red line" at 637 nm. This early work is summarized nicely in Young's (1892) book. Grotrian (1931) obtained spectra of the corona during the 1929 eclipse, confirming earlier work which showed that the spectrum was essentially scattered photospheric light, but with the Fraunhofer absorption lines almost entirely washed out. From the ≈ 20 nm width of the Fraunhofer H and K lines, Grotrian deduced that the thermal velocities for the scattering electrons must be $\approx 7.5 \times 10^6$ m s^{-1}, which corresponds to $T_e \approx 1.1 \times 10^6$ K. During the 1920s and 1930s, the French astronomer Bernard Lyot developed the coronagraph, enabling him to observe the corona without the need for an eclipse (Lyot 1932, 1933). He discovered many new and unidentified emission lines in the corona (Lyot 1939). In 1937, he suggested that the spectral width of the "Green line" might be due to thermal motions, if the radiating ions had temperatures of several million K. Grotrian (1939) proposed tentative identifications for the Red coronal line (Fe X)

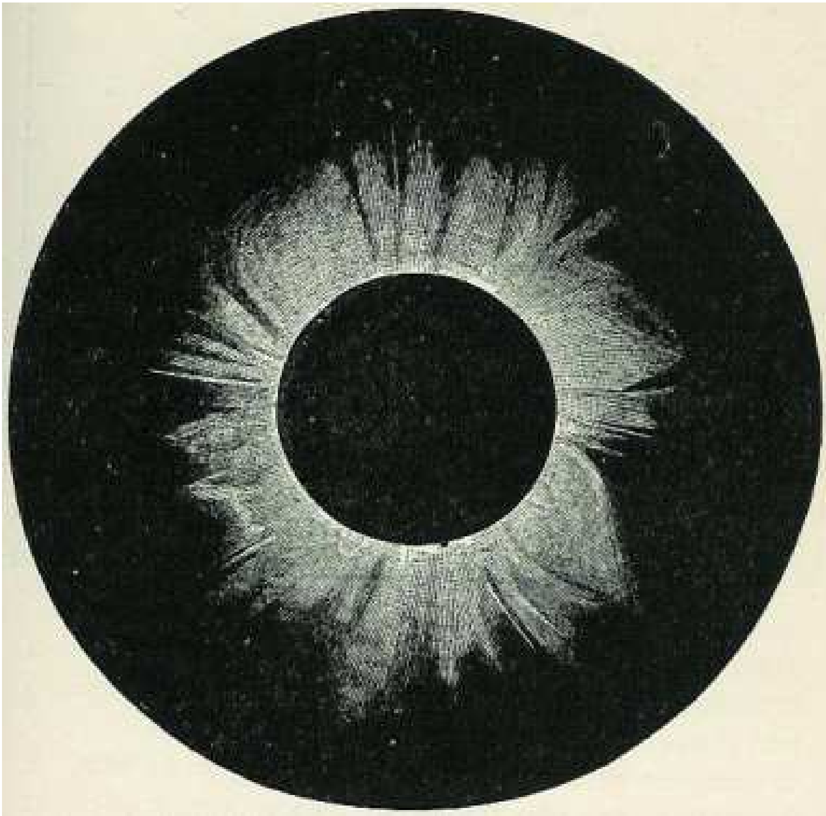

Figure 1.1: Curved and radial structures in the corona as drawn from photographs obtained during the 1871 eclipse, a period close to sunspot maximum. From Young (1892), Fig. 73.

and a line at 789.2 nm (Fe XI)[1]. Following Grotrian, Edlén (1943) identified 4 lines against laboratory measurements, and many other lines between 330 and 1100 nm using wavelengths estimated from regularities in the structure of highly charged ions ("isoelectronic sequences"), with forbidden transitions of ions between 9 and 15 times ionized. In particular, the "Green line" was identified as a forbidden transition of Fe XIV.

To produce such highly charged ions requires between 1 keV and 5 keV to overcome the potential energies I_P of ionization, compared with the 0.5 eV typical energy of the solar photosphere. It was therefore no longer possible to believe that convective or radiative energy transport was responsible for these properties of the corona, unlike the solar photosphere. Whereas Edlén (1943) assumed an electron temperature T_e of 2.5×10^5 K, particle temperatures can also be estimated as follows. If the ionization energy is supplied by a population of thermal particles at temperature T, then a small but not negligible fraction x of the particle population will exceed I_P if $exp(-k_BT/eI_P) > x$ (see Table 1.1 for values of physical and solar constants). In an ionized plasma consisting mostly of hydrogen, collisions with electrons occur more frequently than with heavier particles, thus the relevant temperature is the electron temperature T_e. For $x = 0.1$ say, $T_e \approx eI_P/2.3k_B$, corresponding to $2 \times 10^6 \lesssim T_e \lesssim 10^7$ K when 1 keV $< I_P <$ 5 keV. These temperatures lie within factors of several of modern estimates of T_e (e.g., Noci 2003).

In the 1940s, 50s and 60s, estimates of T_e in the corona were refined when, under the low density conditions typical of the low corona (see table 1.2), Biermann (1947), Woolley and

[1]The spectroscopic notation Fe X and Fe XI refers to the 10^{th} and 11^{th} spectra of iron, i.e. spectra of the ions Fe^{+9} and Fe^{+10} respectively, the spectrum of neutral iron being Fe I.

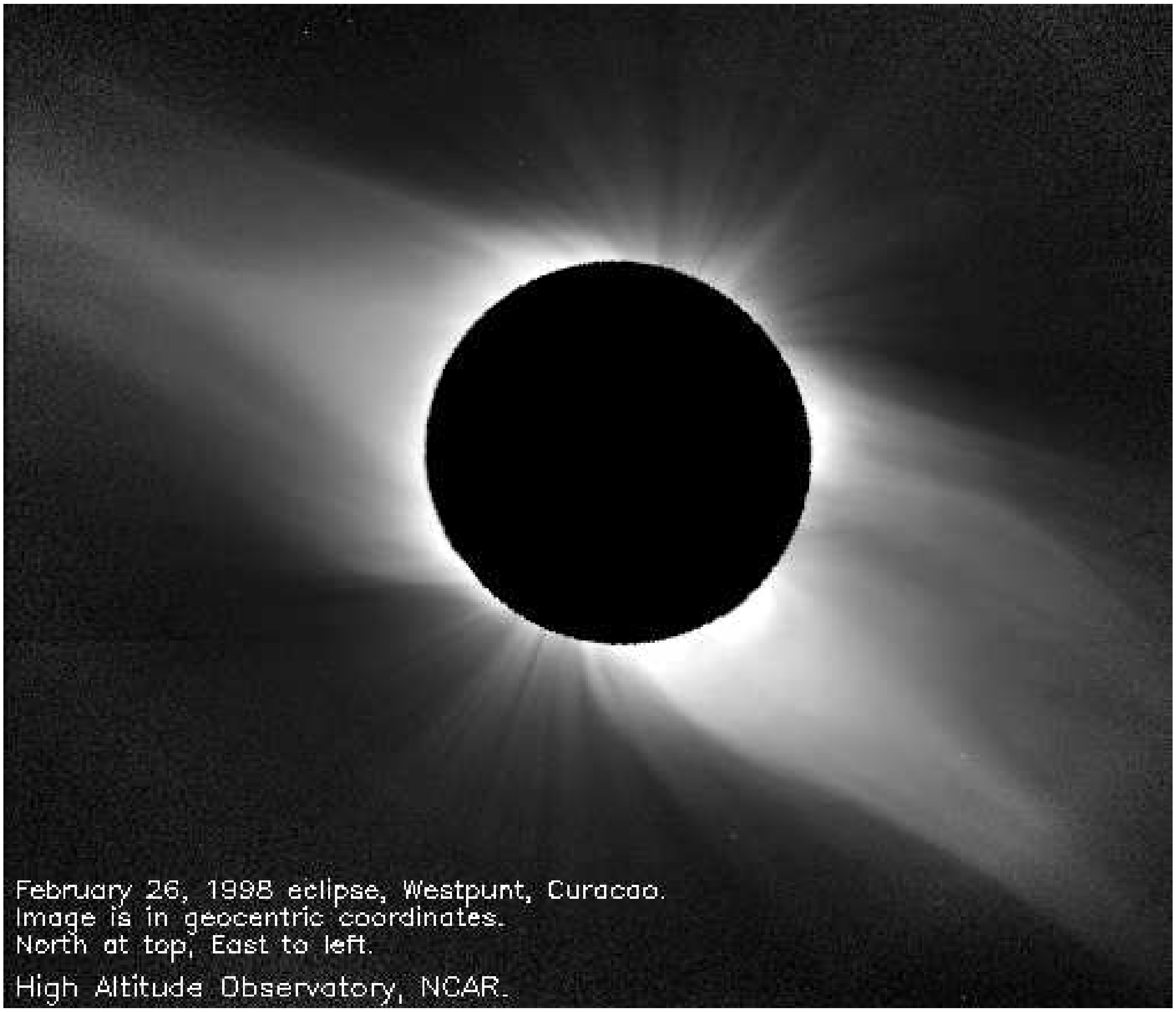

Figure 1.2: Data from HAO's POISE instrument deployed in Curacao in February 1998 are shown. A radial gradient filter was used to enhance the dimmer structure far from the solar surface. The Sun was close to sunspot minimum. The predominant features seen are polar plumes extending in the 1 and 7 o'clock directions, and the large streamers extending in the 4 and 10 o'clock directions. Figure prepared by D. Elmore and A. Lecinski of the High Altitude Observatory.

Allen (1948) and Miyamoto (1949) realized that the statistical balance between the radiating ions of different charges is dominated by *two-body* collisional processes, namely ionization and (radiative) recombination by electron impact. Assuming that these reach a statistical balance, contributions to the emission from line i are peaked functions $G_i(T_e)$ of T_e with full widths at half peak of ~ 0.3 in $\log_{10} T_e$ (see Seaton 1964, Jordan 1969, for example, and Appendix B), with only a weak dependence on electron density n_e or pressure p_e. One could therefore speak of the electron temperature of "ionization equilibrium", being the value of T_e near which $G_i(T_e)$ peaks for emission line i. This contrasts with local the thermodynamic equilibrium (LTE) regime, where the well-known Saha formula for ionization balance depends linearly on the electron density. This is because, in LTE, detailed balance between reciprocal processes

Table 1.1: Physical constants and solar data

Symbol	Physical quantity	Value
e	electron charge	1.602×10^{-19} C
m_e	electron mass	9.109×10^{-31} Kg
m_H	proton or hydrogen mass	1.673×10^{-27} Kg
k_B	Boltzmann's constant	1.381×10^{-23} J K^{-1}
μ_0	permeability of free space	$4\pi \times 10^{-7}$ Hm^{-1}
ϵ_0	permittivity of free space	$(36\pi \times 10^9)^{-1}$ Fm^{-1}
c	speed of light in vacuo $= 1/\sqrt{\mu_0\epsilon_0}$	3×10^8 m s^{-1}
G	gravitational constant	6.670×10^{-11} N m^2 kg^{-2}
$R_\odot$	solar radius	6.9599×10^8 m
$M_\odot$	solar mass	1.989×10^{30} kg
$L_\odot$	solar luminosity	3.826×10^{26} W
$F_\odot$	solar bolometric flux density	6.284×10^7 W m^{-2}
	spatial size of 1 arcsecond at the Sun	0.725×10^6 m
$\overline{\mu} = \sum_i \frac{m_i}{m_H} n_i / \sum_i n_i$	mean mass per solar particle (mostly neutral case)	1.26
	(mostly ionized case)	0.60
$\overline{\mu}_H = \sum_i \frac{m_i}{m_H} n_i / n_H$	mean mass per solar hydrogen nucleus	1.36
n_{tot}/n_e	total density ÷ electron density (ionized plasma)	1.92

Note: Physical constants are from NIST. Solar data are taken from Allen (1973).

must occur, for example between *three-body* recombination and collisional ionization by electron impact.

Typical coronal ionization equilibrium temperatures were found to be 1 to 3MK, but they did not always agree with lower ion temperatures measured from coronal line widths (Evans 1963). Ion and electron collision times are on the order of a minute (see table 1.2). Thus the temperature discrepancies were worrisome for the non-flaring corona whose structure is stable on much longer time scales. The process of dielectronic recombination was then recognized as a major additional two-body recombination process for many coronal ions (Burgess 1964, Burgess and Seaton 1964). Increased recombination lowers ionization recombination temperatures. New ionization equilibrium calculations including this process then brought electron temperatures into better agreement. At the same time, radio data were revealing electron temperatures lower by a factor of two or so (e.g., Kundu 1965). The radio data remain discrepant today (Noci 2003). This is perhaps not a fundamental problem because coronal lines and radio continuum emission depend very differently on T_e, and the corona is obviously thermally inhomogeneous.

Observations using ground-based coronagraphs have continued to the present, but have recently played second fiddle to space-based imagers observing the disk of the Sun at X-ray and EUV wavelengths. X-ray images from the *SKYLAB* mission in 1973 provided clear evidence for dark "coronal holes" which persist over some solar rotation periods. These were identified as unipolar magnetic regions which appeared to be the seat of fast particulate emissions from the Sun, known many decades before to modulate geomagnetic activity, and previously called "M-regions" (e.g., Hundhausen and Holzer 1980).

The late 1980s brought in the era of normal-incidence optics in soft X-ray and EUV telescopes, made possible by the use of multi-layers and narrow passband filters (Underwood et al. 1987, Walker et al. 1988, Golub et al. 1990). These instruments led to the first sub-arcsecond coronal images. At such high resolution the topology of the coronal images is complex and tangled (Golub et al. 1990), implying that the sub-arcsecond corona contains considerable mag-

Table 1.2: Typical conditions at the quiet Sun's coronal base

	Physical quantity	value
Properties		
...Thermal	T_e electron temperature	10^6 K
	n_e electron density ($n_p \approx 0.8 n_e$)	3×10^{14} m^{-3}
	p_e electron pressure $n_e k_B T_e$	4×10^{-3} N m^{-2}
	λ_D Debye length $\sqrt{\epsilon_0 k_B T_e / n_e e^2}$	4×10^{-3} m
	Plasma parameter $\frac{4\pi}{3}\lambda_D^3 n_e$	8×10^7
	ω_{pe} electron plasma frequency $\lambda_D / \sqrt{k_B T_e / m_e}$	9.8×10^8 rad s^{-1}
	ρ mass density	6×10^{-13} kg m^{-3}
	c_S adiabatic sound speed $\sqrt{\gamma p / \rho}$	1.5×10^5 m s^{-1}
	τ_{ee} electron self-collision time	0.044 s
	τ_{pp} proton self-collision time	2.2 s
	τ_{ep} electron momentum changing time (proton collisions)	$\approx \tau_{ee}$
	τ_{ep}^{ε} electron-proton energy exchange time	80 s
	$\lambda_e = \sqrt{3k_B T_e/2m_e}/(\tau_{ee}^{-1} + \tau_{ep}^{-1})$ (electron mean free path)	1.2×10^5 m
	$\lambda_p = \sqrt{3k_B T_p/2m_p}\tau_{pp}$ (proton mean free path)	2.3×10^5 m
	$q_\parallel$ heat flux, parallel to $\mathbf{B}$	$\kappa_\parallel T^{5/2} \nabla T$ W m^{-2}
	$\kappa_\parallel$	10^{-11} W m^{-1} K$^{-7/2}$
	μ coeff. of shear viscosity (unmagnetized) $\nu\rho$	$2.2 \times 10^{-17} T_p^{5/2}$ kg m^{-1} s^{-1}
	σ_0 scalar electrical conductivity	$7.4 \times 10^{-4}\, T_e^{3/2}$ ohm^{-1} m^{-1}
...Magnetic	$\lvert B \rvert$ typical field strength	10^{-3} T
	β plasma/magnetic pressure $p/\frac{B^2}{2\mu_0}$	2×10^{-2}
	c_A Alfvén speed $\sqrt{\frac{B^2}{\rho\mu_0}}$	1.2×10^6 m s^{-1}
	ω_e electron gyro frequency	1.8×10^8 rad s^{-1}
	$r_e = \sqrt{3k_B T_e/2m_e}/\omega_e$ electron gyro radius	0.03 m
	ω_p proton gyro frequency	9.6×10^4 rad s^{-1}
	$r_p = \sqrt{3k_B T_p/2m_p}/\omega_p$ proton gyro radius	1 m
	$\omega_e \tau_{ee}$	7.8×10^6
	$\omega_p \tau_{pp}$	2.2×10^5
	$\kappa_\perp/\kappa_\parallel$, μ'/μ	$(\omega\tau)^{-2\dagger}$
"Closed" fields (loops)		
	L typical loop length	5×10^7 m
	F_M energy flux density needed to sustain loop	6×10^2 W m^{-2}
	Spatially averaged heating rate F_M/L	1.2×10^{-5} W m^{-3}
	v typical flow/micro-turbulent speeds	2×10^4 m s^{-1}
	R Reynolds number (unmagnetized) $vL/\nu = vL\rho/\mu$	25
	R' Reynolds number (magnetized) $vL/\nu' = vL\rho/\mu'$	9×10^{11}
	R_m magnetic Reynolds number $vL\mu_0\sigma_0$	8×10^{11}
	S Lundquist number $c_A L \mu_0 \sigma_0$	5×10^{13}
	L/c_S sound crossing time	330 s
	L/c_A Alfvén crossing time	40 s
	Rad. time scale $t_{rad} \approx \frac{3}{2} n_{tot} k_B T_e / [n_e^2 P_{rad}(T_e)]$	3×10^4 s
	Cond. time scale $t_{con} \approx \frac{3}{2} n_{tot} k_B T_e\, L/(F_C = F_M)$	830 s
"Open" fields (wind)		
	H_{HSE} pressure scale height	5×10^7 m

Note: $T_p \approx T_e$ is assumed in the table. †This is valid in the limit $\omega\tau \gg 1$.

netic free energy driven by the underlying photospheric and chromospheric dynamics. A typical image of the whole corona obtained at EUV wavelengths by the *TRACE* spacecraft is shown in Figure 1.3. The bright loop structures are rooted in magnetic fields associated with active regions seen in the photosphere (but not shown here).

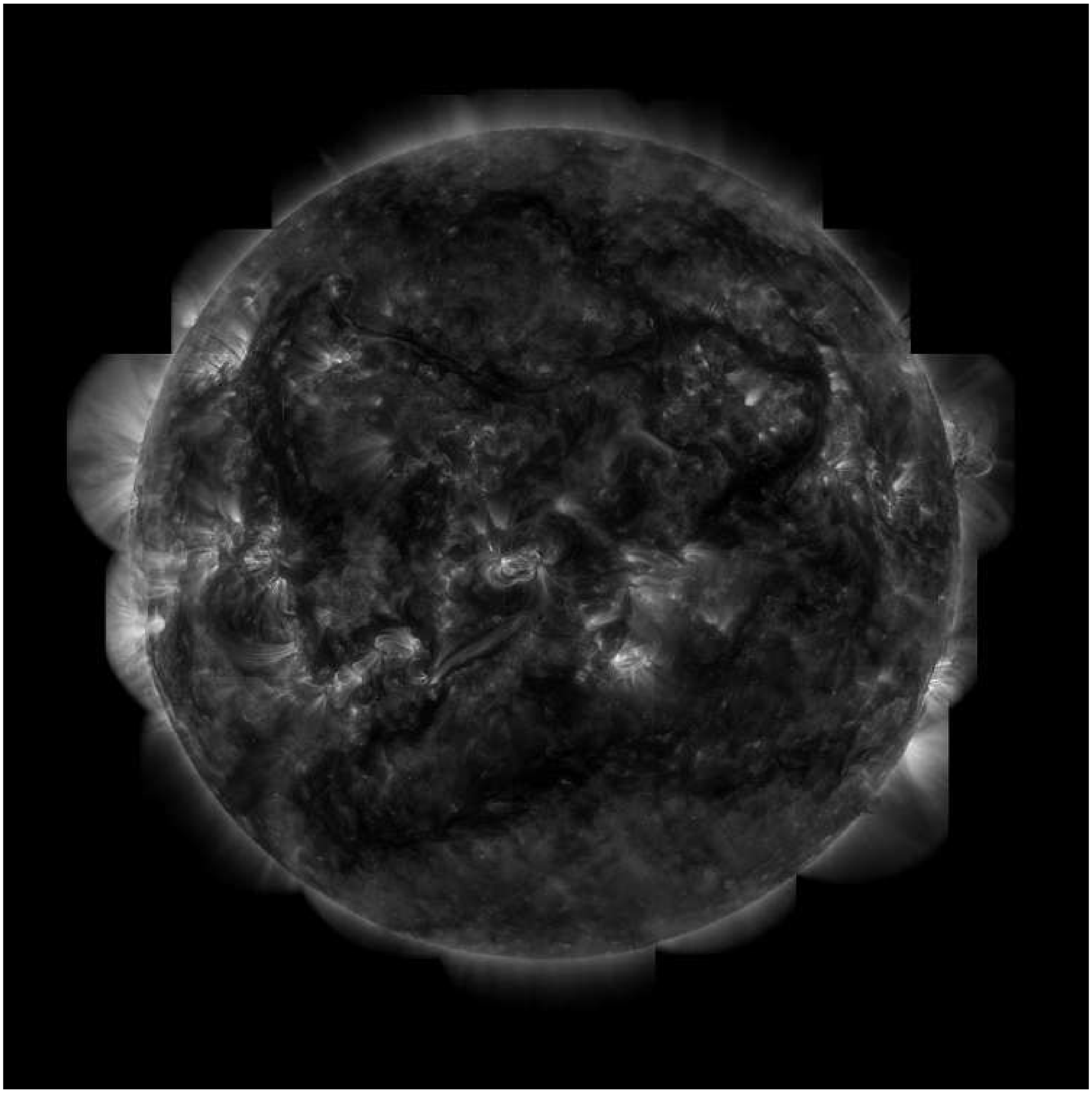

Figure 1.3: A full disk mosaic of the solar corona from the *TRACE* spacecraft, observed at 17.1 nm (emission dominated by lines from Fe IX and Fe X, formed near $T_e \approx 10^6$ K). The Sun was moderately active on 19 February 2001, when these data were acquired. The image shows bright active region loops, diffuse quiet Sun emission (near the bottom), small "bright points", various "filaments" (dark, snake-like features). Image taken from the *TRACE* website.

At the high temperatures and low densities listed in Table 1.2, the Sun's corona emits spectral line radiation very inefficiently in the most abundant chemical species (hydrogen, helium), because these are almost fully ionized. Spectral line radiation is relatively weak because it is dominated by lines of trace species of much lower abundance, such as oxygen or iron. Continuum radiation (at radio and X-ray wavelengths) is not a significant radiation loss channel until temperatures of $T_e \gtrsim 10^7$ K, characteristic of flares, are obtained. In contrast, the high thermal conductivity of the plasma means that heat conduction dominates the transport of energy through the corona, and serve as a net loss of coronal energy when heat is transported to cooler, denser regions which radiate more efficiently. Energy losses from the corona occur also via enthalpy losses associated with flows. The question of why the corona is so hot thus becomes a question of how non-radiative energy is transported to and dissipated in these tenuous, outer regions of the Sun's atmosphere. The energy budget for the corona is summarized in Table 1.3. The quiet corona requires just 1 part in 10^5 of the kinetic energy in the turbulent,

Table 1.3: Energy budgets

Region	Energy flux density W m^{-2}		
	Quiet Sun	corona hole	active region
photospheric radiation		6.3×10^7	
sub-photospheric K.E. flux density		(ditto)	
chromosphere	1.4×10^4	1.4×10^4	$\approx 7 \times 10^4$
spicules (surface average)	10^3	$> 10^3$	...
corona total	8×10^2	5×10^2	$\approx 10^4$
heat conduction %	70	8	1-100
radiation %	30	1	50
wind flow %	< 17	90	< 1

Coronal data were taken from Withbroe and Noyes (1977), Withbroe (1988). Chromospheric data, taken from Anderson and Athay (1989), are larger than those of Withbroe, and more realistic, because they include radiation losses from lines of iron. Active region (plage) chromospheric data were estimated by scaling quiet Sun chromospheric radiation losses by a factor of 5 (Withbroe and Noyes 1977, Chapman 1981).

dense sub-photospheric atmospheric layers to sustain it, the chromosphere ≈ 2 parts in 10^4.

The problem of coronal heating is thus to identify the source(s) of mechanical energy, and the modes of energy transport and dissipation, all in a manner consistent with observations.

Magnetic fields obviously organize the corona. The magnetic fields threading, emerging and buffeted in the sub-photospheric regions act as sources and guides of the mechanical energy needed for heating the corona. As we will see, non-magnetic processes fail to produce enough power, relatively small as it is, to sustain the corona (section 1.5). Beyond this broad conclusion, relatively little progress has been made in identifying the mechanisms in operation.

A real problem is that we suffer from an "embarrassment of riches"- researchers have been prolific in proposing mechanisms to explain why the corona is hot. For example, Mandrini et al. (2000) list 22 "scaling laws" relating coronal heating rates to fluid and magnetic parameters of a dozen or so qualitatively different dissipative models. R. J. Rutten (private communication ca. 2000) wonders, given so many scenarios, why the corona is as cool as it is! An important strategy is therefore to *falsify proposals.* This is a major challenge.

1.2 From turbulent sub-photosphere to corona

The corona is separated from the huge mechanical energy reservoir in the sub-photospheric turbulence by the photosphere and its radial extension, another complex region called the *chromosphere*. By definition, the photosphere is the layer from which the bulk of the solar luminosity is radiated: it is therefore very bright. Its brightness makes it attractive to observers, especially those using techniques developed shortly after Zeeman discovered the effects of magnetic fields

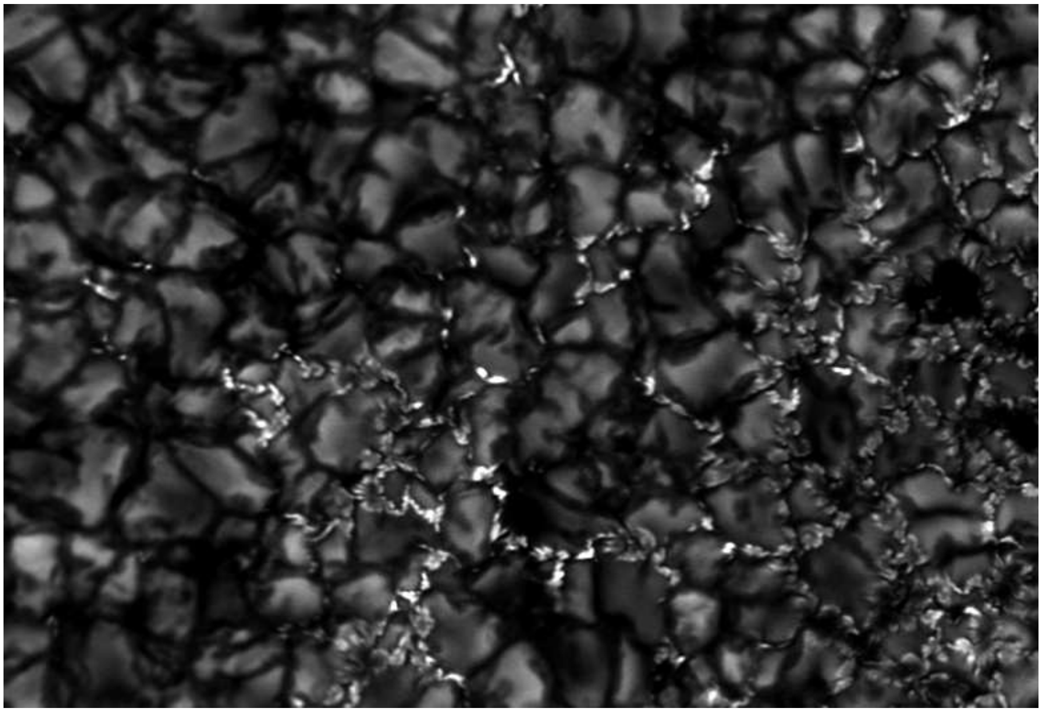

Figure 1.4: A part of one of the highest resolution photospheric images yet obtained, showing the intensity of the "G-band" (430.5 nm) in a roughly 45×30 Mm^2 region of quiet Sun acquired using the 1 meter Swedish Solar Telescope (SST). The granules are typically 1.4 Mm in diameter, and evolve on time-scales of a few minutes. The tiny bright structures in the dark intergranular lanes are associated with strong magnetic field concentrations (Berger et al. 1995), which collectively form the supergranular network. Some of these magnetic fields extend into the corona where they play an important role in heating the coronal plasma. Data were obtained by Carlsson and colleagues of the Institute for Theoretical Astrophysics, Oslo University, on 25 May 2003, and were processed by Mats Löfdahl, Institute for Solar Physics of the Royal Swedish Academy of Sciences.

on spectral lines to try to measure solar magnetic fields (Hale 1908). Nearly all of our knowledge of solar magnetism comes from the analysis of photospheric observations. The photosphere is separated from the corona by 10 or so pressure scale heights[2]. It has become common practice to use photospheric magnetic field measurements, made with relative ease, when studying the role of magnetic fields in the corona. The intervening chromosphere is very often ignored, a worrisome situation discussed further in section 3.3.

High resolution images of the photosphere and corona reveal magnetized plasma in totally different regimes. In the former, a superb example of which is the observation shown in Figure 1.4, the magnetic field is an ever-changing part of a turbulent magneto-fluid. In the latter, it appears more rigid and (for reasons yet to be understood from basic physical principles) in the form of bright loops of plasma embedded in a volume filling magnetic structure (see Figure 1.3).

The radical change in the physical appearance of the top of the photosphere through to the middle-top chromosphere is illustrated in Figure 1.5. The upper panel reflects conditions a few hundred km above the continuum photosphere, showing a magnetic pore (center) and the

[2]By analogy, if the photosphere corresponds to the air that we breathe, the corona corresponds to the ionosphere.

uppermost regions where convection is important. The lower panel shows conditions within a scale height of the overlying corona, just another 1Mm or so above the first image. The sub-photospheric turbulence is reflected in the upper photosphere by the presence of convective cells. No sign of these patterns remain in the chromospheric image. The chromosphere's electrical conductivity is high, so that the morphology of the fibril-like structure must result from the dominance of magnetic forces. While variations of intensity along and between different fibrils seen in chromospheric lines remains to be explained, fibrils should faithfully trace out magnetic lines of force. When observed near the solar limb, the chromosphere includes dynamic jets

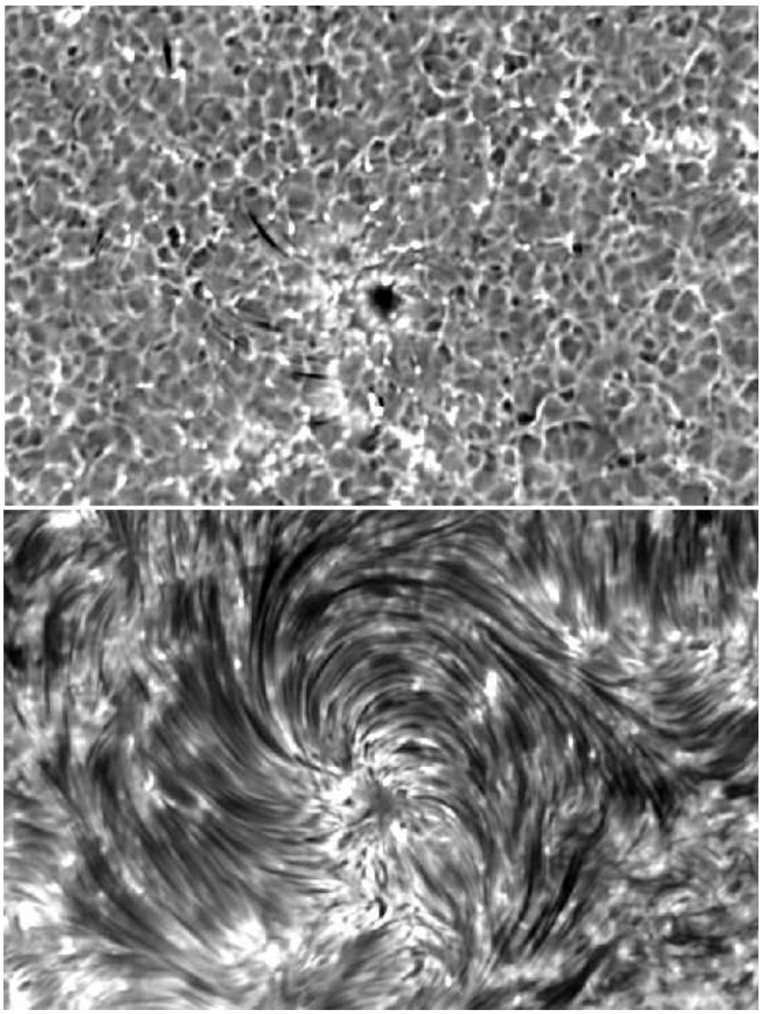

Figure 1.5: A figure showing the upper photosphere (upper panel) and the mid-upper chromosphere (lower panel), of a small pore taken from Cauzzi et al. (2008). These are intensity images (roughly 0.1Å spectral resolution) from the IBIS instrument operated at the Dunn Solar Telescope, obtained on October 1 2005, in the 854.2nm line of Ca II. The field of view is is about $44{\times}30$ Mm^2.

of cool material injected along magnetic fields into the corona. These "spicules", only partly understood but launched from the network chromosphere, thus penetrate the coronal base (see Figure 1.6).

What is the relationship between coronal emission, these chromospheric structures, and the underlying magnetic fields observed in the photosphere? The thermal conductivity of the corona

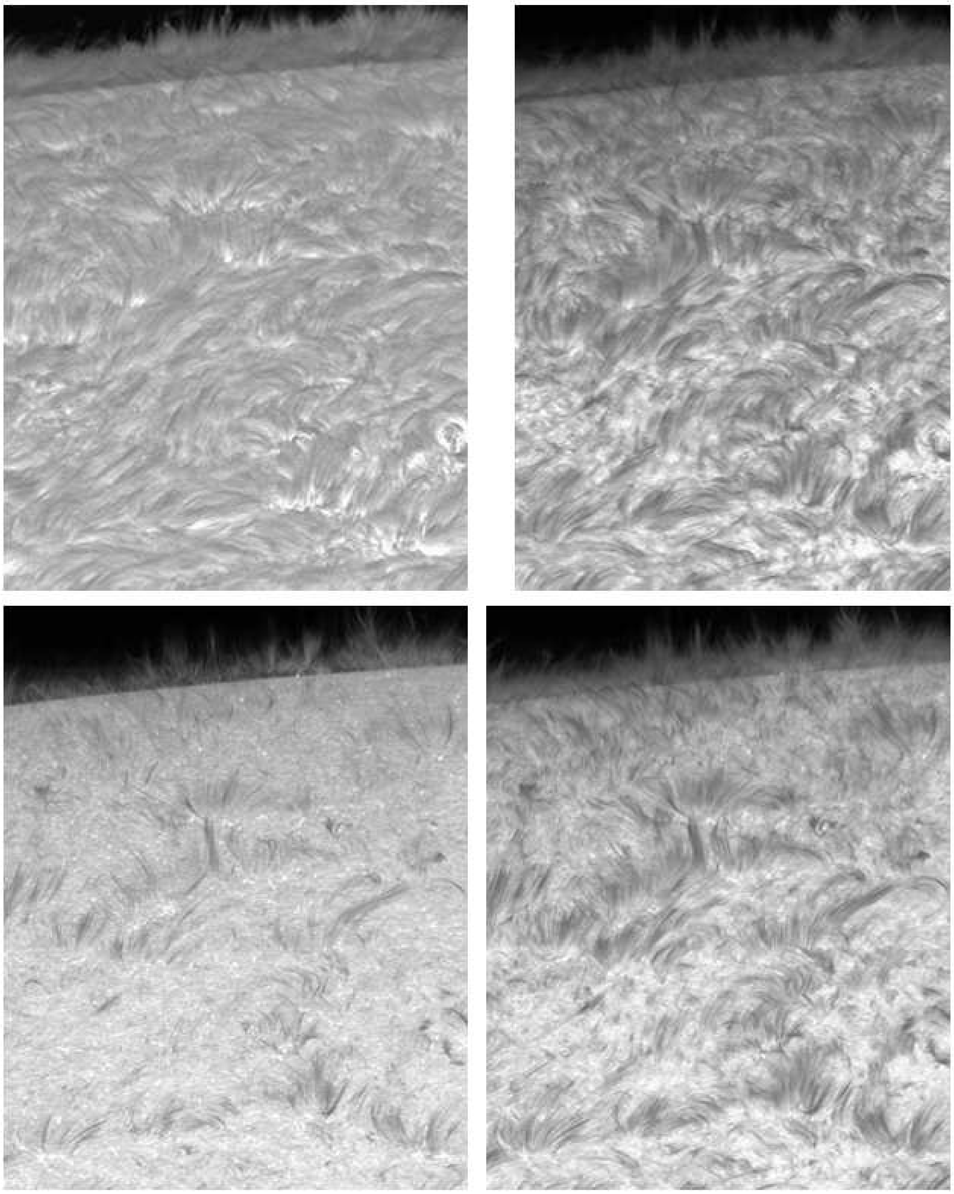

Figure 1.6: Images obtained with the Dutch Open Telescope of the Hα line of a quiet region near the solar limb. The bandpasses of the images are centered near 0, -0.4, -0.6,-0.8 Å, clockwise from the top left panel. The field of view is is about 50×62 Mm^2. From **??**.

is highly anisotropic and directed along magnetic field lines. The electrical conductivity, like the chromospehre, is also high so that plasma must flow along, and trace out, field lines. A major goal of high resolution space physics UV/EUV missions (such as *TRACE*) was therefore to try to connect coronal loops along field lines down into their photospheric roots. While there is a clear relationship between coronal loops and photospheric magnetic fields in a broad sense, this goal has generally proven impossible when examined in detail. There are (at least) three interesting aspects to this problem.

– First, as Figure 1.7 illustrates, EUV coronal emission cannot observationally be followed

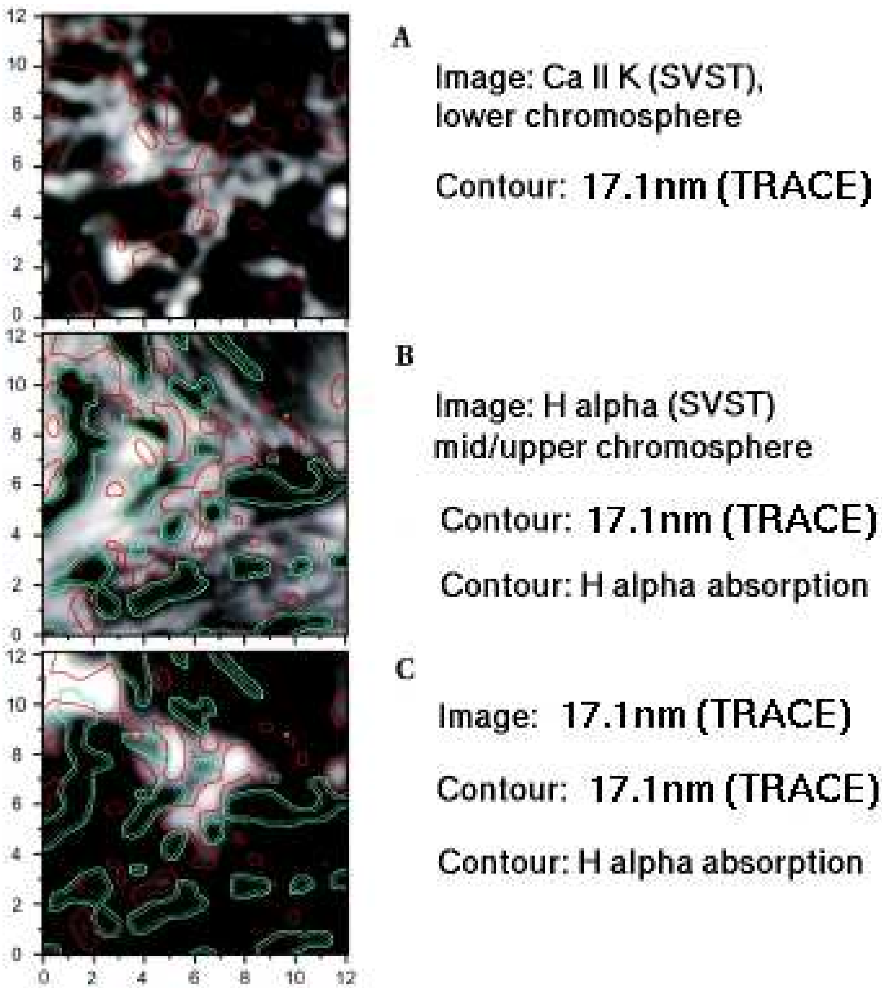

Figure 1.7: These high resolution images illustrate the complexity of the physical interface between the chromosphere and corona. (A) Ca II K-line image, bright areas demarcate the location of magnetic elements in the lower chromosphere, contours outline the regions of bright emission defined from the TRACE 17.1nm image shown in C. (B) Same region seen in a summed image of Hα -0.035 and 0.035 nm filter-grams, green contours outline dark areas of increased absorption which demarcate transient "jets" of chromospheric plasma. (C) TRACE Fe IX/Fe X 17.1 nm image. The length scale is in Mm. Adapted from Berger et al. (1999).

down to the flux sheets or tubes observed at the level of the photosphere. Instead the EUV emission is mixed at its base with cooler chromospheric material, such that no one-to-one relationship of coronal to photospheric magnetic field can be found.

- A second challenge is that active region plasma loops, which attract so much attention in EUV images (e.g. Figure 1.3), are by no means volume-filling, yet the magnetic field itself must essentially fill the volume. Indeed, if loops were volume filling, they would be far less visible. Instead, only certain tubes of magnetic flux are chosen by the Sun to emit EUV radiation. This point is illustrated further by Figure 1.8. What is it that marks these tubes as places where the plasma loops should be seen in the EUV passbands observed?
- Thirdly, most of the 1MK solar corona is not organized into resolvable loops at the angular

resolution of *TRACE*. The lower part of Figure 1.3 shows an example of apparently diffuse emission. Similar *TRACE* images taken close to solar sunpot minimum show that the diffuse EUV emission is more prevalent, perhaps dominant, in such periods. This "quiet Sun" component represents an important part of the corona, whose properties deserve an explanation as much as the more eye-catching active region loops. Tracing field lines using intensity images is not an option when the corona appears diffuse.

The ability to trace field lines into the photosphere would have enabled us to study heating mechanisms directly, since then the energy injected from the sub-photosphere could have been be followed in its upward journey into the corona. However, our inability to do so represents *a significant challenge in the quest to identify the nature of the source and transport of electromagnetic energy into the corona.*

We close this section by adding simple physical considerations. The steep chromospheric stratification implies that the chromosphere almost always contains the (morphologically complex, and dynamically important) plasma $\beta = 1$ surface. Magnetohydrodynamic (MHD) oscillations originating in the (sub) photosphere can change character ("convert") efficiently near this surface. The Sun must constantly struggle to attain force balance in the chromosphere as the relative importance of the Lorentz force varies inversely with β. Later (section 3.3) we will see that the mostly neutral chromospheric plasma can have systematic effects on the flow of magnetic free energy through it. To understand the corona and indeed solve the coronal heating problem, we must try to understand the physics of the chromosphere.

1.3 Essential coronal observations

To guide later theoretical discussion, the following points summarize some properties of the observed, non-flaring corona selected to be of direct relevance to the heating problem. More complete discussions of coronal observations in the pre- and post- space instrumentation era can be found in works by Van de Hulst (1953), Golub and Pasachoff (1997).

1. Coronal emission is always organized by magnetic fields (Figures 1.1, 1.2, 1.3, 1.9).

2. The dominant large-scale structures are cool coronal holes ($T \approx 8 \times 10^5$ K, Noci 2003), quiet Sun emission at intermediate temperatures ($T \approx 1 - 2 \times 10^6$ K), hotter active region loops ($2 \times 10^6 \leq T \leq 5 \times 10^6$ K). Coronal holes, recognized as sources of the fast solar wind (e.g., Hundhausen and Holzer 1980), overlie predominantly unipolar magnetic fields. The quiet corona overlies mixed polarity fields, the active corona is associated with emerging magnetic fields associated with sunspots. At several solar radii the corona is stretched by the large kinetic energy of the solar wind, and the wind's interaction with the surface magnetic fields produces "streamers" seen during eclipse.

3. At intermediate scales, denser "coronal bright points", which are resolved into smaller magnetic loops or plumes in the highest resolution observations, are present over the entire solar disk. They are associated with bipolar emerging magnetic flux concentrations (also called "ephemeral regions"). Within coronal holes, "polar plumes" are seen extending almost radially from the surface from such features (Figure 1.2).

4. These structures have plasma *temperatures* which, remarkably, are also very well organized. Figure 1.9 shows vast and separate areas of blue, green and red, which are associated with quiet Sun and coronal holes, and active regions and the higher corona. The three colors are

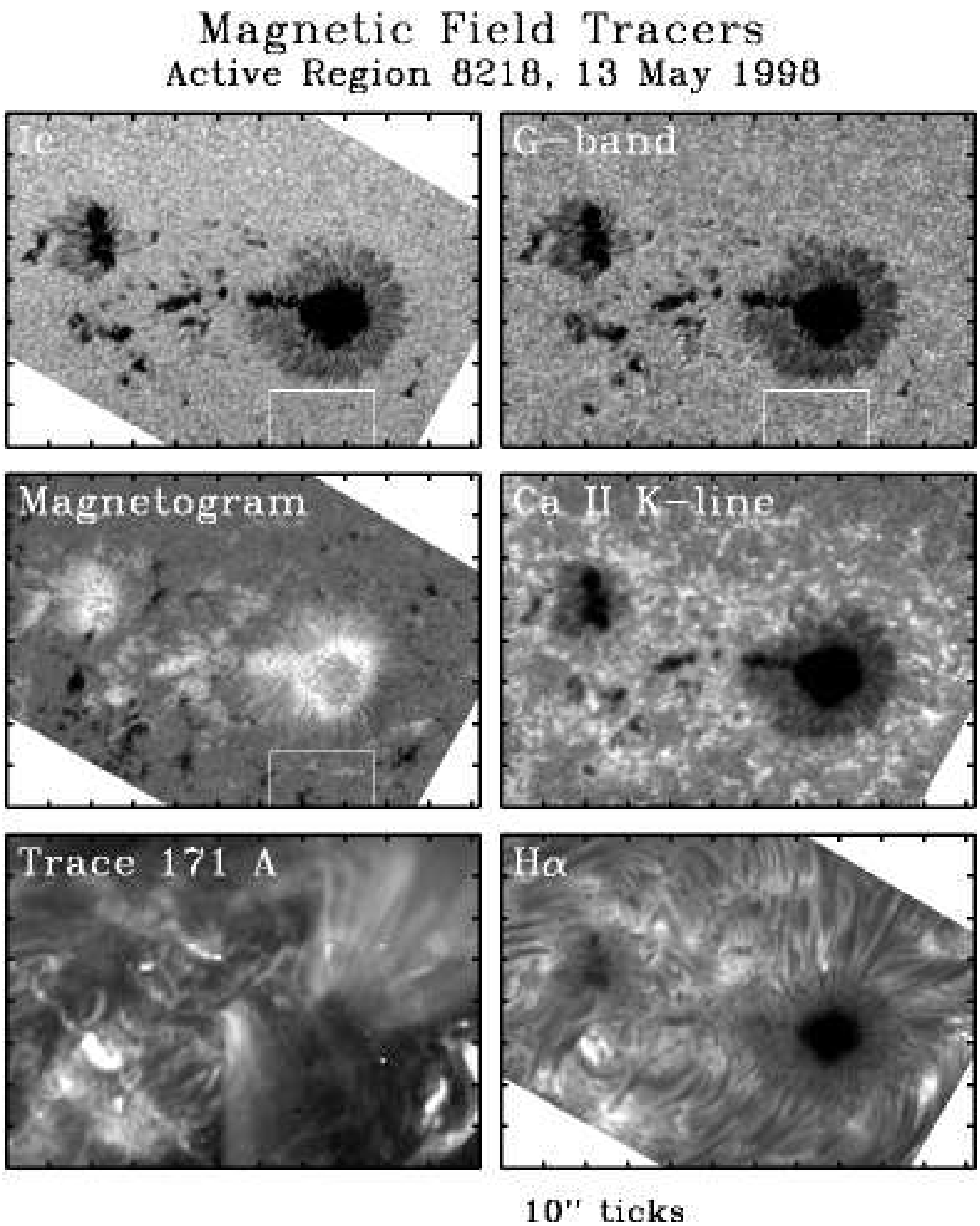

Figure 1.8: Images of a sunspot at a variety of wavelengths indicate the location (in the photosphere) and the topology (above the photosphere) of the magnetic field. Brightenings in the G-band frequently reveal the location of intense photospheric flux tubes, while more diffuse chromospheric emission in the Ca II K-line also overlies locations of magnetic flux. Notice that the Sun has somehow picked several particular foot-points from which particularly prominent 17.1 nm (10^6 K) emitting loops emerge, and not others. The field of view is about 60×80 Mm^2. Figure courtesy of B. W. Lites.

broadly sensitive to plasma at progressively higher temperatures. Only *within* active regions there are areas of white indicating mixed plasma temperatures.

```
More needed ere
```

5. On the smallest resolvable scales, the corona has fine thermal structure. High resolution coronal and chromospheric images reveal a complex physical interface between the chromosphere and corona (Figure 1.7). On small scales the thermal interface, if not the magnetic interface, is quite complex.

6. Hot plasma loops associated with active regions, at temperatures of several $\times 10^6$ K, are intrinsically *more diffuse* than those near 10^6 K. This effect cannot arise from photon scattering because images in the visible forbidden line of the Fe XIV "green line" ($T_e \approx 2 \times 10^6$ K) and the Fe X ($T_e \approx 2 \times 10^6$ K) "red line" show the same effect (e.g., Bray et al. 1991).

7. Curiously, of active region plasma loops, the cooler ones expand very little with height, in a manner in apparent disagreement with fields that are nearly potential (e.g., Klimchuk 2000, Watko and Klimchuk 2000).

8. The total radiation emitted by the corona varies in phase with the number of sunspots, following the emergence and decay of active regions. Just one active region on the Sun can double the soft X-ray emission. The shape of the large-scale corona also varies with the sunspot cycle.

9. Secular variations with time..

10. Waves

11. The corona shows different elemental abundances in different environments. *In-situ* particle fluxes in the slow solar wind reveal a well-known "first ionization potential (FIP) effect – the enhancement of low-FIP elemental abundances by a factor ≈ 3 (Geiss 1982). No FIP effect is present in the fast solar wind. Emission line spectra of coronal structures support these conclusions and show that a FIP effect is present in long-lived coronal structures where diffusion of neutral vs ionized particles has time to be significant (Feldman and Widing 2003).

12. Spectral line widths reveal sub-resolution non-thermal broadening. Typical values are $20-30$ $\mathrm{km\,s^{-1}}$, they are subsonic.

13. Low in the corona (below $R_\odot$, even in tenuous coronal holes), the body of evidence points to magneto-fluid behavior, as opposed to collisionless behavior (see chapter 2).

14. Above $\sim 2R_\odot$ from Sun center in coronal holes, spectroscopic evidence for incomplete collisional coupling between ions, and for departures from isotropic particle distribution functions (chapter 2).

1.3.1 Limitations of coronal observations

Observations have yet to approach the angular resolution needed to study either the mechanical energy sources in the high-β regions or the dissipation of the energy in the low-β coronal regions. Remotely sensed observations of the corona have been made between radio and γ-ray wavelengths. These observations are of two kinds: direct observations of photons originating from thermal emission, non-thermal emission and/or scattering of photons originating in the lower solar atmosphere, and measurements of the scintillation of cosmic radio sources "eclipsed"

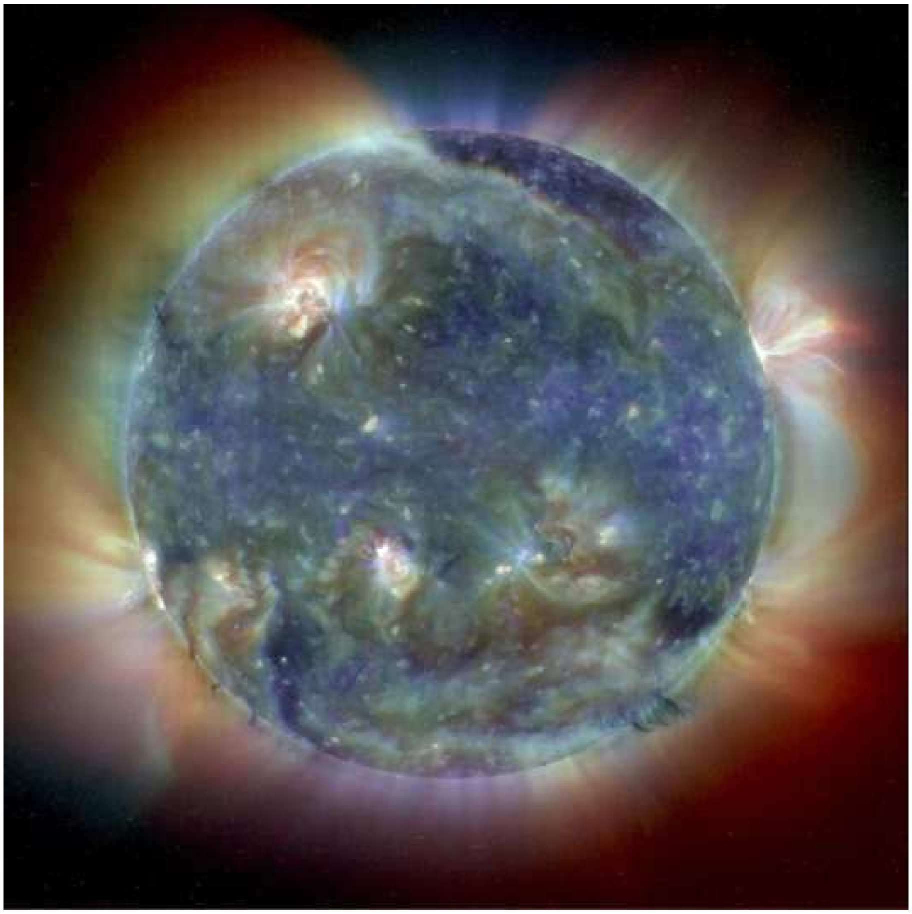

Figure 1.9: A three-color image of the corona as seen in three near-contemporaneous images from the EIT instrument on the *SOHO* spacecraft, from May 1998. Blue represents Fe IX/Fe X emission at 17.1 nm, yellow Fe XII emission at 19.5 nm, red Fe XV emission at 28.4 nm (with a small contribution from He II 30.4 nm). On large scales, the corona is thermally "organized" in the sense that there are huge areas of 17.1 nm emission physically separated from areas of 19.5 and 28.4 nm emission. The active regions and smaller "bright points" show some mixed temperature material, when observed at the ≈ 4 Mm EIT angular resolution. From the *SOHO* web site (`http://sohowww.nascom.nasa.gov/`).

by the corona (e.g., Bird and Edenhofer 1990). *In-situ* measurements from spacecraft, so far made only beyond 62 $R_\odot$ (the closest approach made by a *Helios* spacecraft, Mariani and Neubauer 1990), sample the solar wind which reflect conditions close to the solar surface only indirectly.

Any remote observation has obvious limitations, such as spectral, angular and temporal resolution, imaging and spectral quality, and noise. Additional limitations specific to the corona arise from line-of-sight integrations, and from physical selection effects. Most coronal observations are of optically thin scattered photospheric light obtained during eclipse or with coronagraphs, or of optically thin EUV and X-ray emission lines. Exceptions are optically thick radio emission and thin free-free Bremsstrahlung X-ray emission from rare very hot plasma ($T_e > 10^7$ K). Generally, then, coronal observations are biased in the sense that the intensities are proportional to $\int_{\Delta s} n_e(s)^\alpha ds$ where $1 \le \alpha \le 2$ and $\int_{\Delta s} ds$ defines the line-of-sight path along which the emission must be integrated. Heat conduction along magnetic field lines tends to smooth out gradients in electron temperatures T_e: as a rough approximation one can use a constant conductive flux density as a solution to the (field-aligned) coronal energy equation, which leads to temperature scale lengths $(d\ ln\, T_e/ds)^{-1} \propto T_e^{7/2}$. Thus, coronal images tend to have contributions to EUV and X-ray emission from field-aligned structures ("loops") which are physically much larger than those at lower temperatures. This effect can mask spatial or temporal variations on smaller length/time scales (see Appendix B). Related is the obvious observational distinction between the dynamics of the transition region and the corona. Parametric models of dynamic heating events in the corona show enormous dynamic changes in transition region emission lines, in direct response to the intermittent dissipation of energy *in the corona*. Yet in the same calculation the corona itself appears far less dynamic (Wikstøl et al. 1997). This selection effect is rarely taken into account. It calls into question claims that the transition region is the site of much local heating (as done, for example, by Aschwanden et al. 2007). Equally plausible is the fact that fluctuations in transition region lines are *easier to observe* than in the corona. The bulk of the energy flux from the corona is normally carrried as conduction down to the transition region. A burst of energy released in the corona will be manifested most obviously in the radiation (and motion) of plasma at lower temperatures. In this case, "seeing is not believing".

1.3.2 Questions raised

Solar physicists are of course very familiar with the above observations. This familiarity has perhaps a down-side in that we tend to take observed phenomena as given, and forget to ask the simplest and most fundamental question of all: *Why is the Sun obliged to exhibit the above observational properties?*

The broad correlations between emerging and strong magnetic flux and bright coronal emission implied by points 1-5? above suggest a simple relationship between emerging magnetic field and coronal heating, which has often been explored (e.g., Mandrini et al. 2000, and references therein). However a closer look at the detailed relationship between the two is significantly more complex. As an example, Figure 1.8 shows the relationship between photospheric and low chromospheric tracers of magnetic fields and coronal (10^6 K) emission in a sunspot. Of all the sunspot magnetic field, only a small volume extending to corona heights are loaded with bright plasma. Thus, *the heating mechanisms are selective.* Radio measurements of sunspot coronal magnetic fields through gyro-synchrotron emission have repeatedly failed to find any obvious relationships between the regions of strongest coronal magnetic field and bright EUV images (e.g., White 2000).

At the same time, remarkably, the active region and bright point plasma loops are broken into fine, thread-like loop structures seen down to the resolution limit of current instrumentation ($1''$). The thermal structure, while organized on a large scale, has much finer scales embedded in it. As emphasized by Litwin and Rosner (1993), while many authors have stressed this fine structure in the corona, the coronal temperature structure is actually very *coarsely* structured, when one considers how poorly energy can be transported *across* magnetic field lines in the coronal plasma. A resolution of this interesting issue probably lies in the coupling of the corona to the chromosphere (see section 3.3).

1.4 Is there a *coronal* heating problem?

Let us consider in broad terms what it would take to build a corona "from scratch", i.e. from a (fictional) region of the Sun with negligible magnetic field. It would require a source of plasma and magnetic free energy, both of which the Sun has in abundance. As the magnetic fields emerge at the surface, some processes are needed to heat it and then inject the emerged magnetic field with hot plasma, creating a mini-corona. Two extreme cases can be imagined: (1) the corona emerges fully fledged in a hot (1MK) state, as a result of heating processes within the chromosphere or lower layers; (2) the emerging flux does not heat the plasma until magnetic energy injected from beneath has time to be transported and build up within the much larger coronal volume, and finally dissipate *in situ*.

These two (academic) limits serve to illustrate the point, often ignored, that the corona does not have to arise from *in situ* heating processes, it can arise as a by-product of energetic heating in lower layers. *Nearly all modern research assumes that the heating problem belongs to the the latter, "in situ scenario".* This viewpoint was first adopted explicitly in the remarkable work of Alfvén (1947), published during the WW2 era only a few years after it was proven that the corona was hot. He identified a source of energy (photospheric granular motion), a means of transporting the energy (MHD waves), and of dissipating it (via friction). Unfortunately in the last step Alfvén incorrectly applied a formula from Cowling for frictional dissipation developed for partially ionized plasma, and grossly over-estimated the dissipation.

The bulk of the observed properties of the solar corona are in fact more compatible with the *in situ* scenario. It has indirect support in early flare work which showed that the coronal magnetic field was the only possible source of energy needed to explain the rapid onset and other properties of solar flares (Parker 1957). Clearly the corona can store large amounts of magnetic free energy. Indirect support also comes from observed properties of the solar wind, originating in the corona, in which *in situ* heating at several solar radii is needed to account for the high velocity wind streams from coronal holes (e.g., Withbroe 1988, Holzer et al. 1997). Also, there exist active stars whose coronal X-ray luminosity exceeds the chromospheric luminosity, reaching levels of 10^{-3} of the stellar luminosity (see Haisch and Schmitt 1996).

However, it is important to examine the spill-over scenario. It has been noted that the corona might be formed entirely by overly energetic *chromospheric heating* (Thomas and Athay 1961, Kuperus and Athay 1967). This can occur when the chromospheric heating rate exceeds both the maximum radiative cooling rate possible in the upper chromospheric plasma, and the total rate at which energy can be stored as latent energy of ionization. The heated, overpressured plasma then must evolve dynamically by expanding along magnetic lines of force into less dense, higher regions.

If the chromospheric heating occured rapidly, the corona so-formed would "light up" in a time $\approx L/c_S = 330$ s, where L is a characteristic coronal length scale and c_S the coronal speed of sound. Even if no more chromospheric heating occurred, this corona would then appear bright for a "cooling time" $t_{cool} \approx \frac{3}{2} n_{tot} k_B T\, L/F_C = 10^3$ s, as thermal energy is conducted and radiated away (Table 1.2). Post-flare loops originate in this fashion as very hot chromospheric plasma expands into previously dim flux bundles in the corona, but in this case the chromosphere is heated by energy released in the corona (e.g., Benz 2008) in the manner proposed by Kopp and Pneuman (1976). More direct observational evidence suggests that such a corona, while possible, does not account for the bulk of coronal emission. For example, the above time scale estimates suggest that for $\approx 1/3$ of the time, signatures of upflowing plasma should be seen, as the expanding and hot chromospheric plasma rises to fill the overlying coronal volume. Yet Doppler shifts of lines of ions formed in the transition region between corona and chromosphere indicate a predominance of downflows (Mariska 1992).

In spite of these objections, the spill-over picture still has advocates (recently, Aschwanden et al. 2007). The authors correctly recognize the importance of the chromosphere. The *in situ* proposition is not falsified, however. Instead the article presents a cocktail of arguments, with a careful selection of data, to support the idea that active region coronal loops arise from chromospheric heating[3]. For example, the extra mass observed in bright coronal loops ("loop over-density") must originate from deeper layers. But they then claim it arises from chromospheric heating from beneath. However *in situ* coronal heating can and does achieve this as conductive energy and high energy particles propagate down to the chromosphere. Mass is also lifted into the atmosphere by emerging magnetic fields. The reader is encouraged to read the other arguments.

Let us examine one specific "spill-over" scenario. Scudder has advanced a more specific hypothesis, namely that the hot coronal plasma arises from a small population of highly super-thermal ("fast") particles heated somehow in the upper chromosphere (Scudder 1992a, 1992b, 1994). This hypothesis is inspired by the properties low density space plasmas, such as in the earth's magnetosphere. Scudder notes that the chromosphere requires 1-2 orders of magnitude more energy to support it than the corona. An *in-situ* "coronal heating mechanism" is not needed. The decreasing cross section of Coulomb collisions with increasing energy is invoked, together with the gravitational potential of the Sun, to "filter" the particle distribution functions so that the mean energy per particle ("temperature") increases with height above the chromosphere.

hrom mfp

At coronal energies ($\approx$ 100 eV), ion mean free paths are large. For protons in the quiet corona, the mean free path λ is 0.2 Mm at 10^6 K, but is reduced to 0.2 km in the upper chromosphere, with Knudsen numbers $\lambda d\, lnT/dz$ of $\approx 2 \times 10^{-3}$ in both cases. These Knudsen numbers are large enough that significant departures from collisional behavior might be expected (e.g., Scudder 1992a, Landi and Pantellini 2001). Nevertheless, Landi and Pantellini (2001) have demonstrated that only very strong super-thermal tails can survive thermalizing collisions in the transition region, in agreement with independent calculations of Lie-Svendsen et al. (1999). The hypothesis also faces further challenges from observations. It is again difficult to see how the net red-shift of transition region lines, indicating energy flow down from the corona, might be produced; there is overwhelming evidence for fluid (not collisionless) behavior throughout the transition region and corona (see chapter **??**). Scudder's largely collisionless picture predicts a variation of the intensity of coronal emission with height which should have a dependence on ion mass, which is not observed.

For these reasons we reject the spill-over scenario and look primarily for mechanisms which deposit energy directly into coronal plasma.

1.5 The failure of acoustic-gravity modes

While magnetic fields clearly play a prominent role in structuring coronal plasma, heating by acoustic-gravity modes cannot be immediately dismissed on the basis of coronal plasma morphology. The reason is that acoustic-gravity compressions and rarefactions propagating parallel to magnetic fields experience no Lorentz force, they are pure acoustic modes. We must assess the role of acoustic waves in heating the corona. Wave energy is dissipated via heat conduction and viscosity, finally to be radiated or advected away.

Coronal heating by acoustic waves was first suggested by Biermann (1946), Biermann (1948) and Schwarzschild (1948), and was developed by Schatzman (1949). The proposal was widely accepted for several decades (e.g., Shmeleva and Syrovatskii 1973), but it faced stricter challenges

[3]These include aspects of loop time evolution, loop overdensity, loop upflows (rarely observed), evidence for hot upflows, cool downflows, upward propagating waves, temperature structure along loops, magnetic complexity in the transition region, the low altitudes of nanoflares, "elementary" loop cross sections, MHD heating simulations heating.

in the 1970s. Firstly, in the 1960s, it was clear that the coronal radiation losses used in the early work were underestimated. Then spectral data of UV emission lines were able to set limits on the energy flux carried by acoustic waves. Boland et al. (1973) compared total energy flux densities from the corona and transition region with those which can be carried by acoustic waves, using

$$F_W = \rho \xi^2 c_S, \tag{1.1}$$

where ξ was derived from UV line width observations of lines of Si II, Si III, C II and C IV in the quiet Sun. In their model, they found that $F_W \approx 5 \times 10^2$ W m^{-2} for all lines, just sufficient to account for the estimated coronal energy losses of $4 - 6 \times 10^2$ W m^{-2} in the quiet Sun.

Later, Athay & White (1978, 1979) revisited the problem, based upon a more rigorous analysis of data from the OSO-8 satellite. They again applied the above equation, but used densities ρ, microturbulent velocities ξ and the sound speed c_S derived from chromospheric models determined in part from Si II lines using radiative transfer calculations. In contrast to Boland et al. (1973), they found that $F_W \approx 0.1 F_M$ where $F_M \approx 6 \times 10^2$ W m^{-2} is the average radiative flux density from the uppermost chromospheric scale height (where H Lyman-α contributes half of the total), transition region and corona of the quiet Sun (Table 1.2, from Withbroe and Noyes 1977). In other words, *acoustic waves fall short of supplying the solar radiative losses from both the upper chromosphere and the corona by an order of magnitude.* The sharp contrast with the work of Boland et al. (1973) requires comment, since both studies analyzed lines of Si II near 181 nm. Boland et al.'s values for ρ, ξ^2 and c_S exceed those of Athay & White by factors of 2.4, 2.0 and 1.7 respectively, so that Boland et al.'s estimated flux density is 8 times larger. The study by Athay & White should be more reliable. Re-working their numbers, we find that they omitted the mean molecular weight in evaluating ρ from the hydrogen density. Therefore their flux density estimate is too low by a factor of 1.36, but this error does not invalidate their conclusions.

If more evidence for the failure of acoustic-gravity modes were needed, recent work shows that, at least for the dominant oscillation modes seen in the quiet chromosphere (3 minute oscillations, e.g., Gibson 1973), very little of the observed radiation losses from the weak, internetwork upper chromosphere can be attributed to observable acoustic-gravity waves (Judge and Carpenter 1998, Judge et al. 2003). This gap between theory and observation increases in the magnetically-controlled network and brighter areas of the Sun. Also, in contrast with the linear wave models of McWhirter et al. (1975), Stepien and Ulmschneider (1989) combined the non-linear limiting behavior of acoustic shock waves with transition region pressures from empirical models, to predict X-ray flux densities from sound waves which are 2-3 orders of magnitude smaller than observed in the Sun and other late-type stars. Lastly, it became clear in the 1980s that stellar soft X-ray emission varies by orders of magnitude for solar-like stars and its intensity is related to stellar rotation (e.g., Haisch and Schmitt 1996). Such properties are not consistent with acoustically heated coronae.

We must therefore turn to electromagnetism as the medium through which energy is transported to and dissipated in the corona. It follows that if wave motions are to carry the required energy flux, then, near the formation of the Si II lines discussed above, the Alfvén speed c_A must be higher than c_S. This implies that the plasma β is < 1 there. This is in qualitative agreement with the magnetic structuring of the upper chromosphere as illustrated, fr example, in Figure 1.5.

1.6 The unique challenge of heating the corona

Without delving into philosophical matters, advances in science ideally rely upon the notion of falsifiability, advanced by Popper (1992). Hypotheses (even entire paradigms) are proposed and tested against data. Any aspects found to be inconsistent with data are rejected and one proceeds to revise and/or make a new hypothesis. Alongside falsification lies a powerful principle – "Occam's Razor" – attributed to William of Occam (1285–1349): *One should not increase, beyond what is necessary, the number of entities required to explain anything.*

The problem of coronal heating is, like most problems in astrophysics, one for which we are observers only. Armed with the machinery of modern physics and computers, we nevertheless can capture only photons, and some particles ejected by the Sun as they intercept spacecraft. Let us consider another solar problem to place the heating problem in context.

Over 40 years ago, 5 minute oscillations in Doppler shifts of photospheric spectral lines were reported by Leighton et al. (1962). The physical nature of these oscillations was unclear for over a decade. The measurements inspired Ulrich (1970) and Leibacher and Stein (1971) to investigate a normal-mode model of the Sun, which appeared promising. It was not until 1975 that Deubner was able to obtain data with sufficient cadence, angular resolution, duration and field of view, that the space-time properties of the oscillations were measured. Remarkably, the data were in good qualitative agreement with predictions from normal mode oscillations. No reasonable person could deny that the model contained the simplest ingredients which could conceivably be compatible with the data. The discovery paved the way for the development of a new subject, helioseismology, in which certain properties of the invisible interior of the Sun are made manifest as perturbations of these oscillations seen at the surface. The success of helioseismology hinges upon several facts: First, the normal mode model survived the cut of Occam's Razor. Second, the oscillations are essentially linear perturbations upon well-defined zeroth order models of the Sun. Third, the observations needed for helioseismic work have both the temporal and angular resolution needed for the problem at hand- the problem is well posed. Combined, these facts make helioseismology an ideal subject for application of "inverse methods", in which data yield properties of the models directly via integral (matrix) inversion. Occam's Razor appears again in the inverse methods through the use of "regularization" which mathematically cuts out classes of solution inaccessible to the data (e.g., Craig and Brown 1986), to arrive at "simplest solutions compatible with the data". Even in this linear system, the initial progress was not particularly fast- 13 years elapsed between the appearance of the discovery paper of Leighton et al., the theoretical model of Ulrich, and finally Deubner's identification of the global modes.

By comparison, the problem of heating the corona has qualitative differences, many of which have been long recognized (e.g., Hollweg 1990):

- The corona is far dimmer than the photosphere, coronal observations are always of a lower quality.

- Coronal observations have until recently revealed no relatively simple, clear signature equivalent to the 5 minute oscillations.

- Models of the solar interior are relatively well defined because the physical ingredients are relatively straightforward. No well-defined "zeroth order" model of the corona exists. The physical ingredients needed are more complex.

Recognizing that the corona arises from the sub-photospheric mechanical motion and coupling to magnetic fields, there are other basic difficulties. The problem is observationally ill-posed - very (immeasurably?) small changes in photospheric conditions can in principle cause huge changes in the overlying corona. We do not yet understand the role of the chromosphere. Meaningful zeroth-order equilibrium configurations involve solutions to non-linear force balance equations. Turbulent motion and magnetic field evolution observed lower in the atmosphere (see Figure 1.4) drive the corona in a continuously evolving state that inevitably includes current sheets at (mathematically) tangential discontinuities (Gold 1964; Parker 1972, 1983b, 1988, 1994). Extrapolations of well-determined photospheric magnetic fields are thus subject not only to ill-posed boundary conditions, but the boundary conditions must be treated carefully, and must themselves admit the possibility of discontinuities (Low and Flyer 2007). Without equilibrium configurations, there is no credible zeroth order model upon which a given hypothesis for heating mechanisms can be built. A critical part of the problem involves identifying how magnetic free energy is dissipated. Using Table 1.2, Joule and viscous dissipation occurs on tiny length scales ($\approx 10^{-4}$ m) which are 10 orders of magnitude smaller than scales observable with current imaging instruments. The dissipation is not directly accessible to observation. Lastly, coronal energy transport is inherently non-local, because heat conduction is very efficient. Locally heated regions will, in observations, be smeared out as heat is rapidly diffused along magnetic lines of force.

For these basic reasons, this problem remains unsolved after 60+ years of intense investigation. In contrast, since 1975, progress in global helioseismology has been very rapid (e.g., Zirker 2003).

1.7 Methods of attack

Many authors have used inverse methods to derive emission measures distributions, $\xi(T_e)$, from transition region and coronal lines (see Appendix B). With assumptions of hydrostatic equilibrium, these have been used to determine 1D models from which the heating rate as a function of spatial coordinate can be derived (e.g., Jordan 1992). With the advent of data with arcsecond resolution, other authors have used intensity images to examine the structure and energy balance of plasma loops as a function of spatial coordinate along the loops.

Winebarger
static, & who
lowing that st

In finishing this chapter, it is appropriate to quote a warning from over 50 years ago, the early days of the development of MHD:

> "The discharge theory is, in fact, a good example of the exasperating behavior of electromagnetic theories of solar phenomena. At first sight, everything is in its favor; the motions existing in the presence of a magnetic field imply large electric forces, and the material is highly conducting. But induced currents, whose effect is always to oppose the changes to which they are due, smother the effect which was sought and leave only an unsatisfactory vestige of it remaining. Solar hydromagnetics is a fascinating subject and one which is very imperfectly understood; but it is also one in which the probability of being led astray by seductive theories is very high". – Cowling (1953).

Further reading

Young's book, which appeared in several editions (the fourth is listed below), contains much interesting reading concerning the 1869 eclipse and the contemporary state of knowledge of solar and solar-terrestrial physics:

Young, C.A., "The Sun", London: Kegan Paul, Trench, Trübner & Co. Ltd., 4th edition, 1892.

The following book reviews many observations from the pre-space era, and their interpretation in terms of coronal temperatures and densities:

Billings, D. E.: 1966,*A guide to the solar corona, Academic Press, New York* .

The following contains a nice discussion of coronal observations including those obtained during the "space age":

Golub, L., Pasachoff, J. M., "The solar corona", Cambridge Univ. Press, Cambridge UK, 1997.

This article discusses coronal temperature determinations in a historical context, with emphasis on coronal holes since the 1970s:

Noci, G.: 2003, "The Temperature of the Solar Corona", *Memorie della Societa Astronomica Italiana* **74**, 704–712.

The following review article has a similar perspective to section 1.6 on the challenges associated with coronal heating:

Hollweg, J. V.: 1990, "Heating of the solar corona", *Comp. Phys. Rep.* **12**, 205–232.

Chapter 2

MHD equations

The body of observational evidence indicates that in the first few pressure scale heights of the quiet and active corona (say $< 0.3R_\odot$), the plasma is fluid-like. Spectroscopically determined coronal elemental abundances are not orders of magnitude different from photospheric values. The coronal plasma is in this sense more like a well-mixed fluid than a gravitationally stratified, collisionless atmosphere (Woolley and Allen 1948). There is no evidence for a major discrepancy between the temperatures of coronal electrons and the ions (section 1.1). The thermalization time of coronal electrons and protons is about a minute (Table 1.2). Emission lines of various ions have intensity profiles consistent with strong collisional coupling between ions, i.e. ions with different charge or mass behave in a manner expected for a coupled fluids, not separate fluids. More direct evidence for fluid behavior comes, for example, from the identification of slow modes, essentially field-aligned sound waves, in the low solar corona above sunspots (Brynildsen et al. 2002), and in active region loops (de Moortel et al. 2002). de Moortel et al. state that "It is evident that the [coronal] longitudinal oscillations are a widespread, regularly occurring coronal phenomenon." There is abundant evidence for hydrodynamic, as opposed to collisionless, flows. For example free-fall downflows are very rare. These phenomena result from motion due to pressure gradients in the collisional limit. They are dynamically *slow*, in that the wave periods and flow times greatly exceed collision times. It seems safe to conclude that, for slow processes, the EUV and X-ray corona generally behaves as a *magnetofluid*.

In coronal holes and above a few scale heights ($\gtrsim$ 150Mm, say) in the quiet corona, collisions are less frequent. Collisions can become slow enough for each species to decouple from the other, while the coupling between particles of the same species are more strongly coupled and can often be treated as a single fluid. Spectroscopic analyses of line profiles from coronal holes, obtained with the SUMER and UVCS instruments on the SOHO spacecraft, have indicated departures from collision-dominated conditions. Landi and Cranmer (2008) expanded upon a UV spectral line width study of Tu et al. (1998) to conclude that electrons and ions are at different temperatures between 1.03 and 1.17 solar radii from disk center. Ions with charge to mass ratios > 0.25 have particularly enhanced ion temperatures (line widths). Such a result is of great significance, as it would require non-MHD processes such as high frequency ion cyclotron waves to explain it. To depart from MHD within a couple of scale heights of the coronal base is, however, a major theoretical complication, which therefore requires a clear observational case. In the author's opinion, further work is needed to rule out interpretations consistent with inhomogeneous fluids, before MHD is abandoned from the outset.

The case for non-MHD processes appears much tighter for more tenuous plasmas observed by UVCS at heliocentric distances $> 1.5R_\odot$ above polar holes. Cranmer et al. (2008) re-examined analyses of UVCS line profiles begun by Kohl et al. (1998). The exhaustive parameter study of

Cranmer and colleagues supports Kohl et al.'s finding of *anisotropic* ion distribution functions, at a 90% confidence level, for O^{5+} ions observed above $2R_\odot$. The higher temperatures found perpendicular to magnetic lines of force (assumed radial) indicate ion cyclotron heating. The UVCS seems to span the region between collision-dominated and collisionless conditions implied by *in-situ* measurements of the solar wind. Thus, *credible evidence for non-MHD processes exists for tenuous coronal hole plasmas* $\geq 1R_\odot$ *above the solar surface.* In the broader context of the general coronal heating problem, this evidence shows only that non-MHD processes are required to explain kinetic effects in a small population of the ions high above the Sun. These non-MHD properties might not therefore be significant in the bright, low corona in general, and the active (loop-like) corona in particular.

It is sometimes thought that fluid treatments are applicable only when particle mean free paths are much smaller than physical scales of interest. However, Parker (2007, ch. 8) reviews how the equations of fluid mechanics can describe the dynamics of gases or plasmas, without regard to collisions, because of the conservation of mass, momentum and energy. The validity of the fluid equations requires that the macroscopic quantities (particle densities n) are statistically well-defined, i.e., for a scale length ℓ, $n\ell^3 \gg 1$, without regard to collisions. Also, the motion of individual particles is, between collisions, assumed to be linear. Thus the equations are valid on scales in excess of the largest (ion) gyro-radii of interest. In the corona the gyro-radii are far smaller than the mean free paths, and the issue is not important. Care must be taken, though, to deal with the pressure tensor, heat flux and other terms under weakly collisional, magnetized conditions.

The simplest theoretical framework which might account for the transport and dissipation of electromagnetic energy in the Sun is *resistive MHD*. It can treat a wide variety of, but not all, candidate mechanisms for heating the Sun's corona. This framework is (almost) our starting point for discussing coronal heating. While single-fluid MHD can be approached using phenomenological transport coefficients (e.g., see Ferraro and Plumpton 1966), the nature of energy transport and dissipation is different for the light, negatively charged electrons, and the heavier positively charged ions. Electric currents flow because of the relative motion between ions and electrons, and the associated energy is dissipated by electron-heavy particle collisions. Viscous dissipation of kinetic energy in fluid velocity gradients is dominated by ion motions, whereas heat conduction – which is in part dissipative – is usually dominated by electrons. In the presence of "strong" magnetic fields, in the sense that particles are "magnetized" as in the corona (i.e., $\omega\tau \gg 1$, see Table 1.2 and below), transport and dissipation processes become highly anisotropic, and differ significantly for ions and electrons. Thus, from the outset, we must at least deal with a two-component "simple plasma" (ion-electron) model, from which we discuss the widely-used single fluid MHD equations, including transport coeffeicients from kinetic theory, as an approximation to collision-dominated plasmas. In this way the basic processes which convert magnetic to thermal energy are hopefully made clear.

2.1 Basic approximations

MHD describes the motion of electrically conducting fluids in the presence of magnetic fields, describing physical processes in at least partially ionized plasmas in a series of well-defined approximations outlined below. Magnetic and electric fields, charge densities and currents are treated as spatial averages, assuming that the spatial scales of interest greatly exceed particle mean free paths, and that number of particles in a Debye sphere (the "plasma parameter"), and indeed the plasma as a whole, are both $\gg 1$ (Table 1.2). The plasma's fluid properties are controlled by particle trajectories determined by gyro motion and collisions, through the parameter $\omega\tau$, called the "magnetization", where ω is the gyro frequency and τ the mean collision time. In turn, the particles' "magnetization", determines the nature of the transport and dissipation of energy and momentum in the plasma.

We follow Braginskii's (1965) seminal work, outlining the basic assumptions and results of this work. Deeper insight can be found in the original paper and books by Woods (1987) and Kulsrud (2005). The fluid equations are derived from the Boltzmann equations for each particle species, a. The latter determine the time evolution of the distribution functions $f_a(t, \mathbf{r}, \mathbf{v})$, where $f_a(t, \mathbf{r}, \mathbf{v})d^3\mathbf{r}d^3\mathbf{v}$ is the number of particles in the phase space volume $d^3\mathbf{r}d^3\mathbf{v}$ at time t, position $\mathbf{r}$ and with velocity $\mathbf{v}$ (Chapman and Cowling 1970). For particles with no internal degrees of freedom,

$$\frac{\partial f_a}{\partial t} + \mathrm{div}\,(\mathbf{v} f_a) + \mathrm{div}_{\,v}\left(\frac{\mathbf{F}_a}{m_a} f_a\right) = C_a. \tag{2.1}$$

Here $\mathrm{div}_{\,v}\mathbf{F}_a \equiv \sum_\beta \frac{\partial F_{a\beta}}{\partial v_\beta}$. In MHD the plasma is treated as a fluid with average number and mass densities, n_a and ρ_a, and velocities $\mathbf{u}_a$ defined by

$$\begin{aligned} n_a(t, \mathbf{r}) &= \int f_a(t, \mathbf{r}, \mathbf{v}) d^3\mathbf{v} && (2.2)\\ \rho_a(t, \mathbf{r}) &= m_a n_a(t, \mathbf{r}) && (2.3)\\ \mathbf{u}_a(t, \mathbf{r}) &= \frac{1}{n_a(t, \mathbf{r})} \int \mathbf{v} f_a(t, \mathbf{r}, \mathbf{v}) d^3\mathbf{v} = \langle \mathbf{v} \rangle_a. && (2.4) \end{aligned}$$

The LHS of equation (2.1) contains forces $\mathbf{F}_a$ which are "smoothed", macroscopic values, representing averages over a large number of particles and over times long compared with typical times of flight. The RHS contains all remaining "collisional" terms, $C_a = \sum_b C_{ab}(f_a, f_b)$, which arise from rapidly fluctuating micro-fields originating from the continual mutual bombardment of particles a by particles b. While it is easy to specify $\mathbf{F}_a$ for particles of charge $\mathcal{Q}_a$, electric current $\mathbf{j}$, and mass m_a, given electric, magnetic and gravitational fields $\mathbf{E}$, $\mathbf{B}$[1], $\mathbf{g}$, as

$$\mathbf{F}_a = \mathcal{Q}_a(\mathbf{E} + \mathbf{v}_a \times \mathbf{B}) + m_a \mathbf{g}, \tag{2.5}$$

determination of C_a is far more complex, because these terms depend on all the distribution functions. Also, the RHS should include not only random processes ("collisions"), but also rapid, collective processes such as plasma waves or turbulence which give rise to microscale, fluctuating electric fields. Collisions will be discussed in this chapter, leading to "classical" transport coefficients. Collective processes are harder still to deal with. They lead to "anomalous" transport coefficients, and are left until chapter 4.

The fluid equations describing conservation of particles, particle momenta and energies, are derived by multiplying equation (2.1) by 1, $m_a\mathbf{v}_a$ and $mv_a^2/2$ respectively, and integrating over $\mathbf{v}_a$:

$$\begin{aligned} \frac{\partial n_a}{\partial t} + \mathrm{div}\,(n_a \mathbf{u}_a) &= 0 && (2.6)\\ \frac{\partial \rho_a \mathbf{u}_a}{\partial t} + \mathrm{div}\,(\rho_a \langle \mathbf{v}_a\, \mathbf{v}_a \rangle) - n_a \mathbf{F}_a &= \int m_a \mathbf{v}_a C_a d^3\mathbf{v}_a && (2.7)\\ \frac{\partial}{\partial t}\left(\frac{\rho_a}{2}\langle v_a^2 \rangle\right) + \mathrm{div}\left(\frac{\rho_a}{2}\langle v_a^2 \mathbf{v}_a \rangle\right) - n_a \mathbf{u}_a \cdot \mathbf{F}_a &= \int \frac{m_a v_a^2}{2} C_a d^3\mathbf{v}_a && (2.8) \end{aligned}$$

[1]Here, following convention in solar physics, "magnetic field" refers to $\mathbf{B}$. In the physics literature this term is reserved for $\mathbf{H} = \mathbf{B}/\mu$ (e.g. Jackson 1962), where μ is the magnetic permeability.

The force $\mathbf{F}_a$ in equations (2.7) and (2.8) is given by equation (2.5), but with $\mathbf{v}_a$ replaced with $\mathbf{u}_a$. Since these expressions still contain moments of the particle velocities, $\mathbf{v}_a$, these moments are more familiarly expressed in terms of the random component $\mathbf{v}'_a$ and systematic flow $\mathbf{u}_a$, where

$$\mathbf{v}'_a = \mathbf{v}_a - \mathbf{u}_a. \tag{2.9}$$

The components of the dyad $\langle \mathbf{v}_a \, \mathbf{v}_a \rangle$ (a tensor quantity, see Appendix A) are then, since $\langle u_\alpha v'_\beta \rangle_a = 0$,

$$\langle v_\alpha v_\beta \rangle_a = (u_\alpha u_\beta)_a + \langle v'_\alpha v'_\beta \rangle_a \tag{2.10}$$

Using equation (2.6) the equation of motion takes the more familiar form:

$$\rho_a \frac{\mathrm{d}\mathbf{u}_\mathrm{a}}{\mathrm{dt}_a} = -\mathbf{grad}\, p_a - \nabla \cdot \boldsymbol{\pi}_a + n_a \mathbf{F}_a + \mathbf{R}_a, \tag{2.11}$$

where $\frac{\mathrm{d}}{\mathrm{dt}_a} \equiv \frac{\partial}{\partial t} + \mathbf{u}_a \cdot \mathbf{grad}$, and

$$\begin{aligned} p_a &= \frac{\rho_a}{3} \langle {v'_a}^2 \rangle = n_a k_B T_a, & (2.12)\\ \pi_{a\alpha\beta} &= \rho_a \langle v'_\alpha v'_\beta - \frac{v'^2}{3} \delta_{\alpha\beta} \rangle_a, & (2.13)\\ \mathbf{R}_a &= \int m_a \mathbf{v}'_a C_a d^3\mathbf{v}_a. & (2.14) \end{aligned}$$

p_a is the scalar pressure, the total pressure tensor $\mathbb{P}_a$ has components $P_{a\alpha\beta} = p_a \delta_{\alpha\beta} + \pi_{a\alpha\beta}$. $\boldsymbol{\pi}_a$ is the viscous stress tensor. The α component of the term $\nabla \cdot \boldsymbol{\pi}_a$ is $\sum_\beta \partial \pi_{a\alpha\beta}/\partial x_\beta$, and the force $\mathbf{R}_a$ is the mean change in momentum of the particles of species a with all other particles. Note that equation (2.12) can be used to define T_a for any distribution function, only for Maxwellians is T_a the thermodynamic kinetic temperature. Similarly, the total energy equation becomes

$$\frac{\partial}{\partial t}\left(\frac{\rho_a}{2} u_a^2 + \frac{3}{2} n_a k_B T_a\right) + \mathrm{div}\left\{\left(\frac{\rho_a}{2} u_a^2 + \frac{5}{2} n_a k_B T_a\right)\mathbf{u}_a + \boldsymbol{\pi}_a \cdot \mathbf{u}_a + \mathbf{q}_a\right\} \\ = n_a \mathbf{F}_a \cdot \mathbf{u}_a + \mathbf{R}_a \cdot \mathbf{u}_a + Q_a \tag{2.15}$$

where

$$\begin{aligned} \mathbf{q}_a &= \int \frac{m_a {v'_a}^2}{2} \mathbf{v}_a f_a(t, \mathbf{r}, \mathbf{v}_a) d^3\mathbf{v}_a = \frac{\rho_a}{2} \langle {v'_a}^2 \mathbf{v}_a \rangle, \text{ and} & (2.16)\\ Q_a &= \int \frac{m_a {v'_a}^2}{2} C_a d^3\mathbf{v}_a. & (2.17) \end{aligned}$$

$\mathbf{q}_a$ is the heat flux density, Q_a is the heat generated in particle species a through collisions with all other particles. Subtracting the dot product of equation (2.12) with $\mathbf{u}_a$ from equation (2.15), we obtain the internal energy equation (or heat equation) for species a:

$$\frac{3}{2} n_a k_B \frac{\mathrm{dT}_a}{\mathrm{dt}} + p_a \mathrm{div}\, \mathbf{u}_a = \mathrm{div}\, \mathbf{q}_a - \boldsymbol{\pi}_a : \nabla u_a + Q_a, \tag{2.18}$$

where $\boldsymbol{\pi}_a : \nabla \mathbf{u}_a = \sum_{\alpha\beta} \pi_{a\alpha\beta} \partial u_{a\alpha}/\partial x_\beta$.

For each particle species, equations (2.6), (2.7) and (2.8) comprises a system of five equations for the evolution of the five unknowns n_a, $\mathbf{u}_a$, p_a (or T_a), to which we seek solutions given initial and boundary conditions. To close this system requires "constitutive relations" which specify the following variables in terms of the n_a, $\mathbf{u}_a$, p_a (or T_a) of *all* abundant species a:

Variable	Source	Comments
$\mathbf{F}_a$	equation (2.5)	$\mathbf{E}$, $\mathbf{B}$ must be determined from Maxwell's equations, consistent with charge $\mathcal{Q}$ and current density $\mathbf{j}$
$\mathbf{R}_a$, $\boldsymbol{\pi}_a$, $\mathbf{q}_a$, Q_a	Kinetic theory, or measurements	Use near-LTE theory from Braginskii (1965)

The charge and current densities, $\mathcal{Q}$ and $\mathbf{j}$, needed to determine the electric and magnetic fields are

$$\mathcal{Q} = \sum_a \mathcal{Q}_a n_a; \quad \mathbf{j} = \sum_a \mathcal{Q}_a n_a \mathbf{u}_a \tag{2.19}$$

The systems of n equations for an n-species plasma are closed using kinetic theory taking proper account of the influence of magnetic fields which enforce local rotational symmetry around $\mathbf{B}$, following Braginskii (1965).

2.1.1 Particle trajectories and collisions

The gyrofrequency of particle a in a magnetic field of strength B is

$$\omega_a = \frac{|\mathcal{Q}_a|B}{m_a}, \text{ so that} \tag{2.20}$$

$$\omega_e = 1.76 \times 10^{11} B, \text{ and } \omega_i = 0.96 \times 10^8 \frac{Z_i B}{m_i/m_p}. \tag{2.21}$$

As already noted, the effects of magnetic fields on transport processes depend on $\omega_a \tau_a$, where τ_a is the shortest "relaxation time" for species a. For all charged particles in the corona, $\omega_a \tau_a \gg 1$ (Table 1.2). The particles execute many gyrations between typical collisions. For particle motions parallel to $\mathbf{B}$, the Lorentz force is zero, transport coefficients are identical to the field-free case (as given by Gombosi 1994, for example). But for motion perpendicular to $\mathbf{B}$, recognizing that $\omega_a \tau_a = \lambda_a / r_a$, λ_a being the mean free path and r_a the gyroradius, the perpendicular distance travelled between typical collisions is the smaller of λ_a and r_a. When $\omega_a \tau_a \gg 1$, this distance is reduced by a factor $\omega_a \tau_a$ compared with the field-free case, and perpendicular transport of mass, momentum and energy is accordingly reduced. The transport coefficients are only "laterally isotropic", being isotropic only along $\mathbf{B}$ itself and in the plane perpendicular to it. When $\omega_a \tau_a \ll 1$ the presence of $\mathbf{B}$ has little effect on transport coefficients which become fully isotropic as $\omega_a \tau_a \to 0$.

For a low-density plasma, classical binary Coulomb collisions determine C_{ab}, and hence τ_{ab}. Consider a simple plasma consisting of protons (p) and electrons (e). The energy exchanged between particles of small mass m and large mass M is $\approx m/M$ of the kinetic energy (in the center of mass frame) per collision. Since $m_e/m_p \ll 1$, this means that the electron and ion gases relax to equilibrium in a time τ_{ep}^{ε} which is roughly m_p/m_e times longer than relaxation time τ_{ee} for the electron gas. Now, the Coulomb potential is the same magnitude for $e-e$ and $e-p$ collisions, and since the relative speeds (or energies) of impact are similar, $\tau_{ee} \approx \tau_{ep}$. By the same argument, if $T_p \sim T_e$, $\tau_{pp} \sim \sqrt{m_p/m_e}\tau_{ei}$ because the speed of $p-p$ impacts is reduced by the factor $\sqrt{m_p/m_e}$. Henceforth we write τ_e for either of τ_{ee} or τ_{ei}, and τ_p for τ_{pp}. The electron and ion gases individially relax much faster than electron-ion relaxation, and if $T_p \approx T_e$,

$$\tau_e \,:\, \tau_p \,:\, \tau_{ep}^{\varepsilon} = 1 \,:\, \sqrt{m_p/m_e} \,:\, m_p/m_e. \tag{2.22}$$

To estimate τ_e and τ_p, we must note that the Coulomb potential is long range. Thus relaxation involves not only close collisions (large-angle scattering), which have a cross section for impact energy $m_a v_a^2/2 = \varepsilon_a \sim 3k_B T_a/2$ (measured in the center-of-mass frame) of

$$\sigma_{large} = \pi b^2, \quad b \approx \frac{\mathcal{Q}_a^2}{4\pi\epsilon_0\varepsilon_a}, \tag{2.23}$$

but also must include far more frequent small-angle collisions which are significant to much larger radii, of order $b' = \lambda_D$ where λ_D is the Debye radius (Table 1.2). λ_D is the distance beyond which the Coulomb field is shielded by the plasma. In effect, the collision is formally no longer a binary collision, instead the effects of the surrounding charges are treated by setting the Coulomb potential to zero for distances greater than λ_D. This is reasonable when the "plasma parameter" is large, which is the case for the corona (Table 1.2). The quantity $ln(\lambda_D/b)$, called the "Coulomb logarithm" and designated $ln\ \Lambda$ (Spitzer 1965), is a weak (logarithmic) function of T_a and density n_a. $ln\ \Lambda$ is typically ≈ 20 under coronal conditions. The total cross section is then

$$\sigma_a \approx ln\ \Lambda\, \pi b^2 \propto \varepsilon^{-2}. \tag{2.24}$$

These cross sections do not depend on mass, so they are similar for proton-proton, electron-electron, and electron-proton collisions. The mean free paths and collision times for colliding identical particles a are then

$$\lambda_{aa} = \frac{1}{\sigma_a n_a} \propto \frac{\varepsilon_a^2}{n_a\, ln\ \Lambda} \propto \frac{T_a^2}{n_a\, ln\ \Lambda}, \text{ and} \tag{2.25}$$

$$\tau_{aa} = \lambda_{aa}/v_a = \frac{1}{\sigma_a n_a}\sqrt{\frac{m_a}{2\varepsilon_a}} \propto \frac{m_a^{1/2}\varepsilon_a^{3/2}}{n_a\, ln\ \Lambda} \propto \frac{m_a^{1/2}T_a^{3/2}}{n_a\, ln\ \Lambda} \tag{2.26}$$

For the same impact energy (or mean temperature T), the mean free paths of electrons and protons in a fully ionized hydrogen plasma ($n_p = n_e$) are identical, but the proton-proton collision times are larger.

2.1.2 Transport and dissipation in a near-LTE hydrogen plasma

The coefficients $\mathbf{R}$, $\boldsymbol{\pi}$, $\mathbf{q}$, and Q can be understood physically using ω and τ via mean free path arguments. Instead of evaluating collision integrals, plasma properties are evaluated at specfic locations (e.g. $\pm\lambda_a = \tau_a \langle {v'_a}^2\rangle^{1/2}$ for free propagation between collisions) along and perpendicular to $\mathbf{B}$, where $\langle {v'_a}^2\rangle = 3k_B T_a/m_a$. It is assumed that macroscopic quantities ψ (e.g., T_a) vary little over the mean free path λ_a, e.g.:

$$\psi(x_0 + \lambda_a) \approx \psi(x_0) + \psi'(x_0)\,\lambda_a + \left(\frac{\psi''(x_0)\,\lambda^2}{2!} + \ldots\right) \tag{2.27}$$

When charge neutrality is valid, i.e. $\mathcal{Q} = e(n_p - n_e) \ll n_e$ (see section 2.2),

$$n_e \approx n_p = n, \text{ say, and } \mathbf{j} = e(n_p\mathbf{u}_i - n_e\mathbf{u}_e) \approx -en\boldsymbol{\nu},$$

where

$$\boldsymbol{\nu} = \mathbf{u}_e - \mathbf{u}_i \tag{2.28}$$

is the velocity of the electrons relative to the ions.

Before proceeding, it will be convenient to define three orthogonal components of a vector $\mathbf{q}$ in terms of the unit vector $\mathbf{h} = \mathbf{B}/B$:

$$\begin{aligned}
\mathbf{q}_{\|} &= \mathbf{h}(\mathbf{q}\cdot\mathbf{h}), \\
\mathbf{q}_{\perp} &= \mathbf{h}\times(\mathbf{q}\times\mathbf{h}) = \mathbf{q}-\mathbf{q}_{\|}, \quad \text{and} \\
\mathbf{q}_{\wedge} &= \mathbf{q}\times\mathbf{h}.
\end{aligned}$$

The frictional and thermal forces $\mathbf{R}$

The force $\mathbf{R}$ arises from collisions between electrons and protons. $\mathbf{R}$ consists of two components, a frictional force $\mathbf{R}_\nu$ whose origin is in a non-zero relative velocity between the electron and ion fluids, $\boldsymbol{\nu} = \mathbf{u}_e - \mathbf{u}_i$, and a thermal force $\mathbf{R}_T$ arising because of non-zero macroscopic temperature gradients and the ε^{-2} dependence of the Coulomb cross section on energy:

$$\mathbf{R} = \mathbf{R}_\nu + \mathbf{R}_T \tag{2.29}$$

When colliding with ions, electrons lose their ordered relative velocity $\boldsymbol{\nu}$, and momentum $m_e\boldsymbol{\nu}$ to the ions in a time τ_e.

Then, the frictional force exerted on the electron gas for motion parallel to $\mathbf{B}$ is, per unit volume roughly

$$\mathbf{R}_\nu^{\|} \approx -\frac{m_e n_e}{\tau_e}\boldsymbol{\nu}_{\|} \quad \mathrm{N\ m^{-3}}. \tag{2.30}$$

This estimate, being based upon estimates of τ_e averaged over Maxwellians, cannot take into account the skewing of the electron distribution function that arises because, for a collision with energy $\varepsilon \propto v^2$, $\tau \propto v^3$. Thus, faster electrons experience a smaller Coulomb force. The distribution function is then skewed in a manner which makes $\boldsymbol{\nu}$ depend more on the faster electrons. Since $\tau_{ee} \sim \tau_{ei}$, the thermalizing electron-electron collisions occur at the same rate as the skewing electron-ion collisions. The net result is an effect of order unity which produces a smaller value of $\mathbf{R}_\nu^{\|}$ than suggested by the estimate (2.30). For motion perpendicular to $\mathbf{B}$, $\boldsymbol{\nu}_\perp$, when $\omega\tau \gg 1$, the skewing effect is diminished because the gyro motion significantly alters the momentum in a given direction perpedicular to $\mathbf{B}$ $1/\omega$ times, during each τ. Thus the skewing effect is smaller by $\omega\tau$, and when this is $\gg 1$ this regime the equation (2.30) becomes accurate. The numerical results of Braginskii are

$$\begin{aligned}
\mathbf{R}_\nu &= -\frac{m_e n_e}{\tau_e}(0.51\boldsymbol{\nu}_{\|} + \boldsymbol{\nu}_\perp) && (2.31)\\
&= en\left(\frac{\mathbf{j}_{\|}}{\sigma_{\|}} + \frac{\mathbf{j}_\perp}{\sigma_\perp}\right), && (2.32)
\end{aligned}$$

where the perpendicular and parallel electrical conductivities are

$$\sigma_\perp = \frac{e^2 n_e \tau_e}{m_e}; \quad \sigma_{\|} = 1.96\sigma_\perp \tag{2.33}$$

Thus, in the corona, the frictional force and associated electrical conductivity is anisotropic, but not radically so. The work done against $\mathbf{R}_\nu$ per second is

$$\mathbf{R}_\nu \cdot \boldsymbol{\nu} = \left(\frac{j_{\|}^2}{\sigma_{\|}} + \frac{j_\perp^2}{\sigma_\perp}\right) \tag{2.34}$$

Clearly this conversion of electric currents into thermal energy is irreversible. It is discussed further in section **??** in the context of "Ohm's law".

The "thermal force" $\mathbf{R}_T$ arises from temperature gradients and the special v_e^{-4} dependence of the Coulomb collision cross section. To understand the origin of $\mathbf{R}_T$, we must study collisions as a function of the impacting electron speed v_e. Again we assume $T_p \lesssim T_e$ so that ion motion does not influence collision times, which thus depend only on T_e. Consider a stationary plasma ($\mathbf{u}_e = \mathbf{u}_p = 0$). Under homogeneous conditions, any given plane has a flux of electrons $n_e v_e$ normal to it. The $e - i$ collisions lead to frictional forces $\mathbf{R}_+$ and $\mathbf{R}_-$ from opposite directions, each of magnitude $m_e n_e v_e/\tau_e$. Then $\mathbf{R}_+ + \mathbf{R}_- = 0$. When $\mathbf{grad}\, T \neq 0$, for example when electrons to the "right" are warmer than those to the "left", the hotter electrons are subject to a smaller frictional force than the cooler electrons, because $\tau_e(v_e) \propto v_e^3$. Thus the thermal force drives electrons down temperature gradients. If $\mathbf{B} = (0, 0, B)^T$ and $\nabla T_e = (0, 0, dT_e/dz)^T$, a Taylor expansion of T_e about z_0 gives an unbalanced force of magnitude

$$\mathbf{R}_T \sim \frac{m_e n_e v_e}{\tau_e} \frac{\lambda_e}{T_e} \frac{dT_e}{dz} \sim \frac{m_e v_e^2}{k_B T_e} n_e k_B \frac{dT_e}{dz} \sim n_e k_B \frac{dT_e}{dz}. \tag{2.35}$$

Cross-field thermal forces can be estimated replacing λ_e by r_e in equation (2.35), so they are smaller than the parallel force given by this equation by the factor $\omega_e \tau_e$. Both $\mathbf{R}_\nu$ and $\mathbf{R}_T$ increase with increasing ion charge Z_i, as the strength of the $i - e$ Coulomb forces increases with Z_i and the cross sections of $e - i$ collisions increase as Z_i^2 (see equation 2.23).

Heat flux $\mathbf{q}_\nu$

Like $\mathbf{R}$, the heat flux $\mathbf{q}$ consists of two parts:

$$\mathbf{q} = \mathbf{q}_\nu + \mathbf{q}_T \tag{2.36}$$

Thermal forces lead directly to terms proportional to $\boldsymbol{\nu}$ in the electron heat flux $\mathbf{q}_\nu^e$, both of which arise from the $\tau_e \propto v_e^3$ behavior for Coulomb collisions. We just argued that the electric current along $\mathbf{B}$ is carried mostly by faster electrons. In the frame where $\mathbf{u}_e = 0$, more fast electrons move in the $\boldsymbol{\nu}$ direction, balanced by a larger fraction of slow electrons moving in the $-\boldsymbol{\nu}$ direction. Since the kinetic energy per electron is $m_e v_e^2/2$, the heat flux $\mathbf{q}_\nu^e$ is unbalanced: heat flows in the $\boldsymbol{\nu}$ direction. Parallel to $\mathbf{B}$,

$$q_{u\parallel}^e \sim n_e k_B T_e \nu_\parallel. \tag{2.37}$$

Cross field current flow is accompanied by heat flow whose origin is different, since the ion-electron collisions accelerate and decelerate electrons moving parallel and anti-parallel to $\boldsymbol{\nu}$ respectively. The force is along the direction of $\boldsymbol{\nu} \times \mathbf{B}$. Its magnitude is estimated by noting that the difference in energy between an accelerated and decelerated electron is $\sim (m_e \nu/\tau_e) r_e$, so that, with $r_e = v_e/\omega_e$,

$$q_{u\perp}^e \sim \frac{m_e \nu_\perp}{\tau_e} r_e n_e v_e \sim \frac{n_e k_B T_e}{\omega_e \tau_e} \nu_\perp \tag{2.38}$$

Diffusion

Particle diffusion is estimated retaining just the zeroth and first derivatives in the Taylor expansion (equation 2.27). Diffusion of the particles' number, mass or thermal energy density is described by setting ψ equal to n_a, $n_a m_a$ and $\frac{3}{2} n_a k_B T_a$ respectively, which leads to associated flux densities $\mathbf{f}$:

$$\mathbf{f}_a = -D\,\mathbf{grad}\;\psi, \quad D = \frac{\Delta^2}{2\tau_a}, \tag{2.39}$$

Diffusion of momentum is described by derivatives of tensors, because the equivalent quantity to scalar ψ is a vector, $n_a m_a \mathbf{u}_a$. Equation (2.27) then leads to terms of the form $\frac{\partial u_\alpha}{\partial x_\beta}$ for transfer of the α component of the momentum along coordinate β. Examples of flux densities along the "x" direction are, dropping here the subscript a,

$$f_x(\text{mass}) \approx -D\frac{\partial}{\partial x}(nm), \tag{2.40}$$

$$f_x(y \text{ momentum}) = \pi_{yx} \approx -D\frac{\partial}{\partial x}\left(nmu_y\right), \tag{2.41}$$

$$f_x(\text{thermal energy}) = q_{T,x} \approx -D\frac{\partial}{\partial x}\left(\frac{3}{2}nk_BT\right). \tag{2.42}$$

In terms of the "diffusion coefficient" D, coefficients for viscosity η and thermal conductivity κ are found through their definitions, assuming $n \approx$ constant,

$$\pi_{yx} = -\eta\frac{\partial u_y}{\partial x}, \quad \Rightarrow \eta \approx \frac{nm\Delta^2}{\tau} \approx nmD \tag{2.43}$$

$$q_{T,x} = -\kappa\frac{\partial T}{\partial x}, \quad \Rightarrow \kappa \approx \frac{nk_B\Delta^2}{\tau} \approx nk_BD. \tag{2.44}$$

When $\mathbf{B} = 0$ or, for diffusion along $\mathbf{B}$, $\Delta \approx \lambda \approx v\tau$, and then $D \approx v\lambda$, the standard result from elementary kinetic theory. In this case, from equations (2.43) and (2.44) and when $T_i \approx T_e$ and $u_i \approx u_e$, *momentum is transported mostly via the ions ($\eta \propto \sqrt{m}$), and energy is transported mostly by electrons ($\kappa \propto 1/\sqrt{m}$).*

However, equation (2.39) is more general than the kinetic result $D = v\lambda$, in that the displacement of the particle between collisions Δ need not be the mean free path. Cross-field diffusion is influenced by the Lorentz force, for charged particles.

Diffusive heat flux $\mathbf{q}_T$

The presence of magnetic fields influences $\mathbf{q}_T$ in both obvious and subtle ways. Parallel to $\mathbf{B}$ the particles travel a typically a distance $\Delta = \lambda$ between collisions, parallel to it they travel a distance of order the gyroradius, $\Delta = r$. Using equation (2.39), when $\omega\tau \gg 1$,

$$\kappa_\perp/\kappa_\parallel \approx \omega^{-2}\tau^{-2}, \tag{2.45}$$

$$\kappa^e_\parallel/\kappa^i_\parallel \approx \sqrt{m_i/m_e}, \qquad (T_i \approx T_e), \tag{2.46}$$

$$\kappa^e_\perp/\kappa^i_\perp \approx \sqrt{m_e/m_i}, \qquad (T_i \approx T_e). \tag{2.47}$$

Thus, when $T_e \approx T_e$, electrons dominate the parallel heat conduction, but ions dominate the transverse heat conduction.

More subtly, there arises a transverse heat flux perpendicular to both $\mathbf{B}$ and $\mathbf{grad}\,T$, $\mathbf{q}_\wedge$. (Definitions of these vector components are given in A.4). Consider a situation where $\mathbf{grad}\,T_a$ lines along the x axis, $\mathbf{B}$ lying along the z axis. $\mathbf{q}_\wedge$ arises because particles gyrating at neighboring points x, $x + \Delta$ at different temperatures T_a and $T_a + \Delta\partial T_a/\partial x$ have higher velocities v'_a along the y axis than along $-y$. The result is that if the particle fluxes $+n_a v'_{ay}$ and $-n_a v'_a$

between x and $x+\Delta$ are balanced, the thermal flux densities $n_a v'_{ay} k_B T_a$ are imbalanced by the fraction $(r_a/T_a)\partial T_a/\partial x$ producing the heat flux

$$q_y \approx n k_B v_a r_a \frac{\partial T_a}{\partial x} \approx \frac{n_a k_B T_a}{\mathcal{Q}_a B}\frac{\partial T_a}{\partial x} \tag{2.48}$$

These fluxes are of opposite sign for electrons ($\mathcal{Q}_a = -e$) and ions ($\mathcal{Q}_a = +e$). They have no net effect on the plasma's thermodynamics.

Irreversible heat exchange, $T_i \neq T_e$

Collisions of electrons and ions at different kinetic temperatures lead to irreversible exchange of heat, in addition to the frictional heating given above ($-\mathbf{R}\cdot\boldsymbol{\nu}$). Assuming $\boldsymbol{\nu}=0$, the energy exchanged per unit volume and time from electrons to ions is

$$Q_\Delta \approx \frac{2m_e}{m_i}\frac{n_e}{\tau_e}\frac{3}{2}k_B(T_e - T_i), \tag{2.49}$$

since only $\frac{2m_e}{m_i}$ of the kinetic energy is transferred per collision. When $|\boldsymbol{\nu}| \neq 0$ *and* $T_i \neq T_e$, the energy transferred to the ion and electron fluids are, to order m_e/m_i, additive:

$$Q_i = Q_\Delta, \quad Q_e = -\mathbf{R}\cdot\boldsymbol{\nu} - Q_\Delta = -\mathbf{R}_\nu\cdot\boldsymbol{\nu} - \mathbf{R}_T\cdot\boldsymbol{\nu} - Q_\Delta \tag{2.50}$$

Thus the total energy gains of the plasma are

$$Q_i + Q_e = -\mathbf{R}_\nu\cdot\boldsymbol{\nu} - \mathbf{R}_T\cdot\boldsymbol{\nu} \tag{2.51}$$

of which $-\mathbf{R}_T\cdot\boldsymbol{\nu}$ is reversible, since this term changes sign under time or temperature gradient reversals.

Viscous stress tensor $\boldsymbol{\pi}$

The last needed constitutive relation specifies $\boldsymbol{\pi}$ in terms of spatial derivatives of velocities $\mathbf{w}$ (e.g. $\mathbf{w} = \mathbf{u}_i$). The nature of $\boldsymbol{\pi}$ can be determined within linear approximations by considering the linear translational transformations of the velocity of neighboring fluid elements, i.e.

$$\mathbf{w}(\mathbf{r}+\mathbf{R},t) = \mathbf{w}(\mathbf{r},t) + \mathbf{R}\cdot\nabla\mathbf{w}(\mathbf{r},t) + \mathcal{O}(R^2) \tag{2.52}$$

where $\nabla\mathbf{w}(\mathbf{r},t)$ is the velocity gradient tensor with components $\partial w_\alpha/\partial x_\beta$. Restriction to first order derivatives of $\mathbf{w}$ describes a "Newtonian fluid" in fluid mechanics (e.g., Mihalas and Mihalas 1984, §3.1). From the properties of second order tensors $\nabla\mathbf{w}(\mathbf{r},t)$ can be decomposed into a sum of three "orthogonal" tensors (see Appendix A), the "deviator" $\overset{\circ}{\nabla}\mathbf{w}$, the cross product of the "vector" $\nabla w^\vee$ with the unit tensor $\mathbb{1}$, and the scalar product of the "trace" $\overset{\times}{\nabla} w$ with $\mathbb{1}$:

$$\nabla\mathbf{w} = \overset{\circ}{\nabla}\mathbf{w} - \nabla w^\vee \times \mathbb{1} + \frac{1}{3}\overset{\times}{\nabla} w\, \mathbb{1}. \tag{2.53}$$

Then

$$\mathbf{w}(\mathbf{r}+\mathbf{R},t) = \mathbf{w}(\mathbf{r},t) + \boldsymbol{\Omega}\times\mathbf{R} + \frac{1}{3}\mathbf{R}\,\mathrm{div}\,\mathbf{w} + \mathbf{R}\cdot\overset{\circ}{\nabla}\mathbf{w} + \mathcal{O}(R^2), \tag{2.54}$$

where $\boldsymbol{\Omega}$ is the fluid element's angular velocity. The only term antisymmetric in $\mathbf{w}$ in equation (2.54), containing $\boldsymbol{\Omega}$, describes rotation of a fluid element with no deformation, it can be removed from equation (2.54) by moving to the locally rotating frame, and thus plays no role in viscous processes. The fluid is deformed only by the deviator $\overset{\circ}{\nabla}\mathbf{w}$ in equation (2.54). The $\operatorname{div}\mathbf{w}$ "dilation" or "bulk" component of $\nabla\mathbf{w}$ describes just the changing volume of the fluid element, with no change in shape. The deviator $\overset{\circ}{\nabla}\mathbf{w}$ is traceless and symmetric, as required for $\boldsymbol{\pi}$ (equation 2.13). Aside from the solid rotation and dilation terms, the deviator thus contains the only combinations of derivatives of $\mathbf{w}$ that are allowed by fluid motion, and therefore $\boldsymbol{\pi}$ must be written in terms of the deviator, at least in the present linear approximation. Defining the "rate-of-strain" tensor $\mathbb{W}$ as

$$\mathbb{W} = 2\,\overset{\circ}{\nabla}\mathbf{w} \quad \text{so that} \tag{2.55}$$

$$W_{\alpha\beta} = \frac{\partial w_\alpha}{\partial x_\beta} + \frac{\partial w_\beta}{\partial x_\alpha} - \frac{2}{3}\operatorname{div}\mathbf{w}\,\delta_{\alpha\beta}, \tag{2.56}$$

the relationship between $\boldsymbol{\pi}$ and $\mathbb{W}$ for an isotropic (i.e. field-free) plasma is then

$$\pi_{\alpha\beta} = -\eta_0 W_{\alpha\beta} \tag{2.57}$$

where η_0 refers to the field-free limit. With $\Delta \approx v\tau$, $\eta_0 \approx nk_BT\tau$. This case applies also to the field-aligned case with compression along the field lines: $\partial w_\parallel/\partial x_\parallel \neq 0$, because the parallel momentum is freely transported along $\mathbf{B}$. As stressed by Hollweg (1986,1990), if a field-aligned gradient in $\mathbf{w}$ exists in the corona, this leads to large viscosities and surprisingly small Reynolds numbers (Table 1.2).

```
must add:
1950: Pikelner. Izv. Krymsk. Ap. Obs. 3, 51.  Reynolds number is 200
in coronal "fans" (= streamers, helmets today), VERY SMALL =>
turbulence unlikely.
```

A valid approximation for a perfect gas is to set the dilatation component of $\boldsymbol{\pi}$ to zero, even when $\operatorname{div}\mathbf{w} \neq 0$. It can be important for imperfect gases, such as those undergoing ionization or recombination. This component arises from physical processes different from those outlined above, so we must modify equation (2.57) for field-free plasmas, to read

$$\pi_{\alpha\beta} = -\eta_0 W_{\alpha\beta} - \zeta_0 \operatorname{div}\mathbf{w}\;\delta_{\alpha\beta}. \tag{2.58}$$

The coefficient of "bulk viscosity", ζ_0, is zero for "Maxwellian fluids". This is assumed henceforth.

Viscosity in a magnetized plasma ($\omega\tau \gg 1$) is complicated because it depends on the orientations of two vectors, $\mathbf{w}$ and $\mathbf{B}$, and a tensor whose components depend on $\partial w_\alpha/\partial x_\beta$. Braginskii showed that $\boldsymbol{\pi}$ can be nevertheless still be written generally as linear combinations of $\mathbb{W}$. A symmetric second order tensor with zero trace, such as $\boldsymbol{\pi}$, has five independent components, thus there are just five constants of proportionality $\eta_0, \ldots \eta_4$ for the linear combinations of $\mathbb{W}$ forming $\boldsymbol{\pi}$. The reader should refer to Braginskii's paper for explicit formulae, here we review some examples.

Consider cases where $\mathbf{B} = (0, 0, B_z)^T$, and the specific case where the only non-zero spatial derivative is $\partial w_z/\partial x$. The z-momentum is transported across the field lines in the x direction such that

$$\pi_{zx} \approx -\eta_\perp \frac{\partial w_z}{\partial x}, \quad F_z \approx \frac{\partial}{\partial x}\eta_\perp \frac{\partial w_z}{\partial x}, \tag{2.59}$$

as before, where $F_z(x)$ is the viscous stress, but now

$$\eta_\perp \approx \frac{\eta_0}{\omega^2\tau^2}, \tag{2.60}$$

which is an enormous reduction in viscosity when $\omega\tau \gg 1$. Two of Braginskii's four remaining coefficients, η_1 and η_2 are $\mathcal{O}(\eta_\perp)$.

Another case where $\eta \approx \eta_\perp$ obviously applies is the viscous transport of momentum perpendicular to $\mathbf{B}$, for example when $\partial w_y/\partial x \neq 0$, replacing w_z with w_y in equation (2.59). A slightly different case involves the suppression of viscous energy dissipation by $\mathbf{B}$ even when perpendicular momentum is transported along $\mathbf{B}$. When $\partial w_x/\partial z \neq 0$, for example, $\pi_{xz} \approx \eta_\perp \partial w_x/\partial z$ since the symmetry of $\mathbb{W}$ renders it identical to the case discussed above ($\partial w_z/\partial x \neq 0$). Here $\eta_\perp$ is again the relevant viscosity parameter because the gyrating particles "lose memory" of transverse ordered velocity in a time ω^{-1}, during which time they are displaced only by $\approx r_a$.

The two remaining viscosity coefficients, η_3, η_4 are $\mathcal{O}(\eta_0/(\omega\tau))$. They will not concern us because they are non-dissipative, the stresses being perpendicular to the velocities.

Contributions to viscous stresses $\boldsymbol{\pi}$ *from gyro-relaxation*

For flows with $\operatorname{div}\mathbf{w} \neq 0$, a process leading to additional terms in $\boldsymbol{\pi}$ arises from a quite different physical effect. Consider again $\mathbf{B} = (0, 0, B_z)^T$, but now, for example, $\operatorname{div}\mathbf{w} = \partial w_x/\partial x \neq 0$. The magnetic field lines are compressed, because $-\dot{n}/n = \dot{B}/B = \partial w_x/\partial x$, from equation (2.6). As B increases with time, particle energies perpendicular to the field increase at the expense of those parallel to the field, to conserve the first adiabatic constant (the magnetic moment, $mv_\perp^2/(2B)$ during the period τ before a typical collision occurs. The additional transverse energy makes the transverse pressure exceed the longitudinal pressure by a fraction of order $\tau\dot{B}/B = -\tau\dot{n}/n$, leading to stresses

$$\pi_{xx} = \pi_{yy} \sim -p\tau\frac{\dot{n}}{n} \sim -\eta_0\frac{\partial w_x}{\partial x}, \quad \text{and} \quad \pi_{zz} = \eta_0\frac{\partial w_x}{\partial x}. \tag{2.61}$$

The collisional equipartition of energy between transverse and parallel particle energies is an irreversible process, and so this is a heating mechanism and not just a process for redistributing energy within the plasma. Thus, when $\operatorname{div}\mathbf{w} \neq 0$, the viscosity coefficient is of the same order as that of a field-free plasma. As noted by Hollweg (1986), these effects may be important for dissipating energy in the corona, but have rarely been discussed.

Braginskii also indicates how plasma turbulence can greatly influence transport coefficients in magnetized plasmas (see section 4.1).

2.1.3 Braginskii's closure

Braginskii (1965) presented the first consistent set of calculations for transport coefficients in simple plasmas (consisting of just ions of mass m_i, charge $+Z_ie$, and and electrons of mass m_e and charge $-e$), under conditions where collisions are sufficiently rapid to ensure that departures of particle distribution ¡functions from Maxwellians are small. His work is applicable for arbitrary magnetic field strengths in the non-relativistic limit. Kulsrud (2005) reviews Braginskii's work in the limit $\omega\tau \gg 1$. The essential elements of this work are as follows.

- The calculations are based on the "Chapman-Enskog" perturbative method to obtain solutions to the Boltzmann equations (e.g., Chapman and Cowling 1970). The distribution functions are expanded as a series expansion, $f = f^{(0)} + f^{(1)} + f^{(2)} + \ldots$. Collision integrals are evaluated analytically using an expansion in terms of an infinite series of Laguerre polynomials, which are truncated. Their accuracy is evaluated by examining the magnitude of higher order terms.

- Advantage is taken of the smallness of m_e/m_p, to approximate certain collision integrals and order the perturbative terms. The electron Boltzmann equation is re-written using $m_e/m_p \ll 1$ to permit the derivation of separate solutions for ions and electrons, when $T_i \neq T_e$ and $\mathbf{u}_e \neq \mathbf{u}_i$.
- Collisions are written in "Landau form" (Landau 1937).
- Distribution functions and quantities derived from them are determined keeping systematic track of the magnitude of specific terms in the ion and electron Boltzmann equations $f^{(0)} \gg f^{(1)} \gg f^{(2)}$, $m_e/m_p \ll 1$.

The resulting solutions to the Boltzmann equations are linear in the perturbing macroscopic quantities, ∇T, $\mathbf{u}$, and $\mathbb{W}$.

2.1.4 Coronal heating and energy vs. entropy increases

The LHS of the internal energy equation (2.18) for species a of the plasma describes the evolution of the internal energy in response to "pdV" work done ($p_a \mathrm{div}\, \mathbf{u}_a$). The RHS contains gains and losses of energy via collisional processes of conduction, and the conversion of ordered kinetic energy via viscous and frictional forces. While on might choose to define coronal heating as those processes which increase the internal energy, a more precise definition is to define it in terms of the increase of entropy. The difference is significant in that then just the irreversible (i.e. dissipative) heating processes are isolated, separate from those process which involve reversible heat transfer. Reversibility is usually determined by examining the behavior of terms under reversal of the time coordinate, but some terms in equation (2.18) do not contain explicit time dependence. In such cases a different approach is needed (e.g. section 11.3 of Woods 1987).

2.1.5 Validity

At the heart of the formalism is the assumption that both the electrons and ions relax rapidly. Boltzmann's "H-theorem" states that, if f_a changes only because of collisions, it must relax to a Maxwellian distribution. Relaxation occurs on a time scale $\approx \tau_a$. All spatial averages in the plasma must change slowly in time and space to ensure that the computed "fluxes" $\mathbf{q}$, $\boldsymbol{\pi}$, $\mathbf{R}$ and Q are determined accurately. Thus, all macroscopic quantities ϕ must satisfy

$$\frac{d\ln\phi}{dt} \ll \tau_{>}^{-1}, \tag{2.62}$$

where $\tau_{>}$ is the larger of τ_{ee} and τ_{pp}, which is 2.2 seconds (Table 1.2). More stringently, for a *single fluid* treatment to be valid, $\tau_{>} = \tau_{ep}^{\varepsilon}$, which is of order 10^2 seconds in the corona.

To assess the validity of the approximations under spatial variations, account must be taken of the fact that the motions are highly anisotropic when $\omega\tau \gg 1$. Parallel to $\mathbf{B}$, particle mean free paths of ≈ 0.1 Mm under standard conditions (Table 1.2) are a factor 500 smaller than scales such as the pressure scale height, so these approximations have some justification. However, being of order 0.1Mm , and increasing with $T^{3/2}/n$ (equation 2.26), one must take care when discussing diffusion regions in magnetic reconnection, and/or shocks, for example. Perpendicular to $\mathbf{B}$, under many conditions the formalism is valid if the transverse scales exceed the gyro radii. However, under some configurations the conditions for validity are changed (see Braginskii).

Formal use of Landau's collisional term requires $\lambda_D \ll r_e$ (and also r_p). Physically this inequality means that the magnetic field has little net effect on collisions. From Table 1.2, $\lambda_D = r_e/7$, showing the formalism to be questionable. Braginskii states that the transport coefficients are generally accurate to a factor of $\ln\Lambda$ which is ≈ 20 outside of this approximation, on the basis that the importance of collisions with impact parameters smaller than r_e can be at most $1/\ln\Lambda$ of collisions with large impact parameters.

The accuracy of some of the transport coefficients has been called into question, but that in no case are the coefficients in error by more than a factor of 2.8, and they are usually better than 25% or less, consistent with Braginskii's original claims (Epperlein 1984, Woods 1987). Lastly, the presence of instabilities leading to turbulence can greatly influence these coefficients (section 4.1).

2.2 The electromagnetic fields

Maxwell's equations are

$$\begin{aligned} \operatorname{div}\mathbf{B} &= 0 && (2.63)\\ \operatorname{div}\mathbf{E} &= \mathcal{Q}/\epsilon_0 && (2.64)\\ \mathbf{curl}\,\mathbf{H} &= \mathbf{j} + \frac{\partial \mathbf{D}}{\partial t} && (2.65)\\ \mathbf{curl}\,\mathbf{E} &= -\frac{\partial \mathbf{B}}{\partial t} && (2.66) \end{aligned}$$

where $\mathbf{D} = \epsilon_0\mathbf{E}$ and $\mathbf{B} = \mu_0\mathbf{H}$. ϵ_0 and μ_0 are the permittivity and permeability of free space. The approximations $\epsilon \approx \epsilon_0$ and $\mu \approx \mu_0$ are valid in plasmas (Ginzburg 1970, Woods 1987).

MHD is fundamentally a relativistic theory, in the sense that the transformation of the field and fluid quantities from a laboratory frame to the frame moving with the fluid at velocity $\mathbf{u} \approx \mathbf{u}_i$ must be treated at least to $\mathcal{O}(v/c)$. Denoting quantities evaluated in the frame comoving with the fluid with a prime, with the speed of light $c = 1/\sqrt{\mu_0\epsilon_0}$, the relationships between the field and fluid quantities in the two frames are, to lowest order,

$$\mathbf{E}' \approx \mathbf{E} + \mathbf{u}\times\mathbf{B} \quad ; \quad \mathbf{B}' \approx \mathbf{B} - \frac{\mathbf{u}\times\mathbf{E}}{c^2} \tag{2.67}$$

$$\mathcal{Q}' \approx \mathcal{Q} - \frac{\mathbf{u}\cdot\mathbf{j}}{c^2} \quad ; \quad \mathbf{j}' \approx \mathbf{j} - \mathcal{Q}\mathbf{u} \tag{2.68}$$

To estimate the magnitude of the $\mathbf{u}\times\mathbf{E}$ term we can use an approximate form of Ohm's law, in which the conductivity tensor is replaced with the scalar conductivity σ which applies to isotropic media. Formally this is incorrect in the presence of magnetic fields, but even in this case it is only in error by a factor of two (see equation 2.33). Then, in the moving frame,

$$\mathbf{j}' \approx \sigma\mathbf{E}' \approx \sigma\left(\mathbf{E} + \mathbf{u}\times\mathbf{B}\right) \tag{2.69}$$

Because of the large magnitude of σ (equation 2.33 and Table 1.2), $E' \approx 0$, i.e. the electric field in the moving frame is ≈ 0, thus

$$\mathbf{E} + \mathbf{u}\times\mathbf{B} \approx 0, \tag{2.70}$$

and so $\mathbf{B}' \approx \mathbf{B} + \mu_0\epsilon_0\mathbf{u}\times(\mathbf{u}\times\mathbf{B})$, so that $B' \approx B + \frac{u^2}{c^2}B$. To estimate the transformation $\mathbf{j} \to \mathbf{j}'$ to order u/c, we have $\mathcal{Q} \approx \epsilon_0 \operatorname{div}\mathbf{E} \approx \epsilon_0\operatorname{div}(\mathbf{u}\times\mathbf{B}) \sim \frac{v}{c^2}\frac{H}{\ell}$ for lengthscale ℓ. Thus $\mathcal{Q}v \sim \frac{u^2}{c^2}|\mathbf{curl}\,\mathbf{H}|$ which is $\ll j$. The charge separation is small, since $\mathcal{Q}/ne \sim \frac{u}{c^2}\frac{H}{\ell ne} \sim \frac{u}{c}\frac{u_{\rm drift}}{c}$ which is $\ll 1$. To $\mathcal{O}(u/c)$, then:

$$\begin{aligned} \mathbf{E}' &\approx \mathbf{E} + \mathbf{u}\times\mathbf{B}; \quad \mathbf{B}' \approx \mathbf{B} && (2.71)\\ \mathbf{j}' &\approx \mathbf{j}, && (2.72) \end{aligned}$$

so that we may speak of the magnetic field and electric current density without specifying the reference frame.

The displacement current, $\frac{\partial \mathbf{D}}{\partial t}$, is neglected in MHD. On time-scale t and length scale ℓ, $\frac{\partial \mathbf{D}}{\partial t} \sim \epsilon_0 E/t$, whereas $|\mathbf{curl}\, H| \sim H/\ell$, thus

$$|\frac{\partial \mathbf{D}}{\partial t}|/|\mathbf{curl}\,\mathbf{H}| \sim \epsilon_0 E\ell/tH \sim \mu_0\epsilon_0 E\ell/tB$$

But $E \sim uB$, so that this ratio is $\sim \frac{u(\ell/t)}{c^2}$. Thus, on timescales $t \gg \ell/c$ and length scales ℓ, the displacement current can be neglected. Another way of looking at this approximation is to imagine that $c \to \infty$, so that the electromagnetic state of the system is effectively set instantaneously.

An approximate equation describing the evolution of the magnetic field can be derived using the scalar form of Ohm's law and the transformation equations:

$$\mathbf{curl}\,\mathbf{H} = \sigma\left(\mathbf{E} + \mathbf{u} \times \mathbf{B}\right). \tag{2.73}$$

Assuming that σ is constant,

$$\mathbf{curl}\,\mathbf{curl}\,\mathbf{B} = -\mu_0\sigma\frac{\partial \mathbf{B}}{\partial t} + \mu_0\sigma\mathbf{curl}\ (\mathbf{u} \times \mathbf{B}) \tag{2.74}$$

which can be re-arranged, on expansion of the first term using $\mathbf{curl}\,\mathbf{curl}\,\mathbf{x} = \mathbf{grad}\,\mathrm{div}\,\mathbf{x} - \nabla^2\mathbf{x}$, to give the "induction equation":

$$\frac{\partial \mathbf{B}}{\partial t} = \mathbf{curl}\,(\mathbf{u} \times \mathbf{B}) + \eta\nabla^2\mathbf{B}, \quad \eta = 1/\mu_0\sigma. \tag{2.75}$$

This equation describes the evolution of the magnetic field in terms of the flow of plasma across the fields lines and a diffusion term.

The electromagnetic forces on a unit volume of fluid are

$$\mathbf{F} = \mathcal{Q}\mathbf{E} + \mathbf{j} \times \mathbf{B} = \epsilon_0\mathbf{E}\mathrm{div}\,\mathbf{E} + \frac{1}{\mu_0}\mathbf{curl}\,\mathbf{B} \times \mathbf{B} \tag{2.76}$$

Using Maxwell's equations (2.63) and (2.66), we can make equation (2.76) symmetric in $\mathbf{E}$ and $\mathbf{B}$:

$$\mathbf{F} = \epsilon_0\mathbf{E}\,\mathrm{div}\,\mathbf{E} + \frac{1}{\mu_0}\mathbf{B}\,\mathrm{div}\,\mathbf{B} + \frac{1}{\mu_0}(\mathbf{curl}\,\mathbf{B}) \times \mathbf{B} + \epsilon_0(\mathbf{curl}\,\mathbf{E}) \times \mathbf{E} \tag{2.77}$$

$$+\frac{\partial}{\partial t}\left(\mathbf{B} \times \epsilon_0\mathbf{E}\right) - \mathbf{B} \times \frac{\partial \epsilon_0\mathbf{E}}{\partial t} \tag{2.78}$$

The last term (proportional to the displacement current) is $\mathcal{O}(\frac{u^2}{c^2})$ and is negligible. With equation (2.70), the penultimate term is of order uUB^2/c^2 (with $\frac{\partial}{\partial t} \approx U\,grad$), and is also negligible. The remaining terms are symmetric in $\mathbf{E}$ and $\mathbf{B}$. The i^{th} components of $\mathbf{F}$ dependent on $\mathbf{B}$ are, using tensor notation and the summation convention,

$$\frac{1}{\mu_0}B_i\frac{\partial B_k}{\partial x_k} + \frac{1}{\mu_0}\left(\frac{\partial B_i}{\partial x_k} - \frac{\partial B_k}{\partial x_i}\right)B_k = \frac{1}{\mu_0}\frac{\partial}{\partial x_k}\left(B_iB_k - \frac{1}{2}\delta_{ik}B^2\right), \tag{2.79}$$

where δ_{ik} is Kronecker's delta. The tensor inside the braces is the magnetic component of the electromagnetic stress tensor, having units of energy density. In the limit of small u/c, the energy density of the fields is dominated by the magnetic field, since the equivalent stress tensor for $\mathbf{E}$ is smaller by u^2/c^2. Thus, the i^{th} component of the electromagnetic force reduces to

$$F_i \approx \frac{\partial}{\partial x_k} T_{ik}, \quad T_{ik} = \frac{1}{\mu_0}\left(B_i B_k - \frac{1}{2}\delta_{ik} B^2\right) \tag{2.80}$$

To see the meaning of the stress tensor, if we align the Cartesian axis x_3 locally along $\mathbf{B}$, then

$$\mathbb{T} = \frac{B^2}{2\mu_0}\begin{pmatrix} -1 & 0 & 0 \\ 0 & -1 & 0 \\ 0 & 0 & +1 \end{pmatrix}, \tag{2.81}$$

so that the force $\mathbf{F}$ reduces to the negative gradient of an isotropic pressure $B^2/2\mu_0$ and a tension force which is the gradient of B^2/μ_0 along the magnetic field direction. The electromagnetic fields carry momentum with a density $\epsilon_0 \mathbf{E} \times \mathbf{B}$ which is of order $\epsilon_0 u B^2$. The ratio of this to ρu is c_A^2/c^2, which is, by assumption, $\ll 1$ in MHD, and is the case in most solar applications (c_A is the Alfvén speed, section 2.5.4).

When $u^2/c^2 \ll 1$ the electro-magnetic energy density is dominated by the magnetic component ϵ_M,

$$\epsilon_M = \frac{B^2}{2\mu_0}, \tag{2.82}$$

so that

$$\frac{\partial \epsilon_M}{\partial t} = \frac{1}{\mu_0}\mathbf{B} \cdot \frac{\partial \mathbf{B}}{\partial t} = -\mathbf{H} \cdot \mathbf{curl}\, \mathbf{E} \tag{2.83}$$

Using div $(\mathbf{E} \times \mathbf{H}) = \mathbf{H} \cdot \mathbf{curl}\, \mathbf{E} - \mathbf{E} \cdot \mathbf{curl}\, \mathbf{H}$, and with $\mathbf{curl}\, \mathbf{H} = \mathbf{j}$,

$$\frac{\partial \epsilon_M}{\partial t} + \text{div}\ (\mathbf{E} \times \mathbf{H}) \quad = \quad -\mathbf{E} \cdot \mathbf{j} \tag{2.84}$$

Since $\mathbf{E} \times \mathbf{H}$ is the Poynting flux density, the LHS of this equation is of the form (rate of change of energy density) plus (divergence of energy flux density). The equation is thus the conservative form of the electro-magnetic energy equation, and we can identify the RHS with sources and sinks. Using the approximate scalar form of Ohm's law (equation 2.69), we have

$$\frac{\partial}{\partial t}\frac{B^2}{2\mu_0} + \text{div}\ (\mathbf{E} \times \mathbf{H}) = -\mathbf{j} \cdot \mathbf{E}' - \mathbf{u} \cdot (\mathbf{j} \times \mathbf{B}) = -j^2/\sigma - \mathbf{u} \cdot (\mathbf{j} \times \mathbf{B})\,. \tag{2.85}$$

The first term on the RHS is Ohmic dissipation, and the last term represents the work done on the fluid by the Lorentz force. T!hus, with a scalar conductivity, Ohmic (also called Joule) heating proceeds at the rate:

$$Q_J = j^2/\sigma \quad \text{W m}^{-3} \tag{2.86}$$

More detailed forms of Ohm's law are discussed below, derived from the equations of motion of the plasma components (electrons, ions, even neutrals).

2.3 MHD equations: fully ionized plasma

Having highlighted a kinetic approach from which fluid equations for individual species of coronal plasma can be derived, we now piece together the results to determine equations of conservation of mass, momentum and energy for the fluid, as well as forms for "Ohm's law", which are derived from the momentum equations. We saw in section 2.1.1 (relation 2.22) that Maxwellian distributions are established *within* the electron and proton gases before they are established *between* them. There is therefore a hierarchy of formulations for multi-species plasmas, depending on the magnitude of the collisional coupling within and between the particle species relative to other terms in the momentum equations:

– When all collision times are long the fluid approximation fails and kinetic treatment is needed.

– When collision times between species (e.g., ions and neutrals) are larger, but self-collision times smaller, multi-fluid MHD-like equations can be used for each species, each with its own velocity and temperature.

– When all collision times are short, a single-fluid treatment is valid with appropriate modifications to include the effects of momentum and heat transfer between the different species. All particle distribution functions are close to Maxwellians with a common temperature T.

We assume the latter to be the case. The five conservation equations (2.6), (2.11) and (2.15), can be summed to obtain "single fluid" equations. First consider a purely hydrogen plasma which is completely ionized.

2.3.1 Particle conservation

The particle, mass densities and mean velocity are given by

$$n = n_e + n_p, \quad \rho_e = n_e m_e, \quad \rho_p = n_p m_p, \quad \rho = \rho_e + \rho_p, \quad \mathbf{u} = \frac{\rho_e \mathbf{u}_e + \rho_p \mathbf{u}_p}{\rho}. \tag{2.87}$$

The summed continuity equation is

$$\frac{\partial \rho}{\partial t} + \mathrm{div}\,(\rho \mathbf{u}) = 0 \tag{2.88}$$

With suitable definitions of ρ etc., this equation also applies for mixtures of particle species in general.

2.3.2 Momentum conservation

The momentum equations for the electrons and protons are given by equation (2.11). With $p = p_e + p_p = (n_e + n_p) k_B T$, $\mathbf{j} = -e(n_e \mathbf{u}_e - n_p \mathbf{u}_p)$, and using equation (2.5), the total momentum equation is

$$\rho_e \frac{\mathrm{d}\mathbf{u}_\mathrm{e}}{\mathrm{d}t_e} + \rho_p \frac{\mathrm{d}\mathbf{u}_\mathrm{p}}{\mathrm{d}t_p} = -\mathbf{grad}\, p - \nabla \cdot (\boldsymbol{\pi}_e + \boldsymbol{\pi}_p) + \rho \mathbf{g} + \mathbf{j} \times \mathbf{B} + e(n_p - n_e)\mathbf{E}, \tag{2.89}$$

obtained by summing the two equations. Terms in $\mathbf{R}$ sum to zero because of Newton's third law. In section 2.2 we noted that the charge density $\mathcal{Q}/en_e = e(n_p - n_e)/en_e$ is $\mathcal{O}(\frac{u^2}{c^2}) \ll 1$, thus

$$n_e \approx n_p \approx n, \quad \mathbf{j} \approx en(\mathbf{u}_p - \mathbf{u}_e), \quad \text{and} \quad |e(n_p - n_e)\mathbf{E}| \ll |\mathbf{j} \times \mathbf{B}|, \tag{2.90}$$

to a high degree of approximation. Like Maxwell's equation for $\mathbf{curl}\,\mathbf{H}$, in which the displacement current can be ignored for slowly varying phenomena (when $c_A \ll c$), there are disparate time-scales in the above equation which permit the dropping of additional terms under certain conditions. In equation (2.89), If one is interested primarily in "slow" phenomena, one can ignore the electron inertial term. The reason is that any imbalance in the slower, remaining terms in the equation is rapidly adjusted by the electron inertial term, on a short time scale $t \sim \ell/c_e \approx \ell/43c_S$, where c_e is the electron sound speed. Then, as far as the rest of the equation is concerned, this term can be assumed to be zero over the longer time scales of interest[2]. This is called "quasi-static" evolution. Neglecting then the electron inertial term, and when $T_e = T_p = T$ (so that electron viscosity is small compared with ion viscosity), with $\rho \approx \rho_p$, $\mathbf{u} \approx \mathbf{u}_p$, equation (2.89) becomes

$$\rho \frac{\mathrm{d}\mathbf{u}}{\mathrm{dt}} \approx -\mathbf{grad}\,(2nk_BT) - \mathrm{div}\,\boldsymbol{\pi}_p + \rho\mathbf{g} + \mathbf{j} \times \mathbf{B}. \tag{2.91}$$

Neglecting viscosity, this equation is a starting point for many MHD studies. For phenomena slow compared with ℓ/c_S, the LHS (the proton inertial term) can be ignored and the equation describes magnetostatic equilibrium. For low-β plasmas such as the corona, MHD waves transmit magnetic stresses faster than acoustic-gravity waves, then a reasonable approximation for force balance is to ignore the pressure gradient and gravitational terms in equation (2.91) which leads to the "force free" approximation,

$$\mathbf{j} \times \mathbf{B} \approx 0 \tag{2.92}$$

Note that this equilibrium is non-linear. A special (linear) case of equation (2.92) is the potential field case, $\mathbf{j} = 0$, where $\nabla^2\mathbf{B} = 0$. Force free equilibria do not explicitly involve plasma properties since they apply in the limit $\rho \to 0$. Instead they are determined by appropriate boundary conditions. The validity of the force-free approximations can be checked after a calculation using estimates of plasma properties in equation (2.91).

These considerations of the nature of terms in equation (2.91) describe mathematically some of the difficulties with understanding the corona described physically in section 1.6. We have yet to discuss the energy equation, which is arguably an even more tricky proposition than equation (2.91).

2.3.3 Ohm's law

Momentum conservation in a plasma in which collisions are important takes on additional meaning in terms of a linear relation between current densities and electric fields- none other that Ohm's law. (equation 2.69). When changes in the plasma are slow compared with an electron-ion collisional time, the electron inertia can be neglected in the electron momentum equation (2.11) and the electric field force is balanced by friction, producing a linear relation. Its importance lies in the fact that the thermalization of electromagnetic energy – believed to lie at the heart of the coronal heating problem – occurs at the rate $\mathbf{j} \cdot \mathbf{E}'$ (equation 2.85).

Various forms of Ohm's law can be derived from different forms of the momentum equations for the electrons and ions, depending on what is retained in the equations and whether one works in the laboratory frame or co-moving (fluid) reference frame (equation 2.71). By subtracting the electron equation of motion from that of the protons, ignoring electron inertia, and substituting for the proton inertial term from the proton equation of motion (equation 2.11),

$$\mathbf{grad}\,p_e + en\,\{\mathbf{E} + \mathbf{u} \times \mathbf{B}\} - \mathbf{j} \times \mathbf{B} - \mathbf{R}_\nu - \mathbf{R}_T = 0. \tag{2.93}$$

[2]Rarely can one set a dominant term to zero in an equation! But for linear differential equations of conservative form this approximation can be formally justified, for example, using an eigenfunction expansion (e.g., Wilkinson 1965).

Collecting terms in $\mathbf{j}$ on the RHS of equation (2.93), and using equation (2.32),

$$\mathbf{E}^{\dagger} \equiv \mathbf{E} + \mathbf{u} \times \mathbf{B} + \frac{\mathbf{grad}\, p_e - \mathbf{R}_T}{ne} = \frac{1}{\sigma_{\parallel}}\mathbf{j}_{\parallel} + \frac{1}{\sigma_{\perp}}\mathbf{j}_{\perp} + \frac{1}{ne}\mathbf{j} \times \mathbf{B} \tag{2.94}$$

The term in $\mathbf{j} \times \mathbf{B} = B\mathbf{j}_{\wedge}$ is called the "Hall" electric field, caused by the relative flow between the electron and fluid velocities arising because of quasi-neutrality. Defining $\sigma_{\wedge}$ through

$$\frac{1}{\sigma_{\wedge}} = \frac{B}{ne} = \frac{\omega_e \tau_e}{\sigma_{\perp}},$$

equation (2.94) becomes

$$\mathbf{E}^{\dagger} = \underbrace{\frac{1}{\sigma_{\parallel}}\mathbf{j}_{\parallel}}_{\mathbf{E}^{\dagger}_{\parallel}} + \underbrace{\frac{1}{\sigma_{\perp}}\mathbf{j}_{\perp} + \frac{1}{\sigma_{\wedge}}\mathbf{j}_{\wedge}}_{\mathbf{E}^{\dagger}_{\perp}}. \tag{2.95}$$

The "effective electric field" $\mathbf{E}^{\dagger}$ contains $\mathbf{u}\times\mathbf{B}$, and the "pressure gradient" and "thermoelectric" forces $\mathbf{grad}\, p_e/ne$ and $-\mathbf{R}_T/ne$ respectively. The latter two forces can usefully be thought of as additional electric fields per electron charge, driving current densities and leading to frictional dissipation in the same form as the real electric fields do (Cowling 1956). Under suitable conditions these forces can also generate currents and hence generate accompanying magnetic fields. These terms will be ignored for the corona here, assuming pressure and temperature gradients are small, then $\mathbf{E}^{\dagger} \approx \mathbf{E}'$. But care must be taken in the chromosphere (section 3.3).

Ohmic heating proceeds at the rate $\mathbf{j} \cdot \mathbf{E}'$ where $\mathbf{E}' = \mathbf{E} + \mathbf{u} \times \mathbf{B}$ (see equation 2.84). When $\mathbf{E}'$ is written in terms of $\mathbf{j}$ as above, then the Ohmic dissipation rate is just

$$\mathbf{j} \cdot \mathbf{E}' == \frac{1}{\sigma_{\parallel}} j_{\parallel}^2 + \frac{1}{\sigma_{\perp}} j_{\perp}^2. \tag{2.96}$$

The dissipation is almost isotropic for cases where $j_{\perp} \approx j_{\parallel}$ (see equation 2.33). The question of the relative sizes of $j_{\parallel}$ and $j_{\perp}$ depends on the nature of the predominant terms in the electron momentum equation. In the solar corona, force balance is expected to be close to force-free equilibrium, in which case $j_{\perp} \rightarrow 0$, otherwise (for instance, in magnetostatic equilibrium) $j_{\perp} \neq 0$.

Comments on Ohm's law

Working through the literature on Ohm's law can be confusing. Some authors do not use Braginskii's explicit and convenient split into components parallel and perpendicular to $\mathbf{h}$, which allows tensor analysis to take advantage of the algebra of rotational symmetry about $\mathbf{h}$. The "Hall" field is sometimes carried to the LHS of Ohm's law on the basis that it is non-dissipative, or can be shown to be small (as in very slow phenomena).

Also potentially confusing is use of the "inverse" of equation (2.95), where $\mathbf{j}$ is written in terms of $\mathbf{E}'$. The solution is (see, for example, Appendix A)

$$\mathbf{j} = \underbrace{\sigma_0 \mathbf{E}'_{\parallel}}_{\mathbf{j}_{\parallel}} + \underbrace{\sigma_1 \mathbf{E}'_{\perp} + \sigma_2 \mathbf{E}'_{\wedge}}_{\mathbf{j}_{\perp}}, \tag{2.97}$$

where again the components of the $\mathbf{E}'$ vectors are defined with respect to $\mathbf{h}$. The crucial point to realize is that, starting from this equation, the conductivities are different from those based upon equation (2.95). These new conductivities are

$$\sigma_0 = \sigma_{\parallel} \ ; \ \sigma_1 = \frac{\sigma_{\perp}}{1 + \omega_e^2 \tau_e^2} \ ; \ \sigma_2 = -\omega_e \tau_e \sigma_1.$$

In terms of $\mathbf{E}'$, the Ohmic dissipation rate is simply

$$\mathbf{j}\cdot\mathbf{E}' = \sigma_0 E'^2_{\parallel} + \sigma_1 E'^2_{\perp}. \tag{2.98}$$

In terms of $\mathbf{j}$, note that $\mathbf{j}_\perp$ is comprised of two perpendicular components proportional to $\mathbf{E}'_\perp$ and $\omega_e\tau_e\mathbf{E}'_\wedge$, where usually $\omega_e\tau_e \gg 1$. Then

$$j_\perp^2 = \sigma_1^2 {E'_\perp}^2 + \sigma_2^2 {E'_\wedge}^2 = (\sigma_1^2+\sigma_2^2){E'_\perp}^2, \tag{2.99}$$

and

$$\mathbf{j}\cdot\mathbf{E}' = \frac{1}{\sigma_0} j_\parallel^2 + \frac{\sigma_1}{\sigma_1^2+\sigma_2^2} j_\perp^2 = \frac{1}{\sigma_0} j_\parallel^2 + \frac{1}{\sigma_3} j_\perp^2 \tag{2.100}$$

This form was derived by Piddington (1956) and Cowling (1956). For the case of fully ionized plasmas, we have identically

$$\sigma_3 = \sigma_\perp, \quad \text{(fully ionized plasma)} \tag{2.101}$$

and the dissipation rates agree with equation (2.96), because the Hall and perpendicular conductivities are related. In this case the form using σ_0, σ_1, σ_2 and σ_3 is not needed and is potentially a source for confusion.

However, for a partially ionized hydrogen plasma including neutrals, σ_3 is indeed useful. In this context, there arises yet another confusing point when one tries to argue, in general terms, about how large cross-field current densities are, and their consequent energy dissipation rates. In metal conductors with no bulk motion the current flows because of an applied EMF. However, in a plasma, while this situation might also be set up in the laboratory, in astrophysical plasmas the force balance (including the "external" boundary conditions) determines $\mathbf{j}$ from which $\mathbf{E}$ follows from the conductivities in Ohm's law. Thus, while both equations (2.95) and (2.97) are formally correct, the former gives a more intuitive feeling for cause and effect, having $\mathbf{j} = \mathrm{curl}\mathbf{H}$ as a source term on the RHS of the equation.

2.3.4 Energy conservation

With $T_e = T_i = T$, neglecting again electron inertia, the sum of the energy equations for electrons and protons is

$$\begin{aligned}\frac{\partial}{\partial t}\left(\frac{\rho}{2}u^2 + \frac{3}{2}nk_BT\right) + \mathrm{div}\left\{\left(\frac{\rho}{2}u^2 + \frac{5}{2}nk_BT\right)\mathbf{u} + \boldsymbol{\pi}\cdot\mathbf{u} + \mathbf{q}\right\} \\ = n_e\mathbf{F}_e\cdot\mathbf{u}_e + n_p\mathbf{F}_p\cdot\mathbf{u}_p + \mathbf{E}\cdot\mathbf{j} + Q_G - Q_L\end{aligned} \tag{2.102}$$

Here we have added apparently *ad-hoc* terms, Q_G and Q_L, gain and loss terms lying outside of the approximations stated so far. For example, the corona can gain energy by, for example, wave-particle interations at frequencies higher than typical ion cyclotron frequencies. It loses energy via optically thin radiation arising through *inelastic* collisions of electrons with themselves and with ions, where Q_L has a contribution of the form

$$Q_L \approx n_e^2 P_{rad}(T_e). \tag{2.103}$$

2.4 MHD equations: partially ionized plasma

Although coronal plasma is highly ionized, with neutrals accounting for $\sim$1 in 10^6 particles, the coronal plasma originates from partially ionized plasma in the photosphere and chromosphere. The chromosphere is highly stratified, and its outermost regions are tenuous enough so that incomplete coupling between different particles can occur (e.g., Hansteen et al. 1997). The addition of neutral particles means that additional terms in equations for conservation of mass, momentum and energy are needed, as well as a neutral particle momentum equation. The reader can refer to section 7 of Braginskii (1965) for details, here we give a brief summary of the main differences with the ion-electron fluid picture discussed above, for a pure hydrogen plasma. Thermal, gravitational and viscous forces are neglected to reveal more clearly the new processes which arise.

Collisional coupling is weakest between neutral atoms and ionized particles, because ion-neutral and neutral-neutral collisions are characterized by short-range forces. Classical physics gives the cross section for such collisions as

$$\sigma_{ab} \approx \pi(r_a^2 + r_b^2) \tag{2.104}$$

where r_a and r_b are the classical radii of the particles. These cross sections are therefore a few times πa_0^2 where $a_0 = .53 \times 10^{-10}$ is the Bohr radius. The ion-ion cross sections are, in contrast, $ln\ \Lambda\, \pi b^2$ where

$$b = \frac{\mathcal{Q}^2}{4\pi\epsilon_0\varepsilon},$$

where $\mathcal{Q}$ is the charge on the ions, and ε the impact energy. Then

$$\begin{aligned} \sigma_{in}/\sigma_{ii} &\approx \frac{1}{ln\ \Lambda}\left(a_0 \frac{4\pi\epsilon_0\varepsilon}{\mathcal{Q}^2}\right)^2, && (2.105) \\ &\approx 10^{-4}\left(\frac{10}{ln\ \Lambda}\right)\left(\frac{1}{\mathcal{Q}^4}\right)\left(\frac{\varepsilon}{1\ \mathrm{eV}}\right)^2 && (2.106) \end{aligned}$$

In a simple plasma, the MHD formulation was in terms of $\mathbf{u}_i$ and $\mathbf{u}_e$, or some combination of these with the single fluid fluid velocity $\mathbf{u} \approx \mathbf{u}_i$ and the current density $\mathbf{j} = n_e e(\mathbf{u}_i - \mathbf{u}_e)$. Inclusion of neutrals means that the neutral velocity $\mathbf{u}_n$ or neutral-ion diffusion velocity $\mathbf{w} = \mathbf{u}_i - \mathbf{u}_n$ must be determined also.

Following the same procedure as for the simple plasma, for a pure hydrogen plasma, define

$$n = n_e = n_p, \quad \rho_e = n m_e, \quad \rho_p = n m_p, \quad \rho_n = n_n m_n, \quad \rho = \rho_e + \rho_p + \rho_n \approx \rho_p + \rho_n$$

$$\mathbf{u} = \frac{\rho_e \mathbf{u}_e + \rho_p \mathbf{u}_p + \rho_n \mathbf{u}_n}{\rho} \approx \frac{\rho_p \mathbf{u}_p + \rho_n \mathbf{u}_n}{\rho},$$

$$\mathbf{j} = -en(\mathbf{u}_e - \mathbf{u}_p), \quad \mathbf{w} = \mathbf{u}_p - \mathbf{u}_n, \text{ and}$$

$$f_n = \frac{n_n}{n_n + n}$$

where f_n is the neutral fraction, and the approximate forms ignore terms of order m_e/m_p. With these definitions, the continuity and momentum equations for the whole fluid are identical to those for the simple plasma. The main differences arise in Ohm's law and the energy equation. The frictional forces on species a are now

$$\mathbf{R}_a = \sum_b \mathbf{R}_{ab}, \quad \mathbf{R}_{ab} = -\alpha_{ab}(\mathbf{u}_a - \mathbf{u}_b), \quad \alpha_{ab} = \alpha_{ba} \tag{2.107}$$

Frictional coefficients α are of dimension (mass density / time), related to the integral of cross sections over Maxwellian speeds v, $\langle\sigma_{ab}v\rangle$, and the collision time τ_{ab}, by

$$\alpha_{ab} = n_a n_b m_{ab}\langle\sigma_{ab}v\rangle = m_{ab}n_a/\tau_{ab}, \tag{2.108}$$

Here, m_{ab} is the reduced mass. The equations of motion for electrons, protons and neutrals then include terms in $\mathbf{w}$ as well as $\mathbf{j}$, through the friction forces $\mathbf{R}_\nu$:

$$\begin{aligned}
-m_e n_e\frac{\mathrm{d}\mathbf{u}_\mathrm{e}}{\mathrm{d}\mathrm{t}_e} - \mathbf{grad}\, p_e - en\left\{\mathbf{E}+\mathbf{u}_e\times\mathbf{B}\right\} &= -\alpha_e\frac{\mathbf{j}}{en} + \alpha_{en}\mathbf{w}, &(2.109)\\
-m_p n_p\frac{\mathrm{d}\mathbf{u}_\mathrm{p}}{\mathrm{d}\mathrm{t}_p} - \mathbf{grad}\, p_p + en\left\{\mathbf{E}+\mathbf{u}_p\times\mathbf{B}\right\} &= \alpha_{ep}\frac{\mathbf{j}}{en} + \alpha_{pn}\mathbf{w}, &(2.110)\\
-m_n n_n\frac{\mathrm{d}\mathbf{u}_\mathrm{n}}{\mathrm{d}\mathrm{t}_n} - \mathbf{grad}\, p_n &= \alpha_{en}\frac{\mathbf{j}}{en_e} - \alpha_n\mathbf{w}, &(2.111)
\end{aligned}$$

where viscosity and thermal forces have been ignored. The sum of these is, as expected, the single fluid momentum equation (2.91):

$$-\rho\frac{\mathrm{d}\mathbf{u}}{\mathrm{d}\mathrm{t}} - \mathbf{grad}\, p - en\mathbf{E} + \mathbf{j}\times\mathbf{B} = 0 \tag{2.112}$$

Here, the presence of neutral atoms influences just ρ and the partial pressure due to neutrals, p_n. Collisional terms are absent because of Newton's third law.

The coeffients α have the properties

$$\alpha_e = \alpha_{ep} + \alpha_{en} = m_{ep}n/\tau_{ep} + m_{en}n/\tau_{en} = m_e n/\tau_e, \quad \tau_e^{-1} = \tau_{ep}^{-1} + \tau_{en}^{-1}$$

$$\alpha_n = \alpha_{en} + \alpha_{pn} = \frac{m_n}{2\tau_n}, \quad \tau_n^{-1} = \tau_{np}^{-1} + \tau_{ne}^{-1}$$

Now collisions with neutrals are dominated by those with ions, because momentum transfer is inefficient between particles of very different mass. Thus

$$\tau_{en} \gg \tau_{pn}, \quad \alpha_{en} \ll \alpha_{pn}, \text{and} \quad \epsilon = \alpha_{en}/\alpha_n \ll 1.$$

Solving for $\mathbf{w}$ from equations (2.110) and (2.111), using $\frac{d}{dt}_p\mathbf{u}_p \approx \frac{d}{dt}_p\mathbf{u}_n \approx \frac{d}{dt}\mathbf{u}$, Braginskii finds

$$\begin{aligned}
\mathbf{w} &= \frac{1}{\alpha_n}\left(-\mathbf{G} + f_n\mathbf{j}\times\mathbf{B}\right) + \frac{\epsilon\mathbf{j}}{en}, \quad \text{where} &(2.113)\\
\mathbf{G} &= f_n\nabla(p_e + p_p + p_n) - \nabla p_n. &(2.114)
\end{aligned}$$

Eliminating $\mathbf{w}$ from equations (2.109-2.111) and using $\mathbf{u}_p = \mathbf{u} + f_n\mathbf{w}$,

$$\mathbf{E} + \mathbf{u}\times\mathbf{B} + \frac{1}{en}(\nabla p_e - \epsilon\mathbf{G}) - \frac{f_n}{\alpha_n}\mathbf{G}\times\mathbf{B} = \frac{\mathbf{j}_\parallel}{\sigma} + \frac{\mathbf{j}_\perp}{\sigma_3^n} + \frac{1-2\epsilon f_n}{en}\mathbf{j}\times\mathbf{B}, \tag{2.115}$$

where σ_3^n is, for the neutral case, now

$$\sigma = \frac{e^2 n\tau_e}{m_e}, \quad \frac{1}{\sigma_3^n} = \frac{1}{\sigma} + \frac{f_n^2 B^2}{\alpha_n} \tag{2.116}$$

With $\alpha_n \approx \alpha_{np} = m_p n/\tau_{np}$,

$$\sigma_3^n = \frac{\sigma}{1 + f_n^2 \omega_p \tau_p \omega_e \tau_e} \quad \text{(partly ionized plasma).} \tag{2.117}$$

In this context σ_3^n is often called "Cowling's conductivity" as applied to partially ionized plasmas. We could take the dot product of equation (2.115) with $\mathbf{j}$ to determine the dissipation rate of electromagnetic energy, $\mathbf{E}' \cdot \mathbf{j}$, to yield additional terms dependent on ϵ, $\mathbf{G}$, ∇p_e and f_n. But an equivalent approach looking at the frictional forces reveals more insight. The total heat generated by friction is, omitting some algebra,

$$\begin{aligned} Q_f &= -\mathbf{R}_{ei} \cdot \boldsymbol{\nu} - \mathbf{R}_{en} \cdot (\boldsymbol{\nu} + \mathbf{w}) - \mathbf{R}_{in} \cdot \mathbf{w} \\ &= \alpha_e u^2 + \alpha_n w^2 + 2\alpha_{en} \boldsymbol{\nu} \cdot \mathbf{w} \\ &= \frac{j_\parallel^2 + j_\perp^2}{\sigma} + \frac{1}{\alpha_n} \left(f_n \mathbf{j} \times \mathbf{B} - \mathbf{G} \right)^2 . \end{aligned} \tag{2.118}$$

(A term of order $\epsilon^2 \approx m_e/m_p$ has been omitted here.) Several cases arise according to the behavior of the last term in this equation.

- When $\mathbf{j}$ is parallel to $\mathbf{B}$, the dissipation consists of Ohmic dissipation with σ computed taking into account collisions with ions, electrons and neutrals, plus G^2/α_n, a term dissipating work done by differential pressure gradient forces (equation 2.114).

- When G is small compared with $f_n|\mathbf{j} \times \mathbf{B}|$, we recover equation (2.96) using equations (2.116) and (2.117).

- There are situations where the entire second term in equation (2.118) is small or negligible. If the plasma is close to equilibrium with $\mathbf{j} \times \mathbf{B} - \nabla p \approx 0$, then $f_n \mathbf{j} \times \mathbf{B} - \mathbf{G} \approx \nabla p_n$. The dissipation then consists of the standard Ohmic forms of equations (2.86) and (2.96), plus dissipation due to the pressure gradient of neutral particles. Such situations can be expected in "slow" processes (subsonic flows and wave motions). Thus, quasi-static evolution and slow-mode oscillations are expected to have relatively small frictional dissipation of perpendicular electrical currents, far slower than implied by equation (2.118) when $\mathbf{G} \to 0$.

In all of these cases, as the number of neutral particles becomes negligible, $Q_f \to j^2/\sigma$ in accord with equations (2.86) and (2.96).

In conclusion, neutrals, when present, can have a particularly marked effect on Ohm's law, beyond the reduction of σ caused by the additional collisions of charged particles with neutrals. Under some, *but not all*, conditions σ_3^n can be radically reduced by the denominator given above. When the plasma is close to force balance between the Lorentz and pressure gradient forces, σ_3^n can approach σ, severely limiting the rate of energy dissipation by cross-field current dissipation. More generally, care must be taken when pressure gradients exist, the dissipation rate can differ markedly from σ_3^3 given above.

Cross-field current dissipation may become important at intermediate densities, even where $f_n \omega_p \tau_p$ may be quite small, because $\omega_e \tau_e$ can remain $\gg 1$. This condition occurs low in the solar chromosphere where τ_p is dominated by proton-neutral collisions, where neutral atoms are far more abundant than ions. As first proposed by Cowling (1953), Goodman (2000,2004) has argued that this process is responsible for heating the network chromosphere. Goodman (2000) assumes the ion-neutral dissipation is driven by slow magnetosonic waves.

2.5 MHD equilibria and simple motions

2.5.1 Flux freezing

Consider the induction equation (2.75) The ratio of the two terms on the RHS of this equation, the "magnetic Reynolds number" R_m, is

$$R_m \sim |\mathbf{curl}\,(\mathbf{u} \times \mathbf{B})|/|\eta\nabla^2\mathbf{B}| \sim v\ell/\eta \tag{2.119}$$

The case $R_m \gg 1$ applies to large, highly conducting astrophysical plasmas, such as the corona, so that, in the limit $R_m \to \infty$

$$\frac{\partial \mathbf{B}}{\partial t} = \mathbf{curl}\,(\mathbf{u} \times \mathbf{B}). \tag{2.120}$$

The magnetic flux through a surface S at time t is

$$\Phi(t) = \int_S \mathbf{B} \cdot d\mathbf{S} \tag{2.121}$$

So that, using (2.120)

$$\begin{aligned}
\frac{\partial \Phi(t)}{\partial t} &= \int_S \frac{\partial \mathbf{B}}{\partial t} \cdot d\mathbf{S} + \int_S \mathbf{B} \cdot \frac{\partial d\mathbf{S}}{\partial t} \\
&= \int_S \mathbf{curl}\,(\mathbf{u} \times \mathbf{B}) \cdot d\mathbf{S} + \oint_L \mathbf{B} \cdot (\mathbf{u} \times d\mathbf{l}) \\
&= \oint_L (\mathbf{u} \times \mathbf{B}) \cdot d\mathbf{l} - \oint_L (\mathbf{u} \times \mathbf{B}) \cdot d\mathbf{l} = 0.
\end{aligned} \tag{2.122}$$

Where $d\mathbf{S} = (\mathbf{u} \times d\mathbf{l})dt$ is the change in area S due to the distortion of S by the fluid motions in time dt. Thus, in a perfectly conducting fluid moving in a magnetic field, the magnetic flux through a closed circuit moving with the fluid is constant ("Alfvén's theorem"). The magnetic lines of force move with (or are "frozen to") the fluid.

2.5.2 Comments on ideal MHD equilibria and topology

The frozen-in condition dictates that the MHD dynamics is subject to constraints which are intimately related to the *topology* of the magnetic field. This is simply because the plasma has no way to slip across field lines, so that a volume of plasma remains forever somewhere in the same magnetic flux bundle. The topology is defined by the linkage and intertwining of flux bundles which is therefore fixed for all time.

The simplest, non-trivial MHD equilibrium is that of a potential magnetic field ($\mathbf{j}$=$\mathbf{curl}\,\mathbf{H}$=0, $\mathbf{H} \neq 0$), in which the embedded plasma is in equilibrium in the absence of magnetic forces. When $\mathbf{curl}\,\mathbf{H}$=0 then we can write $\mathbf{H}$= $\mathbf{grad}\,\phi$ so that ϕ satisfies $\nabla^2\phi = 0$. The magnetic field and plasma are decoupled, so this is not really a magneto-hydrodynamic equilibrium. The simplest coupled equilibrium is a *force-free* state (equation 2.92), which requires that $\mathbf{j}$ be parallel to $\mathbf{B}$, or with constant magnetic permeability μ:

$$\mathbf{curl}\,\mathbf{B} = \alpha\mathbf{B}. \tag{2.123}$$

The magnetic field and plasma are implicitly coupled because, although the Lorentz force is zero, $\mathbf{j}$, has to be carried by the plasma. The force free field is the limit in which the Lorentz force *dominates* the other terms in the single-fluid momentum equation (2.91)[3]. Even though equation (2.123) implies that magnetic fields and plasma are dynamically decoupled, they are not completely, since there is always a finite but small contribution to the force balance from the plasma. This approximation is important for the low corona, because the Lorentz force does indeed dominate the equation of motion, so this should be a reasonable approximation to coronal magnetostatic equilibrium configurations.

Although equation (2.123) describes the simplest legitimate MHD equilibrium, its apparent simplicity is misleading. Indeed, solutions to equation (2.123) in highly conducting plasmas are the subject of Parker's (1994) monograph. The equation is the limiting form of the full momentum equation in which the Lorentz force $\propto \mathbf{curl}\,\mathbf{B} \times \mathbf{B}$ is explicitly non-linear. More fundamental is the point, stressed by Parker, that the frozen-in condition with equation (2.123) imposes topological constraints on the solutions. Taking the divergence of equation (2.123), we see

$$\mathbf{B} \cdot \mathbf{grad}\, \alpha = 0, \tag{2.124}$$

i.e the value of α is constant along field lines, and each field line, labelled i, say, can have its own value of $\alpha(\mathbf{B}_i)$. Since α is an implicit function of $\mathbf{B}$, equation 2.123 is generally non-linear. Two special, linear cases are not irrelevant to our discourse. The case of α being a non-zero constant is the lowest energy state available to a current-carrying magnetic field (Woltjer 1958). Clearly the case $\alpha = 0$ (potential field) has the lowest energy of these solutions and is the lowest magnetic energy state.

In general, though, this equation (specifically its generalization to include non-magnetic forces), together with the frozen-in condition, leads to topological constraints which are expressed via the *Fundamental Theorem of Magnetostatics*:

> *"the lowest available energy state of a magnetic field* $\mathbf{B}(\mathbf{r})$ *in an infinitely conducting fluid contains surfaces of tangential discontinuity [...] for all but the most carefully tailored field topologies"* – Parker (1994).

To see how this comes about, apply Ampère's law to equation (2.123) around a small flux bundle of area A and flux $\Phi = BA$, which intercepts the bundle along curve s. α is simply $\oint_s \mathbf{B} \cdot d\mathbf{s}$ per unit magnetic flux. It measures the local twist of the field about the particular field line. But we know that each field line i generally must have its own $\alpha(\mathbf{B}_i)$, so that $\oint \mathbf{B} \cdot d\mathbf{s}$ per unit flux will generally be independent of its neighbor. Therefore adjacent field lines must generally have discontinuous values of the peripheral fields (those along the path $d\mathbf{s}$), unless the boundary conditions/initial state are chosen very particularly. The relevance of this theorem to the coronal heating problem is now painfully clear. The photospheric and chromospheric magnetic fields, controlled by sub-photospheric turbulence, are not of a form in which neighboring flux bundles can be expected to accomodate these special, tailored conditions. Therefore we must expect the corona to contain the physical counterpart to the ideal tangential discontinuities, current sheets. We cannot expect to arrive at continuous solutions to the equations for the magnetic field.

The above arguments neglect non-ideal processes without which there is no heating. Yet we have already reached two conclusions: (1) the lowest energy state accessible to a magnetic field a potential field, in which the field is generated by currents wholly outside of the boundaries of the problem studied; (2) (Woltjer's result) if the magnetic field generally carries electrical

[3] This curious situation of setting the largest term in an equation to zero can be understood if one remembers that the equation describes the time evolution of the system. When the Lorentz force is not zero and not balanced by other (far smaller) terms, the system will rapidly evolve towards the force-free state. After this fast adjustment, the force-free equilibrium approximation becomes valid.

currents, then the state with the lowest magnetic energy is a constant α state. Any non-ideal effects will evolve towards the constant-α and, in particular, the $\alpha = 0$ states, subject to imposed constraints (e.g., boundary conditions). During the evolution, energy within the magnetic field is dissipated by friction, ultimately to be radiated away, for example. Thus it appears then that the study of *ideal* MHD equilibria can yield some information on the nature of coronal heating. This seemingly contradictory statement is analogous to problems in equilibrium thermodynamics. In neither case can studies of equilibria shed light on the rate at which such equilibria are approached, but both can identify the accessible states and the direction in which evolution must proceed.

Topological constraints in MHD become crucial as the system tries to accomodate force balance while at the same time maintaining the frozen-in condition. Parker argues that during the evolution, the topological constraints cannot, except for very contrived configurations not to be found in nature, be reconciled with force balance in a continuous way. Thus the natural evolution of the system must include the spontaneous generation of tangential discontinuities.

The subject of magnetostatic equilibria lies largely, but not completely, in the realm of numerical modeling, even in "simple" cases. The difficulties arise because such problems are non-linear, ???

2.5.3 Comments on non-ideal MHD

In the presence of non-ideal effects tangential discontinuities will lead to current sheets of finite thickness, as dissipation sets in to limit the current densities which can flow. Parker (1988) argues that when a system is driven "untidily" to a steady state, such as may be present in the active or quiet solar corona, the injection of magnetic energy is balanced by the continuous build up and dissipation of current sheets throughout the plasma. Given that plasma instabilities are expected to arise before dissipation via classical transport theory can become significant, Parker suggests that the release of energy is intermittent. An evaluation of the energy released (see section ???) prompted Parker to name these events "nanoflares".

It has been shown that, among other measures of topology, a quantity called magnetic relative helicity is approximately conserved, even in high R_m non-ideal plasmas.

2.5.4 MHD waves in homogeneous plasmas

Perhaps the simplest non-trivial form of MHD motion is that of waves in static homogeneous plasma. All non-ideal effects are ignored, so that the energy equation is restricted to the adiabatic form (equation **??**). More details and a nice physical discussion of MHD waves can be found in ch. 5 of the book by Kulsrud (2005). Consider small disturbances $\delta\rho$, δp, $\mathbf{u}$ and $\delta\mathbf{B}$, which, through equations (2.88), (**??**) and (2.75), are functions of the small displacement $\boldsymbol{\xi}$:

$$\begin{aligned} \delta\rho &= -\rho_0 \,\mathrm{div}\, \boldsymbol{\xi}; \quad \delta p = -\gamma p_0 \,\mathrm{div}\, \boldsymbol{\xi} \\ \mathbf{u} &= \partial\boldsymbol{\xi}/\partial t; \quad \delta\mathbf{B} = \mathbf{curl}\, \boldsymbol{\xi} \times \mathbf{B}_0 \end{aligned} \tag{2.125}$$

where subscript 0 refers to unperturbed state. Setting perturbed variables to the form $\delta\rho = \rho_1 exp(\mathbf{k}\cdot\mathbf{r} - \omega t)$, and substituting these into the momentum equation with equation (2.125), yields a set of three equations for the three vector components of the amplitudes $\boldsymbol{\xi} = (\xi_x, \xi_y, \xi_z)^T$:

$$\gamma p_0 \mathbf{k}(\mathbf{k}\cdot\boldsymbol{\xi}) + \frac{1}{\mu_0}\left[\mathbf{k} \times \{\mathbf{k} \times (\boldsymbol{\xi} \times \mathbf{B}_0)\}\right] \times \mathbf{B}_0 = \rho_0 \omega^2 \boldsymbol{\xi} \tag{2.126}$$

Without loss of generality, we follow ch. 5 of Kulsrud (2005) and orient wave vector $\mathbf{k}$ and background magnetic field $\mathbf{B}_0$ as shown in Figure 2.1. In this case, the linearized momentum

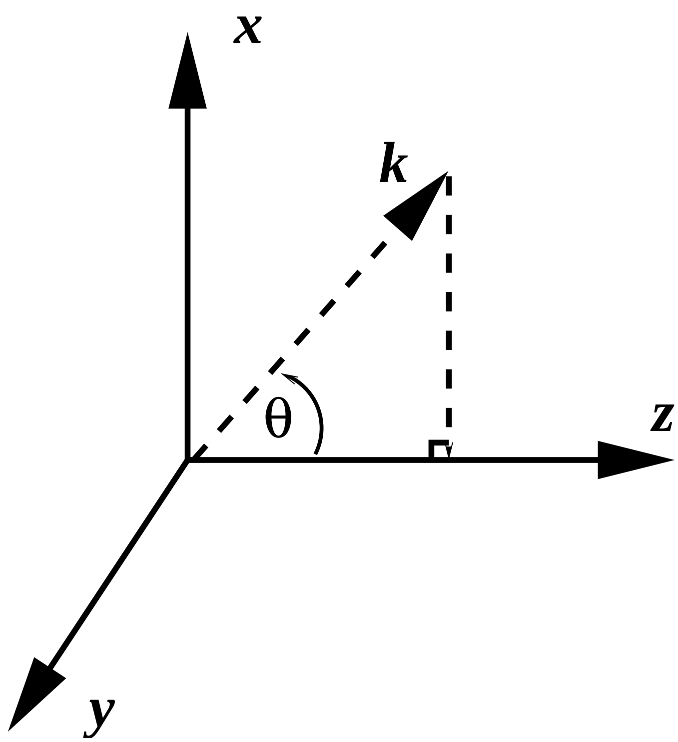

Figure 2.1: Geometry of wavevector of MHD waves relative to the background magnetic field $\mathbf{B}_0$, aligned along the z-axis. The x and y axes are chosen so that $\mathbf{k}$ lies in the plane $y = 0$.

equation can be written in matrix form as

$$\begin{pmatrix} k^2(c_s^2 \sin^2\theta + c_A^2) & 0 & k^2 c_s^2 \sin\theta\cos\theta \\ 0 & c_A^2 k^2 \cos^2\theta & 0 \\ k^2 c_s^2 \sin\theta\cos\theta & 0 & k^2 c_S^2 \cos^2\theta \end{pmatrix} \begin{pmatrix} \xi_x \\ \xi_y \\ \xi_z \end{pmatrix} = \omega^2 \begin{pmatrix} \xi_x \\ \xi_y \\ \xi_z \end{pmatrix}. \tag{2.127}$$

This equation is an eigensystem with eigenvalues ω^2. The equation for ξ_y is completely uncoupled from the other components- and its eigenvalue leads to the dispersion relation

$$\omega = \pm c_A k \cos\theta, \quad \text{with} \tag{2.128}$$

$$c_A^2 = \frac{B^2}{\mu_0 \rho_0} \tag{2.129}$$

The two different signs correspond to two different directions of wave propagation. The eigenvector is $\boldsymbol{\xi} = (0, 1, 0)^T$ so that the oscillations are perpendicular both to the magnetic field and $\mathbf{k}$ vector. The restoring force is the magnetic tension force only. This is called the "Alfvén" or "intermediate" mode. The two other modes can be found by solving the characteristic equation of the remaining rows/columns of the above matrix:

$$\omega^4 - k^2(c_S^2 + c_A^2)\omega^2 + k^4 c_S^2 c_A^2 \cos^2\theta = 0, \tag{2.130}$$

with roots

$$\frac{\omega^2}{k^2} = \frac{c_S^2 + c_A^2}{2} \pm \frac{1}{2}\sqrt{(c_S^2 - c_A^2)^2 + 4 c_S^2 c_A^2 \sin^2\theta}. \tag{2.131}$$

There are thus two roots for the square of the phase speed, ω^2/k^2, a "fast" mode and a "slow" mode. The restoring forces for these modes depend on the interplay between gradients in gas and magnetic pressure, and the tension force. Generally, in the corona, $\beta \ll 1$ and $c_S^2 \ll c_A^2$. In this particular case the fast and slow mode dispersion relations become:

$$\frac{\omega_f^2}{k^2} = c_A^2 + c_S^2 \sin^2\theta, \tag{2.132}$$

$$\frac{\omega_s^2}{k^2} = c_S^2 \cos^2\theta. \tag{2.133}$$

The intermediate mode's phase speed is, as the name implies, between these two modes. Since the matrix is symmetric, eigenvalues ω^2 are real, and the three eigenvectors are orthogonal to one another. Strictly speaking, the three "ideal" modes apply to waves in homogeneous media, yet these modes are often referred to in the solar physics literature. This is because any local oscillation can be projected on to these eigenvectors, so that one can speak of "Alfvén-like" local oscillations whenever $\boldsymbol{\xi} \approx (a, 1, b)^T$, $a, b \ll 1$, for example. The WKB limit, where the background varies little over a wavelength, is one physical limit of interest.

While WKB-like oscillations may behave locally like these three modes, inhomogeneities introduce new physical processes because the assumption of homogeneity de-couples the oscillatory motions. The coupling introduces physical processes otherwise absent which have particularly important consequences for wave energy dissipation. Kulsrud (2005) provides a more detailed discussion of the properties of these modes, wave momentum, energy and pressure, and the properties of waves propagating in weakly inhomogeneous media.

2.6 MHD waves and inhomogeneities

The corona is clearly inhomogeneous. Not only is it stratified (radial density gradients), but also coronal plasma is highly structured by the magnetic field anchored in an inhomogeneous fashion to the solar photosphere. MHD oscillations must in general be described by a set of coupled partial differential equations, of which the above solutions are the simplest, decoupled cases (e.g., Thomas 1983).

Much attention has been given to "tube waves", those modes obtained when a cylindrically symmetric tube of magnetic flux is embedded in an otherwise homogeneous medium. The Alfvén speed is assumed different within and outside of the tube. The motivation appears to be (1) that the EUV and X-ray corona consists of plasma loops, and (2) that the photospheric magnetic field is organized into strong concentrations by magneto-convective processes. The magnetic field emerging into the corona is expected to be in the form of expanding sheets or tubes, depending on the surface field distribution (see Figure 1.4).

using the "thin flux tube approximation" (Defouw 1976, Roberts and Webb 1978, Spruit 1981). In this case, the horizontal scales inside each "tube" are assumed to be smaller than the pressure scale height, and simplified equations of motion are solved for three modes – longitudinal ("sausage"), transverse ("kink") and torsional ("Alfvén) modes – corresponding to the three degrees of freedom of the tube. For the sausage and kink modes, which are dispersive, the motion takes account of the extra inertia of the surrounding field-free fluid, which changes the propagation characteristics of these modes.

2.7 Summary

Further reading

Much of this chapter follows:

Braginskii, S. I.: 1965, "Transport processes in a plasma", *Reviews of Plasma Physics.* **1**, 205–311.

Woods' book has an elegant mathematical treatment and enlightening physical discussion, particularly of thermodynamics and transport processes:

Woods, L. C.: 1987, *Principles of Magnetoplasma Dynamics*, Oxford University Press, Oxford.

The following book offers much physical insight into MHD phenomena, applied to space plasmas including the Sun's corona:

Kulsrud, R. M.: 2005, *Plasma physics for astrophysics*, Princeton University Press, Princeton and Oxford.

Chapter 3

MHD and coronal heating

In the solar corona, magnetic free energy is transported from the lower atmosphere via magnetic stresses generated by fliud motions. In MHD, the magnetic free energy is dissipated via frictional dissipation (electron-ion, ion-neutral, electron-neutral collisions), heat conduction (dominated by electron-electron collisions), viscosity (dominated by ion-ion collisions). In the present chapter, using MHD we examine the nature of the generation, transport and dissipation of magnetic energy in the Sun, from photosphere to corona. The nature and magnitude of the energy flux is difficult to estimate from basic principles, for reasons to be discussed below. We must be guided by observations.

3.1 The nature of the MHD problem

Of the $1L_\odot$ of power generated by nuclear reactions in the solar core, all but 2 parts in 10^4 is radiated into space within the few hundred km-thick photosphere. Of the $2 \times 10^{-4} L_\odot$ of power used to maintain the chromosphere, just $10^{-5} L_\odot$ is needed to maintain the quiet corona and wind. Thermodynamics dictates this this energy be transported mechanically. Immediately below the photosphere, turbulent convection carries most of the solar luminosity in the form of kinetic energy. The Sun apparently converts just a fraction 2×10^{-4} of this energy flux into mechanical energy propagating into the overlying atmosphere.

At and below the photosphere, plasma densities and pressures are high because of the atmospheric stratification. Under normal conditions the mechanical energy density is dominated by the kinetic energy of turbulent convection. In contrast, the mechanical energy in the corona is dominated by the magnetic energy. The chromosphere is a challenging region in which convection cells have turned over, where the energy density can be mostly magnetic, or kinetic/thermal, depending on the the chromospheric stratification and local magnetic conditions. Typical conditions in the three regions are listed in table 3.1.

Photospheric plasma is a sufficiently good conductor (section 3.2) so that it is almost frozen to field lines. Photospheric motions perpendicular to the magnetic field do work on the magnetic fields (see the last term of equation 2.85). This energy is stored in the form of magnetic stresses which, depending on the magnetic topology, will often extend into the corona.

While photospheric motions are dominated by granulation, the Sun has (at least) two other sources of non-radiative energy: global solar oscillations and emerging magnetic fields. Global oscillations (eigenmodes of the entire Sun) are characterized by periods near 5 minutes, with a total energy of order 10^{27} J (Libbrecht et al. 1986) which decays in about 5 days. The total oscillation power corresponds to a flux density of 300 W m^{-2}, insufficient to sustain the quiet

Table 3.1: Representative conditions from photosphere to the base of the corona

Physical quantity	photosphere	temperature minimum	mid chromosphere	coronal base
height	0 ($\tau_{500} = 1$)	515 km	1280 km	2104 km
density ρ kg m^{-3}	2.7×10^{-4}	4.9×10^{-6}	9.8×10^{-9}	1.2×10^{-10}
temperature T	6420	4170	6220	9500
pressure scale height H m	2×10^{5}	8×10^{4}	2×10^{5}	1.8×10^{5}
neutral density n_H m^{-3}	1.2×10^{23}	2.1×10^{21}	4.2×10^{18}	5.2×10^{16}
electron density n_e m^{-3}	6.4×10^{19}	1.7×10^{17}	7.5×10^{16}	3.7×10^{16}
n_e/n_H	5.5×10^{-4}	1.2×10^{-4}	1.8×10^{-2}	2.3
electrical conductivity σ s m^{-2}	100	25	1900	3200
magnetic diffusivity η m^2 s^{-1}	8200	3.1×10^{4}	420	250
diffusion time $\tau_{0.1} = \ell^2/\eta$ s ($\ell = 0.1$ Mm)	1.2×10^{6}	3.3×10^{5}	2.4×10^{7}	4.1×10^{7}
c_A(B=0.01T) m s^{-1}	540	4000	9×10^{4}	8×10^{5}
H/c_A(B=0.01T) s	380	19	2	0.2
H/c_S s	24	12	21	12

Thermodynamic properties are from model "C" of Vernazza et al. (1981). Electrical conductivities are computed using electron-atom collision cross sections from Kopecký and Obridko (1968), and equation (2.24) for ion-electron collisions.

corona which requires about 800 W m^{-2} (Table 1.3). The bulk of the oscillation power is trapped beneath the surface anyway. While oscillations of 5 minute periods are observed in the corona and in the solar wind, they cannot provide energy sufficient to heat the corona (see also Ulmschneider 1976).

The wavelength-integrated solar radiation measured near earth's orbit- the irradiance- varies with the 11 year sunspot cycle, with a peak-to-peak amplitude of $\approx 0.1\%$ (Willson et al. 1986). This cycle is characterized by variations in the surface magnetic fields caused by the emergence and evolution of magnetic fields generated by a global-scale magnetic dynamo. If these irradiance variations correspond to luminosity variations, then it seems that emerging magnetic fields might constitute an average non-radiative perturbation of order $\sim 10^{-3}L_\odot$ to the energy flux at the solar photosphere. A fraction of this additional energy source clearly contributes significantly to heating the chromosphere and corona, because spectral features formed in these regions vary not by 0.1% but by 40% in the low chromosphere and by a factor of 10 in coronal X-ray emission.

The Sun therefore provides electromagnetic energy significant for the overlying layers in at least two ways:

- New magnetic flux emerges into and through the atmosphere from the interior. The new flux may itself carry free energy, but it will almost always produce current sheets at contact surfaces with mis-aligned, previously emerged fields.

- Some fraction of the enormous sub-photospheric kinetic energy does work on pre-existing magnetic fields. The magnetic stresses of fields connecting to the overlying atmosphere carry magnetic energy into it.

It is reasonable to think of the photosphere as providing physical boundary conditions for the chromosphere and corona, because the energy and mass densities there are far higher. The (sub) photosphere *"drives"* the corona. This is a convenient situation since, of course, the huge flux of visible radiation from the photosphere makes it the most easily observed region of the Sun. Observations from the 19th century onwards have shown that these boundary conditions are not simple because of the turbulent convection and other motions. With interesting exceptions, coronal structures are generally long-lived compared with dynamic time scales in the corona, i.e. the time taken for Alfvén waves to cross, and the ~ 8 minute evolution time of granulation. Thus in both of these cases one can imagine the energy from these two sources being injected slowly into a pre-existing atmospheric structure. In both cases the new magnetic field components are determined in part by the changing conditions at the lower boundary, so that the atmosphere will lose any previously existing force balance. For the same reason, the magnetic topology of the new field components must induce thin current sheets, the physical equivalent of tangential discontinuities, which are subject to dissipation (Parker 1994).

It is useful to give a couple of historic examples of where the dense photosphere "drives" the corona. The first MHD model of coronal heating was the Alfvén wave driven model (Alfvén 1947). The paper is well worth reading since it contains all the elements needed to describe coronal heating: a source of energy (granular motions), the mode and propagation of magnetic energy through the atmosphere and into the corona (Alfvén waves), and its dissipation (friction). Equally worth reading is the criticism of Alfvén's paper by Cowling (1953) who showed that the resistivity used by Alfvén was applicable to partially ionized plasmas, and was vastly over-estimated in the corona. In another example, Parker (1972) examined the basic MHD of slowly driven magnetic fields tied to the photosphere, by "straightening out" coronal loops as shown in figure 3.1. Convective motions at the two plates drive the tubes of magnetic flux in a random fashion. Magnetic energy is transported into the inter-plate (coronal) volume via magnetic stresses. The stresses, because of constraints set by topology of the frozen-in fields and by force balance, build up current sheets and thereby dissipate free magnetic energy. Parker's scenario is discussed further in section 3.4.

3.2 The photospheric boundary

Table 3.2 lists observed properties of photospheric structures. Diffusive decay times for features of order a pressure scale height $\sim 10^5$ m (coincidentally, also the smallest scale of features resolved by current instruments) are $\tau_{0.1} \approx$several hours (Table 3.1). In comparison, granulation evolves on time scales of a few minutes, so magnetic Reynolds numbers R_m for scales of 10^5 m are $\sim 10^3$. Structures with $\ell \geq 10^5$ m are effectively frozen to the granular motions.

Table 3.2: Properties of representative photospheric features

Physical quantity	granule cell	inter-granular lane	super-granule cell	flux tube or sheet	pore	sunspot umbra
diameter/width m	1.4×10^6	1×10^5	3×10^7	1×10^5	$\lesssim 3 \times 10^6$	$\sim 1 \times 10^7$
lifetime s	500	500	7×10^4	10^3?	$\sim 8 \times 10^4$	$\sim 5 \times 10^5$
flow speed m s^{-1}	2000	...	400	...	...	...
B T	...	...	...	0.05- 0.15	0.15	0.3
T K						4000
n_e/n_H						1.3×10^{-5}

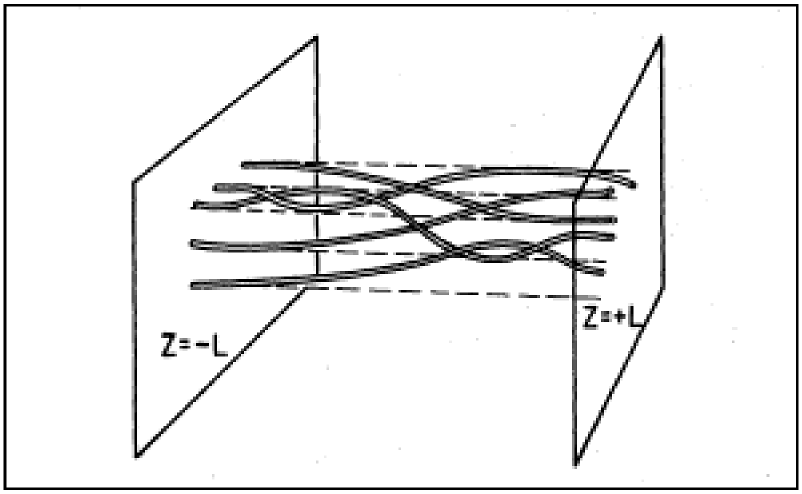

Figure 3.1: Parker's simplified geometry of magnetic fields driven by convective motions. Representative tubes of magnetic flux are attached to two plates of infinite electrical conductivity. The plates represent the two different places on the photosphere where the tubes intercept the surface, the space in between them the chromosphere and corona. Initially the tubes are considered parallel (dashed lines). The tube footpoints within the plates are then subject to random motions relative to one another, representing approximately the effects of the forcing of magnetic fields by surface convection.

But diffusion is not necessarily unimportant, even in the absence of smaller length scales associated with tangential discontinuities. On time scales of a few hours diffusion will influence the dynamics of magnetic elements which are the roots of longer lived coronal structures. Also, Table 3.1 omits special conditions such as exist in sunspot umbrae. The umbral atmosphere is so cool that conductivities are significantly smaller. When $n_e \ll n_H$, $\tau_e^{-1} = n_H \langle v\sigma_{en}\rangle$, so the conductivity $n_e e^2 m_e/\tau_e$ is

$$\sigma \approx \frac{n_e e^2 m_e}{n_H \left(3k_B T/m_e\right)^{1/2} \sigma_{en}} = 8 \times 10^5 \frac{n_e}{n_H} \left(\frac{4000}{T}\right)^{1/2} \quad \text{s m}^{-2}. \tag{3.1}$$

The value of σ_{en} used was taken from Kopecký and Obridko (1968). n_e/n_H approaches 7×10^{-6} in photospheric umbral models (Maltby et al. 1986). The umbral conductivity can drop to just 1.6 s m^{-2}, and the smallest diffusion time for $\ell = 10^5$ m becomes 2×10^4 s. Thus, even in this case, the lifetimes and length scales of individual photospheric structures are such that magnetic diffusion is not expected to be dominant. In fact, observations show that magnetic pores and flux tubes or sheets in intergranular lanes have lifetimes less than the expected diffusion times. Clearly the magnetic fields in these structures evolve via the advection term in the induction equation, perhaps because of emergence/submergence, and/or that the process of magnetic reconnection occurs at a rate exceeding the diffusion rate.

In principle, low electric conductivities can support significant electric fields in the frame moving with the plasma ($\mathbf{E}' \neq 0$). Feldman (1993) has argued that such fields might serve to generate electric currents flowing into the chromosphere and corona. In practice, the conductivities are not likely to approach the small values suggested by Feldman, which arise ???.

Table 3.1 also lists wave propagation time scales (pressure scale height divided by wave phase speed), for a uniform magnetic field strength of 0.01T. But the solar magnetic field is inhomogeneous and drops with height through the chromosphere, the value of 0.01 T was chosen only to estimate the order of magnitude of c_A. Waves propagate magnetic and Reynolds stresses from the photosphere into the chromosphere on time scales far less than diffusion times $\tau_{0.1}$. Sound wave propagation times from photosphere to corona are 3 minutes. For Alfvén waves in flux concentrations, a more realistic calculation in a credible magnetostatic structure is needed. Calculations of flux concentrations expanding into the chromsphere and corona by Cranmer and van Ballegooijen 2005 indicate Alfvén chromospheric crossing times about 1/2 of the sound crossing time. The listed photospheric Alfvén speed is less than the characteristic speed of granular motions (Table 3.2). This condition, computed using $B = 0.01$T, makes coupling of the granular motions to the magnetic field inefficient as pointed out by Parker (1991). However, Parker used a field strength of just 0.001T appropriate for a surface averaged field strength. Photospheric flux is concentrated into bundles where $B \sim 0.1$T. Thus, granular to bundle coupling should be efficient.

We proceed with the picture that the conductivity in the photosphere is high enough to treat the magnetic fields as frozen to the plasma, and that the coupling between photospheric magnetic fields and granular motion is not inefficient.

3.3 The chromosphere: the coronal mediator

The corona begins at the top of the chromosphere, yet it is common practice to study the corona in relation to magnetic fields measured only in the photosphere. The chromosphere is mostly viewed as a passive stratified layer through which the magnetic field emerges and in which the plasma pressure drops to coronal values. There are understandable, practical reasons for this. The chromosphere is geometrically thin compared with the corona. Linear magnetic field extrapolations from photospheric sources are solutions to elliptic partial differential equations[1]. In the bulk of the corona, such extrapolated fields will depend little on small scale structures. Quantitative measurements of thermal and magnetic fields in the chromosphere are notoriously difficult to make, as the fields are relatively weak, chromospheric diagnostic spectra are formed out of LTE and perhaps even are out of ionization equilibrium. The chromosphere is full of dynamic fine structure on scales $\lesssim$ 1Mm, compounding the difficulties of thermodynamic and MHD problems (Low 1990).

For certain problems, for example if one wishes to examine the global magnetostatic structure, stability or oscillation modes of a coronal structure, one might ignore the chromosphere as a justifiable first step. But here we are specifically interested in coronal heating, so that one must constrain the injection of magnetic free energy *and its dissipation* in the corona. Herein lies a problem. The energy responsible for coronal heating is not necessarily related to components of the field which can be extrapolated from the photospheric surface. This is because dissipation requires structure on tiny scales (section 2.3), be they induced by quasi-static evolution or by rapid wave-like motions, and because the chromosphere can in principle have a large effect on the small scale structure of the magnetic field.

In general, then, the chromosphere is not expected to be such a passive layer. Just ≈ 1 part in 20 of the total energy eventually dissipated and radiated away survives the journey through the chromosphere to heat the corona (Table 1.3). The bulk of the dissipation is associated with magnetic fields so that the chromosphere strongly modifies the free energy available to the corona.

[1]At present, it is unclear that meaningful *non-linear* extrapolations have even been achieved, see Low and Flyer (2007)

The chromosphere acts as a thermostat, resisting attempts to raise its temperature by transfering energy to latent heat of ionization and to radiation losses. Thus is is the "thickest" part of the solar atmosphere, spanning 9 pressure scale heights. This steep stratification implies that the chromosphere contains the (morphologically complex, and dynamically important) plasma $\beta = 1$ surface. The field changes from a forced to force-free regime across this surface. MHD oscillations originating in the (sub) photosphere change character- or "convert"- efficiently near this surface (Bogdan et al. 2002). The chromosphere is partially ionized, and the bulk of it contains vastly more neutral atoms than ions and electrons. Element fractionation seems to occur there- the momentum coupling between different species of particles appears to be incomplete. Spicules, only partly understood but launched from the network chromosphere, penetrate the coronal base. Given these properties, *it is important to understand how the chromosphere might modify the flow of mass, momentum and (magnetic) energy into the coronal base.*

A decade ago, a problem concerning the solar wind mass flux was identified. The measured mass flux remains remarkably constant, yet standard Parker-type models (Parker 1958) predicts an exponential dependence of the flux on the electron temperature in the low corona. It is evident from EUV observations (e.g., Figure 1.9) that the low coronal temperature varies significantly. Holzer et al. (1997) found a resolution to this apparent paradox by placing the lower boundary of their calculation *within the chromosphere*, and by solving fluid equations for mass, momentum and energy for parametric heating functions. They showed that the chromospheric mass reservoir mediates the mass flux of the solar wind, as the coupled system adjusts to changes in the dissipated energy. Prescribing a coronal base temperature instead of allowing the hydrodynamic system to determine its own thermal structure led to a paradox. Clearly, care must be taken when studying the corona in isolation from the chromosphere.

Hydrodynamic chromospheric/coronal coupling is manifested in a different way within magnetic fields which return to the solar surface. The ready supply of chromospheric mass is required implicitly in order that energy and force balance can be maintained in well known static "coronal loop scaling laws" (e.g., Rosner et al. 1978). Rosner and colleagues found empirical relationships between the brightness, temperatures and lengths of active region loops observed with instruments on SKYLAB. By assuming

It is well known that the force balance must change character from photosphere and into the corona. The corona must be close to a force-free state since any departure from this state induces a large Lorentz force, unbalanced in the low-β plasma by gravity, pressure gradients or thermal forces. The system then rapidly evolves to the force-free state. Thus, any electrical currents present in the corona must satisfy

$$\mathbf{j} \times \mathbf{B} = \mathbf{0},$$

or equivalently $\mathbf{j}_\perp = \mathbf{0}$. Currents perpendicular to $\mathbf{B}$ are zero. Yet $\mathbf{j}$ has no such constraint in the high-β environment of the photosphere. Somehow, then, the chromosphere must dynamically adjust itself such that the electrical currents become parallel to the magnetic field before the low β corona is reached. Perhaps exotic phenomena such as spicules arise naturally from this awkward transition, as well as the obvious chromospheric canopy.

A critical property of chromospheric plasma is that it is partially ionized, which, independent of force bal;ance considerations, tends to reduce any $\mathbf{j}_\perp$ components present in the chromosphere. This was shown recently by T. Arber and colleagues in the context of flux emergence (Leake and Arber 2006, Arber et al. 2007). The physics of this process was first studied in the 1950s with Schlüter and Cowling. Under conditions where protons and electrons are *magnetized*, i.e. they undergo many gyrations around field lines between collisions, the charged particles are obliged to move with varying magnetic fields. But the neutrals are not. Any motion of the charged particles across field lines is quickly damped out via collisions, resulting in frictional heating. The cross-field conductivity is reduced and magnetic fields can slip more easily across the plasma. Cowling 1956 showed that this process was important in star formation. The chromosphere happens to be in a regime in which these conditions are met and there is an abundance of neutral atoms Goodman 2000. Taking results from Braginskii 1965, the work done against frictional forces is

$$Q_{fr} = \frac{j^2}{\sigma} + \left(\xi_n \mathbf{j} \times \mathbf{B} - \mathbf{G}\right)^2 / \alpha_n.$$

Here, σ is the usual scalar conductivity for a fully ionized plasma, $\mathbf{G} = \xi \nabla p - \nabla p_n$, ξ_n is the neutral fraction, p and p_n the total pressure and partial pressure due to neutrals, and $\alpha_n = m_n n_n / \tau_n$, τ_n the neutral collision time. Goodman, Arber and associates adopt $\mathbf{G} = 0$ to arrive at

$$Q_{fr} = \frac{j_\parallel^2}{\sigma} + \frac{j_\perp^2}{\sigma_\perp^*},$$

where the "Cowling conductivity" $\sigma_\perp^*$ is given by

$$\frac{1}{\sigma_\perp^*} = \frac{1}{\sigma}\left(1 + 2\xi_n \omega_e \tau_e \omega_i \tau_i\right),$$

and the term in brackets is > 1 when, as in the network chromosphere, the electrons and ions are magnetized ($\omega_e \tau_e > 1$, $\omega_i \tau_i > 1$ respectively, $\omega =$ gyro-frequency, $\tau_i =$ modified ion collision time). The net effect is that *cross field currents tend to be dissipated within the chromosphere.* The effects can be dramatic: Arber and collagues found that the chromospheric dissipation of $\mathbf{j}_\perp$ allowed more plasma to slip across fields, so that far less plasma was lifted up into the corona during flux emergence. The subsequent dynamics was then not subject to Rayleigh-Taylor instabilities which occur if the dissipation were switched off. This example clearly illustrates again the importance of chromospheric physics in getting the conditions at the base of the corona right. Sometimes observations suggest that cross-field currents exist within the corona, but this does not imply that dissipation of such currents within the underlying chromosphere is negligible. Instead it implies that gravitational and/or pressure gradient forces are significant.

Schlüter 1951 first pointed out that there are conditions where, in Braginskii's notation, $\mathbf{G} \approx \xi_n \mathbf{j} \times \mathbf{B}$. This is true for slow motions where pressure gradients have time to adjust to a varying $\mathbf{j} \times \mathbf{B}$ force. Such motion includes subsonic flows (certain phases of flux emergence through the chromosphere?), quasi- magnetostatic conditions and linear slow magnetosonic waves. Faster motions (fast modes, supersonic motion) experience the large Cowling dissipation rate, as do Alfvén waves which have identically $\mathbf{G} = \mathbf{0}$. This issue has not been addressed, to the author's knowledge, in the chromosphere, but is expected to be important.

```
October 19, 2005.  Add parag on what is meant by energy transport
and dissipation.  Parker's mechanism (diffusion of helium atoms/ions
through hydrogen) fails to reach the level of losses needed & other
obs. charcateristics would be hard to explain.  But, the transport
of energy is assumed to have been done and the energy stored in the
gravitational energy of heavy atoms.  The dissipation occurs as
these atoms move under the force of gravity, collide with the
hydrogen particles. The collisions ``randomize'' or ``thermalize''
the ordered motion, which is a heating mechanism.
```

3.3.1 The role of heat conduction

Coulomb collision cross sections decrease with energy of the impacting particles ϵ as ϵ^{-2}. In an ionized plasma, the mean free path between collisions is thus $\lambda \propto \epsilon^2/n$ where n is the particle density. When the plasma is sufficiently collisional that the distribution functions are close to LTE at temperature T, $\lambda \propto T^2/n$. The heat flux $\mathbf{q}$ carried by the particles is given by equation (**??**). Using the mean free path approximation (Gombosi 1994, section 4.3), $q = |\mathbf{q}|$ along $\mathbf{B}$ is on the order of

$$\begin{aligned} q &\approx n\frac{\langle u\rangle}{3}\frac{3}{2}k_B\left[(T+\lambda\frac{dT}{ds})-(T-\lambda\frac{dT}{ds})\right] \\ &\approx nk_B\,\lambda\,\langle u\rangle\,\frac{dT}{ds}, \end{aligned} \tag{3.2}$$

(Biermann and Ten Bruggencate 1947), where $\langle u\rangle/3$ is the mean thermal speed of the particles along $\mathbf{B}$, and s measures distance along $\mathbf{B}$. Because $\langle u\rangle \propto \sqrt{T/m}$ where m is the particle mass, electrons dominate q when $T_p \approx T_e$. Therefore the scalar conductivity K varies as $T_e^{5/2}$ (Spitzer 1965), so that heat conduction parallel to $\mathbf{B}$ becomes more effective in hotter plasmas. In contrast, in a gas consisting of rigid spheres (collision cross sections are constant with energy), K varies with just $T^{1/2}$.

The importance of parallel heat conduction in mediating coronal temperature fluctuations was recognized in the 1940s (Alfvén 1941, Giovanelli 1949,Van de Hulst 1953). When important, heat conduction serves as a thermostat, which is illustrated simply by analytical and numerical results from a static numerical model heated by the conductive damping of acoustic waves (McWhirter et al. 1975). In their calculations, an eight-fold increase in the mechanical energy flux deposited in the corona was accompanied only by a 46% increase in T_e. Throughout most of their model, the electron pressure p_e is nearly constant $\approx p_0$, and the energy balance is between field-aligned conduction and optically thin radiative losses:

$$\frac{d}{ds}\left(kT_e^{5/2}\frac{dT_e}{ds}\right) - A_R n_e^2 T_e^{-1/2} \approx 0, \tag{3.3}$$

where $A_R = 5\times10^{-33}$ W m^3 K$^{1/2}$ defines their radiative loss function. Using $p_e = p_0$, the solution to equation (3.3) is

$$T_e^3 = 3\left(\frac{2A_R}{k}\right)^{1/2}\frac{p_0}{k_B}s = 6.9\times10^{12}\,p_0 s, \quad \text{or} \tag{3.4}$$

$$T_e = 1.9\times10^4\,(p_0\,s)^{1/3}\ \ \text{K}, \tag{3.5}$$

The energy flux density needed to support the radiative losses is

$$F = (2A_R k)^{1/2}\frac{p_0}{k_B}T_e^{1/2} = 23\,p_0\,T_e^{1/2}\ \ \text{W m}^{-2}. \tag{3.6}$$

Eliminating first T_e and then p_0 using equations (3.5) and (3.6),

$$F = 23\,p_0^{7/6}s^{1/6}\ \ \text{W m}^{-2}, \text{ and} \tag{3.7}$$

$$F = \frac{k}{3}\frac{T_e^{7/2}}{s} = 3.3\times10^{-12}\,\frac{T_e^{7/2}}{s}\ \ \text{W m}^{-2}. \tag{3.8}$$

It is remarkable that, armed only with equations (3.7) and (3.8), and with simple assumptions concerning the distribution of F across the solar surface, one can explain qualitatively many of the salient thermal features of the corona, as seen in Figure 1.9, for example.

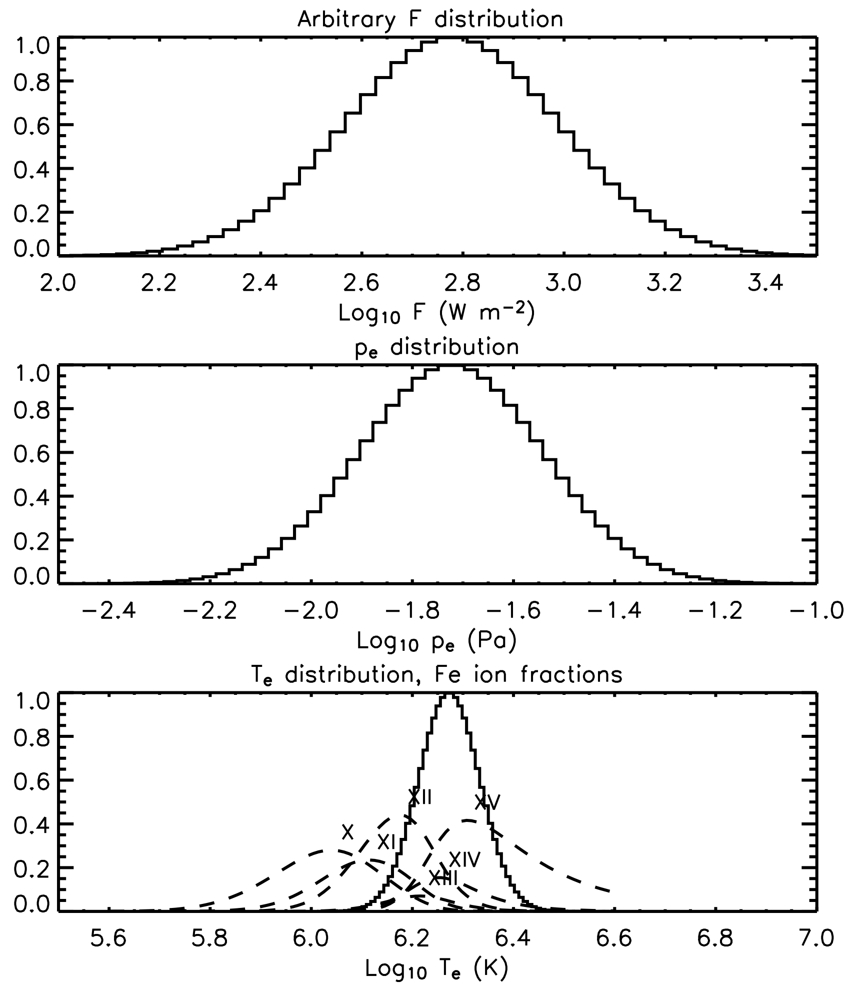

Figure 3.2: A log-normal distribution of dissipated mechanical flux densities F for a coronal structure of length $s = 5 \times 10^7$ m is shown in the top panel. Distributions of coronal electron pressure p_0 and temperature T_e from equations (3.7) and (3.8) are shown in the lower panels. The bottom panel also shows ionization fractions of coronal ions of iron. The distribution for p_0 is similar to that for F, but that for T_e is far narrower. Given a narrow enough distribution for F on the solar surface, the EUV and X-ray corona should appear almost isothermal, but the intensities should vary considerably as F varies across the solar surface.

– First, equation (3.7) shows that, for a magnetic structure of fixed length s, determined for example by a potential, force-free or magnetostatic magnetic field, the pressure of the corona should vary almost linearly with the energy flux density ($p_0 \propto F^{6/7} s^{-1}$). These equilibrium calculations implicitly assume that, as F changes and a new equilibrium is established, material is either condensed to or evaporated from chromospheric plasma to provide lower or higher values of p_0. This point again emphasizes the coupling between corona and chromosphere.

– Second, equation (3.8) shows that the corona acts as a thermostat, with $T_e \propto (F\,s)^{2/7}$. The exponent simply arises from the inverse of the dimensional dependence of F on T_e, and is independent of the assumed form for the radiation losses.

– Third, the electron density scales as $n_e \propto F^{4/7}\,s^{-3/7}$, and so $n_e^2 \propto F^{8/7}\,s^{-6/7}$. Since the intensities I of X-rays or EUV emission lines depend on $\int n_e^2(z)\ G_i(T_e(z))\,dz$ (equation B.8), $I \propto F^{8/7}\,s^{-6/7}\Delta z$ where Δz is the thickness of the structure along the line-of-sight.

These scalings enable one to argue how the corona should appear in X-rays and EUV lines, in response to varying flux densities F for a given s. Figure 3.2 shows schematically how p_0 and T_e vary with an arbitrary (log-normal) distribution of flux densities F for a given s of 5×10^7 m. For distributions of F with FWHM $\lesssim 1$ in $\log_{10}F$ at the coronal base, *the corona should appear almost isothermal*, because the logarithmic width of the distribution function for T_e is 2/7 that for F, and it is narrower than widths of typical $G_i(t)$ functions which depend mostly on atomic processes determining the ionization fractions. At the same time, the X-ray and EUV intensities should vary as $F^{8/7}s^{-6/7}\Delta z$. *The X-ray and EUV intensities should vary considerably from place to place as F and Δz vary, while appearing nearly isothermal.* These results might explain simply the large-scale "order" seen in Figure 1.9, namely the large and separate apparently isothermal regions, *if* F is similar in magnitude across the quiet Sun, and F is considerably higher in active regions and bright points. (The energy balance of coronal holes must take account of the flow of enthalpy in the energy equation e.g., Withbroe and Noyes 1977).

The considerations may also resolve a conundrum pointed out by Litwin and Rosner (1993). They sought a mechanism for efficiently transporting heat *across* magnetic field lines in the corona, to explain why active region plasma loops are apparently isothermal (see section **??**). The above analysis shows that cross-field transport may not be needed at all. Field-aligned heat conduction provides a natural thermostat to explain this phenomenon.

l Shmeleva and Sy-
1973 as another exam-
ling laws

These results were obtained from an energy equation (3.3) which contains *no explicit heating term.* Rosner et al. (1978) (henceforth "RTV") derived identical results, applied to conditions at the apex of a symmetric plasma loop, but they included a heating mechanism which deposited energy (per unit volume) uniformly along a plasma loop. The results are identical because McWhirter et al.'s assumptions of constant pressure and dominance of heat conduction are also valid in the RTV models. Thus, the dominance of field-aligned heat conduction in the energy equation renders the thermal structure of the corona, unfortunately, *relatively insensitive to the heating function.* For some reason the set of equations (3.4) to (3.8) have become attributed to Rosner et al. and they have become known as the "RTV laws", even though they appeared in earlier literature.

```
...add Hearn's minimum flux theory
...add CJ's and others attempt to get heating as fn. Te- fruitless
   because it is invalid perhaps?
...add need to remove deposited energy below 10^5K
```

3.3.2 Pressure balance

The body forces $\mathbf{F}$ in the momentum equation (**??**) to be considered are gravity and the Lorentz force:

$$\mathbf{F} = -\frac{GM_\odot \rho}{r^2}\hat{\mathbf{r}} \qquad + \qquad \underbrace{\frac{1}{\mu_0}\mathbf{curl}\,\mathbf{B} \times \mathbf{B}}_{-\mathbf{grad}\left(\frac{B^2}{2\mu_0}\right) + \frac{d}{dx}|_{\hat{\mathbf{b}}}\left(\frac{B^2}{\mu_0}\right)\ \hat{\mathbf{b}},} \tag{3.9}$$

where $\frac{d}{dx}|_{\hat{\mathbf{b}}}$ is the spatial derivative along the direction of the magnetic field specified by the unit vector $\hat{\mathbf{b}}$. The electric field is zero in the frame of reference of the plasma, because of the large conductivity. The forces arising from pressure gradients in the fluid and magnetic fields are both of the form $-\mathbf{grad}\,(scalar)$, so one can define the "plasma-β" measuring the ratio of the fluid pressure to that of the magnetic field:

$$\beta = p/\frac{B^2}{2\mu_0} \tag{3.10}$$

In the lower atmosphere of the Sun, the particle temperatures are relatively low, so the forces are dominated by gravity and steep vertical pressure gradients. Any imbalance in these forces makes the LHS of equation (**??**) evolve rapidly (via acoustic-gravity waves) to a state of hydrostatic equilibrium, given by:

$$\frac{dp}{dz} = -\rho g; \quad g = GM_\odot/R_\odot^2. \tag{3.11}$$

With equation (**??**) the pressure scale height is

$$H_{HSE} = -\left(d\,ln\,p/dz\right)^{-1} = p/\rho g = \frac{k_B T}{\overline{\mu} m_H g}. \tag{3.12}$$

For the photosphere and chromosphere, $T \approx 6000$ K, $H_{HSE} = 1.43 \times 10^5$ m. In the corona where $T \approx 10^6$ K, it is 5×10^7 m, an order of magnitude less than $R_\odot$ (Table 1.1). The top of the chromosphere is typically 2×10^6 m, ≈ 14 scale heights, above the photosphere (Vernazza et al. 1981): the fluid pressure thus drops exponentially by over 6 orders of magnitude between the photosphere and base of the corona. In contrast, the magnetic field strength drops at most algebraically with height z. A dipole field seated at height z_0 varies as $(z - z_0)^{-3}$, for example. Hence, for a given distribution of photospheric magnetic field, the average plasma-β must decrease rapidly with height throughout the photosphere and chromosphere. Under typical quiet conditions (Table 1.2) the $\beta = 1$ surface lies in the upper chromosphere (Figure **??**). This surface marks the layer where magnetic stresses begin to dominate in the force balance, so that when $\beta \lesssim 0.1$, say, the magnetic field should be almost "force free" (i.e. $\mathbf{j} \times \mathbf{B} \approx 0$) because there is little to compete with this force in the momentum equation. Furthermore, when $\beta < 1$ the magnetic field tends to fill the available space, and because $c_S \approx c_A$ in this layer, the phase speeds of acoustic and Alfvén waves become equal, potentially leading to mode conversion (see section 2.5.4). Metcalf et al. (1995) were able to show that for an active region, the magnetic field is not "force-free" below roughly 400 km above the photosphere, but is force-free above this height. This height corresponds to the $\beta = 0.1$ surface, as expected.

A quantity related to the plasma β is the ratio of the kinetic fluid stresses (the $\rho\mathbf{uu}$ term in equation **??**) to the magnetic stresses. The kinetic fluid stresses are not of the form $-\mathbf{grad}\,(scalar)$, but nevertheless the magnitude of the $\rho\mathbf{uu}$ term is ρu^2 and the ratio analogous to β is

$$|\rho\mathbf{uu}|/(\frac{B^2}{2\mu_0}) \sim u^2/c_A^2. \tag{3.13}$$

In the convection zone and photosphere of the Sun, plasma motions are vigorous but typically sub-sonic yet super-Alfvénic, so that this ratio is still $\gg 1$. Thus the magnetic field is forced by the plasma motions in these layers.

3.4 Coronal heating by current sheet formation

3.5 Coronal heating by wave motions

3.6 Limitations of MHD

Chapter 4

Plasma processes

```
Solar wind results from radio and SoHO (UVCS) -
evidence for high frequency processes (f > ion
gyrofrequencies) - careful assessment - turbulent
fields
```

4.1 Bohm diffusion

In the framework of near-LTE kinetic theory, Braginskii gives an estimate of the magnitude of the effects of plasma turbulence on the kinetic transport coefficients discussed in section 2.1. Assuming that the plasma generates fluctuating electric fields of amplitude E', which become spatially uncorrelated over length scales ℓ', the fields cause particle drifts with speeds $w' \sim E'/B$ which become uncorrelated over length scales ℓ'. Using equation (2.39), we find a "turbulent" diffusion coefficient by using w' and ℓ' in place of the particle mean free path and thermal speed, so that

$$D_{\text{turb}} \sim \ell' w' \sim E'\ell'/B \tag{4.1}$$

If the amplitudes of the turbulence are limited by the supply of thermal energy, and the turbulence is fully developed, then we expect $\mathcal{Q}_a E'\ell' \sim k_B T_a$, whence

$$D_{\text{turb}} \sim \frac{k_B T_a}{\mathcal{Q}_a B} \tag{4.2}$$

Bohm (1949) published an expression of the same form, but multiplied by the numerical factor 1/16, without justification. Note that the ratio of equation (4.2) to the classical cross-field expression (equation (2.39) with $\Delta = r_a$) is

$$\frac{D_{\text{turb}}}{r_a^2/\tau_a} \sim \omega_a \tau_a. \tag{4.3}$$

Thus, in magnetized plasmas, turbulence can cause substantial enhancements in cross-field diffusion of mass, momentum and energy.

Chapter 5

Some clues from laboratory plasma experiments

The power of laboratory measurements to illuminate challenging problems in astrophysics was demonstrated already by the work of Kirchoff and Bunsen in the 1850s and 1860s, which provided a physical basis for understanding the solar Fraunhofer spectrum, and its "reversal" seen during later eclipses by Young. Marking perhaps the beginning of modern astrophysics, with an abiding interest in the Sun and stellar evolution, Hale wanted to understand the thermal properties of sunspots. His laboratory work (e.g. Hale et al. 1906) demonstrated his earlier contention that

> "...the correlated study of solar, stellar and laboratory phenomena offers a most promising means of attacking the problem of stellar evolution" – cited by Goldberg (1953).

Of course, laboratory plasma physics can help illuminate the coronal heating problem.

...

Chapter 6

Conclusions

TBD . . . new missions/experiments

We shall not cease from exploration
and the end of all our exploring
will be to arrive where we started
And know the place for the first time.

–T. S. Eliot

Appendix A

Useful vector and tensor algebra

Some knowledge of Cartesian tensors is useful. They are defined through their invariance to rotational coordinate transformations (see chapter 15 of Riley 1974, for example). Scalars, position vectors, and "dyads" are examples of tensors of zeroth, first and second order respectively. A dyad $\mathbf{x}\,\mathbf{y}$ is simply an array constructed from two first order tensors (e.g. position vectors, velocities, forces) $\mathbf{x}$, $\mathbf{y}$ such that the i^{th} and j^{th} component of $\mathbf{x}\,\mathbf{y}$ is

$$\mathbb{Z}_{ij} = (\mathbf{x}\,\mathbf{y})_{ij} = x_i y_j.$$

Any second order tensor can be written as a linear combination of three dyads. Tensor operators ":", "·" and the unit tensor $\mathbb{1}$ are defined as

$$\mathbb{Y} : \mathbb{Z} = \sum_{i,j} \mathbb{Y}_{ij}\mathbb{Z}_{ij}, \quad (\mathbb{Y}\cdot\mathbb{Z})_{ij} = \sum_k \mathbb{Y}_{ik}\mathbb{Z}_{kj}, \quad (\mathbb{Y}\cdot\mathbf{x})_i = \mathbb{Y}_{ij}x_j, \quad \mathbb{1}\cdot\mathbb{Z} = \mathbb{Z}\cdot\mathbb{1} = \mathbb{Z}$$

Then

$$\mathbf{xy} : \mathbb{Z} = \mathbf{y}\cdot\mathbb{Z}\cdot\mathbf{x} = \mathbb{Z} : \mathbf{xy}, \quad \text{and in particular } \mathbb{1} : \mathbf{xy} = \mathbf{y}\cdot\mathbb{1}\cdot\mathbf{x}.$$

The "×" operator has the following property

`add more to enable readers to figure out ‘‘x’’ operator...`

$$(\mathbb{1}\times\mathbb{1}) : \mathbf{xy} = \mathbf{y}\cdot(\mathbb{1}\times\mathbb{1})\cdot\mathbf{x} = \mathbf{y}\times\mathbf{x}.$$

Any second order tensor $\mathbb{A}$ can be decomposed as

$$\mathbb{A} = \overset{\circ}{\mathbb{A}} - \mathbb{A}^{\vee}\times\mathbb{1} + \frac{1}{3}\overset{\times}{A}\,\mathbb{1}. \tag{A.1}$$

Here, $\overset{\times}{A}$ is the trace of $\mathbb{A}$, $\mathbb{1}$ the unit tensor, $\mathbb{A}^{\vee} = -\frac{1}{2}\mathbb{1}\times\mathbb{1} : \mathbb{A}$ is the "vector" of $\mathbb{A}$, $\mathbb{A}^s = \frac{1}{2}(\mathbb{A} + \widetilde{\mathbb{A}})$ is the symmetric component of $\mathbb{A}$, and $\overset{\circ}{\mathbb{A}} = \mathbb{A}^s - \frac{1}{3}\mathbb{1}\,\overset{\times}{A}$ is the "deviator" of $\mathbb{A}$. $\widetilde{\mathbb{A}}$ is the transpose of $\mathbb{A}$. This decomposition has several important properties. $\overset{\circ}{\mathbb{A}}$ and $\overset{\times}{A}$ are symmetric and $\mathbb{A}^{\vee}$ is antisymmetric, $\overset{\circ}{\mathbb{A}}$, $\mathbb{A}^{\vee}$ and $\overset{\times}{A}$ are "orthogonal" in the sense that

$$\mathbb{A} : \mathbf{B} = \overset{\circ}{\mathbb{A}} : \overset{\circ}{\mathbb{B}} + 2\mathbb{A}^{\vee} : \mathbb{B}^{\vee} + \frac{1}{3}\overset{\times}{A}\overset{\times}{B}, \tag{A.2}$$

i.e. there are no cross-terms. For details see section 1.10 of Woods (1987).

An example of a useful tensor decomposition includes the tensor $\mathbb{A} = \nabla\mathbf{w}^{\vee}$ where $\mathbf{w}$ is a fluid velocity. Then $\nabla\mathbf{w}^{\vee} = \frac{1}{2}\nabla\times\mathbf{w} = \mathbf{\Omega}$, where $\mathbf{\Omega}$ is the angular velocity of the fluid undergoing rigid body rotation. Thus, the $\nabla \mathbf{w}^{\vee}$ component of $\nabla \mathbf{w}$ contains no compression or shear and thus does not contribute to viscosity. That this is clear mathematically can be seen because the stress tensor $\boldsymbol{\pi}$ is symmetric, so that $\boldsymbol{\pi}^{\vee} = 0$, and then the dissipative term in the energy equation becomes

$$\boldsymbol{\pi} : \nabla \mathbf{w} = \overset{\circ}{\boldsymbol{\pi}} : \overset{\circ}{\nabla \mathbf{w}} + \frac{1}{3} \overset{\times}{\pi} \operatorname{div} \mathbf{w}, \tag{A.3}$$

because $\overset{\times}{\nabla \mathbf{w}} = \operatorname{div} \mathbf{w}$. Equation (A.3) is thus a simplified form of equation (A.2), and furthermore the two terms can be identified with shear and compression as done in the main text.

Rotational symmetry

Under the conditions of local rotational symmetry, in particular about a magnetic field $\mathbf{B}$, it is convenient to define three orthogonal vectors. Given

$$\mathbf{h} = \mathbf{B}/B,$$

any other vector $\mathbf{u}$ can be decomposed into the three orthogonal compnents:

$$\mathbf{u}_{\parallel} = \mathbf{h}(\mathbf{u} \cdot \mathbf{h}), \quad \mathbf{u}_{\perp} = \mathbf{h} \times (\mathbf{u} \times \mathbf{h}), \quad \text{and } \mathbf{u}_{\wedge} = \mathbf{u} \times \mathbf{h}. \tag{A.4}$$

Where $\mathbf{u}_{\perp}$ is also identically

$$\mathbf{u}_{\perp} \equiv \mathbf{u} - \mathbf{u}_{\parallel}$$

.

It is also convenient to define the equivalent second order tensors $\mathbb{A}$, which have lateral isotropy about $\mathbf{h}$ if and only if $\mathbf{h} \times \mathbb{A} = \mathbb{A} \times \mathbf{h}$. The most general tensor satisfying this is (p. 59 of Woods 1987):

$$\mathbb{A} = \alpha_{\parallel} \mathbb{1}_{\parallel} + \alpha_{\perp} \mathbb{1}_{\perp} + \alpha_{\wedge} \mathbb{1}_{\wedge}, \tag{A.5}$$

where

$$\mathbb{1}_{\parallel} = \mathbf{hh}, \quad \mathbb{1}_{\perp} = \mathbb{1} - \mathbf{hh}, \quad \mathbb{1}_{\wedge} = \mathbf{h} \times \mathbb{1}, \tag{A.6}$$

and where $\alpha_{\parallel}$ and $\alpha_{\perp}$ are even functions of $\mathbf{h}$ (e.g. a scalar), and $\alpha_{\wedge}$ is an odd function. For example, the electrical conductivity tensor is

$$\boldsymbol{\sigma} = \sigma_{\parallel} \mathbf{hh} + \sigma_{\perp} (\mathbb{1} - \mathbf{hh}) + \sigma_{\wedge} \mathbf{h} \times \mathbb{1} \tag{A.7}$$

where $\sigma_{\parallel}$ and $\sigma_{\perp}$ are even in $\mathbf{h}$, and $\sigma_{\wedge}$ is odd. On choosing $\mathbf{h}$ along the z-axis, this becomes

$$\begin{pmatrix} \sigma_{\perp} & \sigma_{\wedge} & 0 \\ -\sigma_{\wedge} & \sigma_{\perp} & 0 \\ 0 & 0 & \sigma_{\parallel} \end{pmatrix}. \tag{A.8}$$

The conductivity in the field-free case is, by comparison, $\sigma \mathbb{1}$.

A common vector equation arising in magnetized plasmas involves solving for vector $\mathbf{A}$ in terms of $\mathbf{C}$ given

$$\left[a_{\parallel} \mathbf{hh} + a_{\perp} (\mathbb{1} - \mathbf{hh}) + a_{\wedge} \mathbf{h} \times \mathbb{1} \right] \cdot \mathbf{A} = \mathbf{C} \tag{A.9}$$

The solution is simply

$$\mathbf{A} = \left[c_{\parallel} \mathbf{hh} + c_{\perp} (\mathbb{1} - \mathbf{hh}) + c_{\wedge} \mathbf{h} \times \mathbb{1} \right] \cdot \mathbf{C} \tag{A.10}$$

where

$$c_\parallel = \frac{1}{a_\parallel}, \quad c_\perp = \frac{a_\perp}{a_\perp^2 + a_\wedge^2}, \quad c_\wedge = \frac{-a_\wedge}{a_\perp^2 + a_\wedge^2} \tag{A.11}$$

(Woods 1987).
As an example consider equation (2.95):

$$\mathbf{E}^\dagger = \frac{1}{\sigma_\parallel}\mathbf{j}_\parallel + \frac{1}{\sigma_\perp}\mathbf{j}_\perp + \frac{1}{\sigma_\wedge}\mathbf{j}_\wedge,$$

which is of the form of equation (A.9), with vectors $\mathbf{C}$ and $\mathbf{A}$ chosen as $\mathbf{E}^\dagger$ and $\mathbf{j}$ respectively, because of the dot product of the second order tensor with $\mathbf{A}$. The solution for $\mathbf{j}$ in terms of components $\mathbf{E}^\dagger_\parallel$, $\mathbf{E}^\dagger_\perp$ and $\mathbf{E}^\dagger_\wedge$ follows immediately, yielding

$$\mathbf{j} = \sigma_\parallel \mathbf{E}^\dagger_\parallel + \frac{\sigma_\perp}{1 + \sigma_\perp^2/\sigma_\wedge^2}\mathbf{E}^\dagger_\perp - \frac{\sigma_\wedge}{1 + \sigma_\wedge^2/\sigma_\perp^2}\mathbf{E}^\dagger_\wedge$$

which, with $\sigma_\perp = \omega_e \tau_e \sigma_\wedge$, gives equation (2.97).

Appendix B

Differential Emission Measures

Differential emission measures $\xi(T_e)$ are the solution to the problem of the inversion of emission line intensities, when the emission lines are formed under certain conditions: Only 2 body collisions are important (the "coronal approximation", this is valid at low densities); stimulated emission can be neglected (valid for solar lines between X-ray and UV wavelengths) ; the gas is optically thin to all radiation that can effect the level populations n of the ions of interest; statistical equilibrium is valid *i.e.* $Dn_i/Dt = 0$; the electron distribution function is Maxwellian; the gas is fully ionized; the elemental abundances are constant.

Under optically thin conditions, the emergent intensity at frequency ν from the top of a slab of thickness z viewed at an angle θ to the normal of the slab is

$$I_{\nu\mu}(z) = \int_0^z \epsilon_\nu(z)\ \frac{dz}{\mu}\ + I_{\nu\mu}(0) \quad \mathrm{W\ m^{-2}\ sr^{-1}\ hz^{-1}}, \tag{B.1}$$

where $\mu = \cos(\theta)$. $I_{\nu\mu}(0)$ is the background specific intensity, which at UV wavelengths is usually weak and only weakly dependent on frequency. By measuring intensities at frequencies adjacent to the emission line, this is subtracted from both sides of the equation, to yield the contribution to the intensity from the line alone. The line emissivity at frequency ν is

$$\epsilon_\nu(z) = \frac{h\nu}{4\pi}\ \phi_\nu\ n_u^i(z) A_{u\ell}\ \mathrm{W\ m^{-3}\ sr^{-1}\ hz^{-1}} \tag{B.2}$$

where $n_u^i(z)$ is the population density of the upper level of radiative transition i, ϕ_ν is the emission line profile (normalized so that $\int_0^\infty \phi_\nu\ d\nu = 1$) and $A_{u\ell}$ is the Einstein A-coefficient of the transition. Integrating over all frequencies, the total line intensity becomes

$$I_i = \frac{h\nu_i}{4\pi} \int_z n_u^i(z) A_{u\ell}\ dz \quad \mathrm{W\ m^{-2} sr^{-1}}. \tag{B.3}$$

For illustration consider an atom with two atomic levels. In practical cases more detailed calculations of level population densities are made. In statistical equilibrium, the transition rate to the upper level u equals that from the lower level ℓ:

$$n_\ell C_{\ell u} = n_u(A_{u\ell} + C_{u\ell}) \approx n_u A_{u\ell} \tag{B.4}$$

The last approximation is valid when $A_{u\ell} \gg C_{u\ell}$, usually valid at low densities in the corona/transition region. With equation (B.3)

$$I_i = \frac{h\nu_i}{4\pi} \int_z n_\ell^i(z) C_{\ell u}\ dz \quad \mathrm{W\ m^{-2} sr^{-1}}. \tag{B.5}$$

The coefficient for collisional excitation can be written as:

$$C_{\ell u} = 8.63 \times 10^{-12} \frac{\Upsilon_{\ell u}(T_e)}{g_\ell \sqrt{T_e}} \exp(-E_{\ell u}/k_B T_e)\; n_e \quad \sec^{-1}. \tag{B.6}$$

Here, $\Upsilon_{\ell u}(T_e)$ is the Maxwellian-averaged collision strength, g_ℓ the degeneracy of level ℓ, and $E_{\ell u}$ is the difference in energy between the two levels. The population of the lower level can be written as:

$$n_\ell = \frac{n_\ell}{n_{ion}} \frac{n_{ion}}{n_{el}} \frac{n_{el}}{n_H} \frac{n_H}{n_e} n_e, \tag{B.7}$$

where n_{ion}, n_{el}, n_e and n_H are the population densities of the ion and element to which the transition belongs, electrons and hydrogen respectively. Now $n_\ell/n_{ion} \approx 1$, and n_{ion}/n_{el} is the ionization fraction, which at low densities in statistical equilibrium is a function of T_e only. n_{el}/n_H is constant by assumption. For a fully ionized plasma with solar abundances, $n_H/n_e \approx 0.8$. These conditions make n_u a product of n_e^2 with a function of T_e only. Using equations (B.6), (B.7) and (B.5),

$$I_i = \int_z n_e^2 G_i(T_e)\; dz \quad \mathrm{W\ m^{-2} sr^{-1}}, \tag{B.8}$$

where $G_i(T_e)$ is determined by atomic properties alone, under the assumptions made. The $G_i(T_e)$ functions for most coronal ions are simple (Gaussian-like) peaks with full widths at half-peak of ≈ 0.3 in $\log_{10} T_e$ (e.g., House 1964, Seaton 1964, Pottasch 1964, Jordan 1969). Transform independent variable from z to T_e via

$$n_e^2(z) G_i(T_e(z)) dz = \xi(T_e) G_i(T_e) dT_e, \tag{B.9}$$

where $\xi(T_e)$, the differential emission measure, is to be understood as a positive-definite distribution function. It is fixed by the plasma thermal structure alone, such that along the line of sight, any plasma between T_e and $T_e + dT_e$ which has density $n_e(T_e)$ and a thickness $dz(T_e)$, $\xi(T_e)dT_e = n_e^2(T_e)dz(T_e)$.

Craig and Brown (1976) give a formal mathematical definition of $\xi(T_e)$ in terms of the geometry of the thermal plasma structure. To visualize the differential emission measure, one can imagine the plasma volume filled with an arbitrary distribution of electrons at a distribution of temperatures. In principle, though not in practice, $n_e(T_e)$ for the plasma could be measured between T_e and $T_e + dT_e$, and $n_e^2(T_e)$ plotted as a function of T_e. Similarly, the path lengths $dz(T_e)$ could be determined for those populations of electrons with temperatures between T_e and $T_e + dT_e$, and the product $n_e^2(T_e)dz(T_e)/dT_e$, the differential emission measure, plotted as a histogram. Understanding dz/dT_e in terms of this distribution function, and not strictly a differential, we can write

$$\xi(T_e) = n_e^2 \frac{dz}{dT_e}, \qquad \left(\frac{dz}{dT_e} \text{ not formally a differential}\right). \tag{B.10}$$

The line intensity becomes

$$I_i = \int_{T_e} \xi(T_e) G_i(T_e) dT_e \tag{B.11}$$

$\xi(T_e)$ can be determined, to within well-documented mathematical ambiguities (e.g., Craig and Brown 1986), from a set of measurements of I_i and their corresponding functions $G_i(T_e)$ by inverting this integral equation.

ξ is often written as a function of $\tau = \ln T_e$, or $t = \log_{10} T_e$ so that

$$\xi(\tau) = n_e^2 \frac{dz}{d \ln T_e} = T_e \, \xi(T_e) \tag{B.12}$$

and

$$\xi(t) = n_e^2 \frac{dz}{d \log_{10} T_e} = \log_{10} \mathrm{e} \; T_e \, \xi(T_e) \tag{B.13}$$

Frequently, because the functions $G(T_e)$ are roughly the same width when plotted against t, integrals of $\xi(t)$ over a constant width Δt are given. Thus, for example, Raymond and Doyle (1981) determine $\xi_{0.1}(t)$, where

$$\xi_{0.1}(t) = \int_{-0.05}^{+0.05} \xi(t) dt = 0.1 \overline{\xi(t)} = 0.1 \; \overline{\log_{10} \mathrm{e} \; T_e \, \xi(T_e)}, \tag{B.14}$$

and where $\overline{\xi(t)}$ is the average value over the temperature range.

Observational determination of ξ allows one to examine terms in the energy equation with temperature as the independent variable, since the radiation losses integrated along the line of sight through the plasma are simply

$$\int_{\Delta s} Q_R(t) ds = -\xi(t) \, P_R(t) \quad \mathrm{W \ m^{-2}} \tag{B.15}$$

where $P_R(t)$ is the radiated power divided by n_e^2. P_R is a function of temperature alone to a good approximation (e.g., Cox and Tucker 1969).

Lastly, $\xi(t)$ can directly reflect heating mechanisms when other assumptions are brought to bear (e.g., Jordan 1992). For example, in a 1D conductively dominated plasma at constant pressure p and electron pressure p_e, $\mathrm{div}\, \mathbf{q} = k_{\|} T_e^{5/2} dT_e/dz =$ constant, so $dz/dt \propto T_e^{7/2}$. Then

$$\xi(t) = \left(\frac{p_e}{k_B T_e} \right)^2 \frac{dz}{dt} \propto T_e^{3/2}.$$

Between $T_e = 10^5$ and 2×10^6K, measurements have consistently shown that $\xi(t) \propto T_e^{3/2}$, in both quiet and active regions, when proper account of expanding geometry is used to evaluate the divergence of the conductive flux density $\mathbf{q}$ (Jordan 1976).

Bibliography

Alfvén, H.: 1941, "??", *Ark. Mat. Astron. Fys.* 27A(25)

Alfvén, H.: 1947, "Magneto hydrodynamic waves, and the heating of the solar corona", *Mon. Not. R. Astron. Soc.* **107**, 211–219

Allen, C. W.: 1973, *Astrophysical Quantities*, Athlone Press, Univ. London

Anderson, L. S. and Athay, R. G.: 1989, "Chromospheric and Coronal Heating", *Astrophys. J.* **336**, 1089–1091

Arber, T. D., Haynes, M., and Leake, J. E.: 2007, "Emergence of a Flux Tube through a Partially Ionized Solar Atmosphere", *Astrophys. J.* **666**, 541–546

Aschwanden, M. J., Winebarger, A., Tsiklauri, D., and Peter, H.: 2007, "The Coronal Heating Paradox", *Astrophys. J.* **659**, 1673–1681

Athay, R. G. and White, O. R.: 1978, "Chromospheric and coronal heating by sound waves", *Astrophys. J.* **226**, 1135

Athay, R. G. and White, O. R.: 1979, "Chromospheric oscillations observed with OSO 8. II. average power spectra for Si II.", *Astrophys. J. Suppl. Ser.* **39**, 333–346

Benz, A. O.: 2008, "Flare Observations", *Living Reviews in Solar Physics* **5**, 1

Berger, T. E., De Pontieu, B., Schrijver, C. J., and Title, A. M.: 1999, "High-resolution Imaging of the Solar Chromosphere/Corona Transition Region", *Astrophys. J. Lett.* **519**, L97–L100

Berger, T. E., Schrijver, C. J., Shine, R. A., Tarbell, T. D., Title, A. M., and Scharmer, G.: 1995, "New Observations of Subarcsecond Photospheric Bright Points", *Astrophys. J.* **454**, 531

Biermann, L.: 1946, "??", *Naturwiss.* **33**, 118–??

Biermann, L.: 1947, " ", *Naturwiss.* **34**, 87

Biermann, L.: 1948, "Über die Ursache der chromosphärischen Turbulenz und des UV-Exzesses der Sonnenstrahlung", *Zeitschrift für Astrofysik* **25**, 161–177

Biermann, L. and Ten Bruggencate, P.: 1947, "Über die Ursachen der hohen Temperatur der Sonnenkorona nebst einer Bemerkung über das Nachthimmellicht", *Veroeffentlichungen der Universitaets-Sternwarte zu Goettingen* **5(83)**, 223–228

Bigelow, F. H.: 1889, *The Solar Corona*, Smithsonian Institution, Washington, D. C.

Billings, D. E.: 1966, *A guide to the solar corona*, Academic Press, New York

Bird, M. K. and Edenhofer, P.: 1990, *Physics of the Inner Heliosphere I. Large-Scale Phenomena.*, Vol. 20 of *Physics and Chemistry in Space*, Chapt. 2. Remote Sensing Observations of the Solar Corona, 13–97, Springer-Verlag, Berlin Heidelberg

Bogdan, T. J., Rosenthal, C. S., Carlsson, M., Hansteen, V., McMurry, A., Zita, E. J., Johnson, M., Petty-Powell, S., McIntosh, S. W., Nordlund, Å., Stein, R. F., and Dorch, S. B. F.: 2002, "Waves in magnetic flux concentrations: The critical role of mode mixing and interference", *title* **323**, 196–202

Bohm, D.: 1949, "?", in A. Guthrie and R. K. Wakerling (Eds.), *The Characteristics of Electrical Discharges in Magnetic Fields*, McGraw-Hill, New York, ?

Boland, B. C., Engstrom, S. F. T., Jones, B. B., and Wilson, R.: 1973, "The Heating of the Solar Corona. I. Observation of Ion Energies in the Transition Zone", *Astron. Astrophys.* **22**, 161

Braginskii, S. I.: 1965, "Transport processes in a plasma", *Reviews of Plasma Physics.* **1**, 205–311

Bray, R. J., Cram, L. E., Durrant, C. J., and Loughhead, R. E.: 1991, *Plasma Loops in the Solar Corona*, Cambridge Astrophysics Series, Cambridge University Press, Cambridge, England

Brynildsen, N., Maltby, P., Fredvik, T., and Kjeldseth-Moe, O.: 2002, "Oscillations Above Sunspots", *Solar Phys.* **207**, 259–290

Burgess, A.: 1964, "Dielectronic recombination and the temperature of the solar corona", *Astrophys. J.* **139**, 776

Burgess, A. and Seaton, M. J.: 1964, "The ionization equilibrium for iron in the solar corona", *Mon. Not. R. Astron. Soc.* **127**, 355–358

Cauzzi, G., Reardon, K. P., Uitenbroek, H., Cavallini, F., Falchi, A., Falciani, R., Janssen, K., Rimmele, T., Vecchio, A., and Wöger, F.: 2008, "The solar chromosphere at high resolution with IBIS. I. New insights from the Ca II 854.2 nm line", *Astron. Astrophys.* **480**, 515–526

Chapman, G. A.: 1981, "Active regions from the photosphere to the chromosphere", in F. Q. Orrall (Ed.), *Solar Active Regions: A monograph from Skylab Solar Workshop III*, 43–82

Chapman, S. and Cowling, T. G.: 1970, *The mathematical theory of non-uniform gases. An account of the kinetic theory of viscosity, thermal conduction and diffusion in gases*, Cambridge University Press, Oxford, 3rd edition

Cowling, T. G.: 1953, "Solar Electrodynamics", in G. P. Kuiper (Ed.), *The Sun*, Chicago University Press, Chicago, 532—591

Cowling, T. G.: 1956, "The dissipation of magnetic energy in an ionized gas", *Mon. Not. R. Astron. Soc.* **116**, 114–124

Cox, D. P. and Tucker, W. H.: 1969, "Ionization Equilibrium and Radiative Cooling of a Low-Density Plasma", *Astrophys. J.* **157**, 1157–1167

Craig, I. J. D. and Brown, J. C.: 1976, "Fundamental Limitations of X-Ray Spectra as Diagnostics of Plasma Temperature Structure", *Astron. Astrophys.* **49**, 239–250

Craig, I. J. D. and Brown, J. C.: 1986, *Inverse problems in astronomy*, Hilger, Bristol

Cranmer, S. R., Panasyuk, A. V., and Kohl, J. L.: 2008, "Improved Constraints on the Preferential Heating and Acceleration of Oxygen Ions in the Extended Solar Corona", *Astrophys. J.* **678**, 1480–1497

Cranmer, S. R. and van Ballegooijen, A. A.: 2005, "On the Generation, Propagation, and Reflection of Alfvén Waves from the Solar Photosphere to the Distant Heliosphere", *Astrophys. J. Suppl. Ser.* **156**, 265–293

de Moortel, I., Ireland, J., Walsh, R. W., and Hood, A. W.: 2002, "Longitudinal intensity oscillations in coronal loops observed with TRACE I. Overview of Measured Parameters", *Solar Phys.* **209**, 61–88

Defouw, R. J.: 1976, "Wave propagation along a magnetic tube", *Astrophys. J.* **209**, 266–269

Deubner, F.-L.: 1975, "Observations of Low Wavenumber Nonradial Eigenmodes of the Sun", *Astron. Astrophys.* **44**, 371–375

Edlén, B.: 1943, "Die Deutung der Emissionslinien im Spektrum der Sonnenkorona", *Zeitschrift für Astrofysik* **22**, 30–64

Epperlein, E. M.: 1984, "The accuracy of Braginskii's transport coefficients for a Lorentz plasma ", *J. Phys. D: Appl. Phys.* **17**, 1823–1827

Evans, J. W. (Ed.): 1963, *The Solar corona; proceedings of IAU Symposium no. 16 held at Cloudcroft, New Mexico, U.S.A. 28-30 August, 1961.*

Feldman, U.: 1993, "Is it justified to assume that 'Everywhere in the sun's photosphere-corona domain the electric conductivity is HIGH?'; or, what drives the solar upper atmosphere?", *Astrophys. J.* **411**, 896–908

Feldman, U. and Widing, K. G.: 2003, "Elemental Abundances in the Solar Upper Atmosphere Derived by Spectroscopic Means", *Space Sci. Rev.* **107**, 665–720

Ferraro, V. C. A. and Plumpton, C.: 1966, *An introduction to magneto-fluid mechanics*, Clarendon Press, Oxford, 2nd edition

Geiss, J.: 1982, "Processes Affecting Abundances in the Solar Wind"', *Space Sci. Rev.* **33**, 201–217

Gibson, E. G.: 1973, *The quiet sun*, NASA SP, Washington: National Aeronautics and Space Administration

Ginzburg, V. L.: 1970, *The propagation of electromagnetic waves in plasmas*, International Series of Monographs in Electromagnetic Waves, Pergamon Press, Oxford, 2nd revised, enlarged edition

Giovanelli, R. G.: 1949, "A Note on Heat Transfer in the Upper Chromosphere and Corona", *Mon. Not. R. Astron. Soc.* **109**, 372–

Gold, T.: 1964, "Magnetic Energy Shedding in the Solar Atmosphere", in W. Hess (Ed.), *The Physics of Solar Flares, NASA-SP50*, 389

Goldberg, L.: 1953, "Introduction", in G. P. Kuiper (Ed.), *The Sun*, Chicago University Press, Chicago, 1–35

Golub, L., Herant, M., Kalata, K., Lovas, I., Nystrom, G., Pardo, F., Spiller, E., and Wilczynski, J.: 1990, "Sub-arcsecond observations of the solar X-ray corona", *Nature* **344**, 842–844

Golub, L. and Pasachoff, J. M.: 1997, *The Solar Corona*, Cambridge Univ. Press, Cambridge UK

Gombosi, T. I.: 1994, *Gaskinetic Theory*, Cambridge University Press, Cambridge, England

Goodman, M. L.: 2000, "On the Mechanism of Chromospheric Network Heating and the Condition for Its Onset in the Sun and Other Solar-Type Stars", *Astrophys. J.* **533**, 501–522

Goodman, M. L.: 2004, "On the efficiency of plasma heating by Pedersen current dissipation from the photosphere to the lower corona", *Astron. Astrophys.* **416**, 1159–1178

Grotrian, W.: 1931, "Ergebnisse der Potsdamer Expedition zur Beobachtung der Sonnenfinsternis am 9. Mai 1929 in Takengon (Nordsumatra). 6. Mitteilung. Über die Intensitätsverteilung des kontinuierlichen Spektrums der inneren Korona.", *Z. Astrophys.* **3**, 199–226

Grotrian, W.: 1939, "??", *Naturwissenschaften* **27**, 214

Haisch, B. and Schmitt, J. H. M. M.: 1996, "Advances in Solar-Stellar Astrophysics", *Publ. Astron. Soc. Pac.* **108**, 113–129

Hale, G. E.: 1908, "On the Probable Existence of a Magnetic Field in Sun-Spots", *Astrophys. J.* **28**, 315–

Hale, G. E., Adams, W. S., and Gale, H. G.: 1906, "Preliminary Paper on the Cause of the Characteristic Phenomena of Sun-Spot Spectra", *Astrophys. J.* **24**, 185–213

Hansteen, V., Leer, E., and Holzer, T.: 1997, ""The role of helium in the outer solar atmosphere"", *Astrophys. J.* **482**, 498–509

Hollweg, J. V.: 1986, "Viscosity and the Chew-GOldberger-Low equations in the solar corona", *Astrophys. J.* **306**, 730–739

Hollweg, J. V.: 1990, "Heating of the solar corona", Comp. Phys. Rep. **12**, 205–232

Holzer, T. E., Hansteen, V. H., and Leer, E.: 1997, in J. R. Jokipii, C. P. Sonett, and M. S. Giampapa (Eds.), *Acceleration of the solar wind, Cosmic Winds and the Heliosphere*, Univ. of Arizona Press, 239–258

House, L. L.: 1964, "Ionization equilibrium of the elements from H to Fe", *Astrophys. J. Suppl. Ser.* **8**, 307

Hundhausen, A. J. and Holzer, T. E.: 1980, "Large-scale solar magnetic fields, coronal holes and high-speed solar wind streams", *Phil. Trans. R. Soc. Lond. Series A* **297**, 521–529

Jackson, J. D.: 1962, *Classical Electrodynamics*, Wiley & Sons, New York

Janssen, J.: 1879, *Annuiare du bureau des Longitudes*

Jordan, C.: 1969, "The ionization equilibrium of elements between carbon and nickel", *Mon. Not. R. Astron. Soc.* **142**, 501–521

Jordan, C.: 1976, *Phil. Trans. R. Soc. London*, A281 , 391

Jordan, C.: 1992, "Modelling of solar coronal loops", *Memorie della Societa Astronomica Italiana* **63**, 605–620

Judge, P. G., Carlsson, M., and Stein, R.: 2003, "On the origin of the "basal" emission from stellar atmospheres: analysis of solar C II lines", *Astrophys. J.* **597**, 1158–1177

Judge, P. G. and Carpenter, K. G.: 1998, "On Chromospheric Heating Mechanisms of "Basal Flux" Stars", *Astrophys. J.* **494**, 828

Klimchuk, J. A.: 2000, "Cross-sectional properties of coronal loops", *Solar Phys.* **193**, 53–75

Kohl, J. L., Noci, G., Antonucci, E., Tondello, G., Huber, M. C. E., Cranmer, S. R., Strachan, L., Panasyuk, A. V., Gardner, L. D., Romoli, M., Fineschi, S., Dobrzycka, D., Raymond, J. C., Nicolosi, P., Siegmund, O. H. W., Spadaro, D., Benna, C., Ciaravella, A., Giordano, S., Habbal, S. R., Karovska, M., Li, X., Martin, R., Michels, J. G., Modigliani, A., Naletto, G., O'Neal, R. H., Pernechele, C., Poletto, G., Smith, P. L., and Suleiman, R. M.: 1998, "UVCS/SOHO Empirical Determinations of Anisotropic Velocity Distributions in the Solar Corona", *Astrophys. J. Lett.* **501**, L127

Kopecký, M. and Obridko, V.: 1968, "On the Energy Release by Magnetic Field Dissipation in the Solar Atmosphere", *Solar Phys.* **5**, 354–358

Kopp, R. and Pneuman, G.: 1976, "Magnetic reconnection in the corona and the loop prominence phenomenon.", *Sol. Phys.* **50**, 85–98

Kulsrud, R. M.: 2005, *Plasma physics for astrophysics*, Princeton University Press, Princeton and Oxford

Kundu, M. R.: 1965, *Solar radio astronomy*, New York: Interscience Publication, 1965

Kuperus, M. and Athay, R. G.: 1967, "On the Origin of Spicules in the Chromosphere-Corona Transition Region", *Solar Phys.* **1**, 361–370

Landau, L. D.: 1937, "??", *Zh.ETF (J. Expt. Theoret. Phys. USSR* **7**, 203

Landi, E. and Cranmer, S. R.: 2008, "Ion Temperatures in the Low Solar Corona: Polar Coronal Holes at Solar Minimum", *ArXiv e-prints*

Landi, S. and Pantellini, F. G. E.: 2001, "On the temperature profile and heat flux in the solar corona: Kinetic simulations", *Astron. Astrophys.* **372**, 686–701

Leake, J. E. and Arber, T. D.: 2006, "The emergence of magnetic flux through a partially ionised solar atmosphere", *Astron. Astrophys.* **450**, 805–818

Leibacher, J. W. and Stein, R. F.: 1971, "??", *Ap. Lett.* **7**, 191–192

Leighton, R. B., Noyes, R. W., and Simon, G. W.: 1962, "Velocity Fields in the Solar Atmosphere. I. Preliminary Report.", *Astrophys. J.* **135**, 474

Libbrecht, K. G., Popp, B. D., Kaufman, J. M., and Penn, M. J.: 1986, "The excitation and damping of solar oscillations", *Nature* **323**, 235–238

Lie-Svendsen, Ø., Holzer, T. E., and Leer, E.: 1999, "Electron Heat Conduction in the Solar Transition Region: Validity of the Classical Description", *Astrophys. J.* **525**, 1056–1065

Litwin, C. and Rosner, R.: 1993, "On the structure of solar and stellar coronae - Loops and loop heat transport", *Astrophys. J.* **412**, 375–385

Low, B. C.: 1990, "Equilibrium and dynamics of coronal magnetic fields", *Ann. Rev. Astron. Astrophys.* **28**, 491–524

Low, B. C. and Flyer, N.: 2007, "The Topological Nature of Boundary Value Problems for Force-Free Magnetic Fields", *Astrophys. J.* **668**, 557–570

Lyot, B.: 1932, "Étude de la couronne solaire en dehors des éclipses.", *Zeitschrift für Astrophysics* **5**, 73

Lyot, B.: 1933, "The Study of the Solar Corona without an Eclipse ??CHECK", *Journal of the Royal Astronomical Society of Canada* **27**, 265

Lyot, B.: 1935, "Some observations of the solar corona and of prominences in 1935", *L'Astronomie* **51**, 203

Lyot, B.: 1939, "A Study of the Solar Corona and Prominences without Eclipses", *Mon. Not. R. Astron. Soc.* **99**, 580

Maltby, P., Avrett, E. H., Carlsson, M., Kjeldseth-Moe, O., and Kurucz, R. L.: 1986, *Astrophys. J.* **306**, 284

Mandrini, C. H., Démoulin, P., and Klimchuk, J. A.: 2000, "Magnetic field and plasma scaling laws: their implications for coronal heating models", *Astrophys. J.* **530**, 999–1015

Mariani, F. and Neubauer, F. M.: 1990, *Physics of the Inner Heliosphere I. Large-Scale Phenomena.*, Vol. 20 of *Physics and Chemistry in Space*, Chapt. 4. The Interplanetary Magnetic Field, 183–206, Springer-Verlag, Berlin Heidelberg

Mariska, J. T.: 1992, *The Solar Transition Region*, Cambridge Univ. Press, Cambridge UK

McWhirter, R. W. P., Thoneman, P. C., and Wilson, R.: 1975, "Heating of the solar corona II. A model based on energy balance", *Astron. Astrophys.* **40**, 63–73

Metcalf, T. R., Jiao, L., McClymont, A. N., Canfield, R. C., and Uitenbroek, H.: 1995, "Is the solar chromospheric magnetic field force-free?", *Astrophys. J.* **439**, 474–481

Mihalas, D. and Mihalas, B. W.: 1984, *Foundations of Radiation Hydrodynamics*, Oxford Univ. Press, New York

Miyamoto, S.: 1949, "Ionization Theory of Solar Corona", *Publ. Astron. Soc. Japan* **1**, 10–13

Noci, G.: 2003, "The Temperature of the Solar Corona", *Memorie della Societa Astronomica Italiana* **74**, 704–712

Parker, E. N.: 1957, "Acceleration of Cosmic Rays in Solar Flares", *Physical Review* **107**, 830–836

Parker, E. N.: 1958, "Dynamics of the Interplanetary Gas and Magnetic Fields", *Astrophys. J.* **128**, 664–676

Parker, E. N.: 1972, "Topological Dissipation and the Small-Scale Fields in Turbulent Gases", *Astrophys. J.* **174**, 499

Parker, E. N.: 1983, "Magnetic neutral sheets in evolving fields. II - Formation of the solar corona.", *Astrophys. J.* **264**, 642

Parker, E. N.: 1988, "Nanoflares and the solar X-ray corona", *Astrophys. J.* **330**, 474–479

Parker, E. N.: 1991, "Heating solar coronal holes", *Astrophys. J.* **372**, 719–727

Parker, E. N.: 1994, *Spontaneous Current Sheets in Magnetic Fields with Application to Stellar X-Rays*, International Series on Astronomy and Astrophyics, Oxford University Press, Oxford

Parker, E. N.: 2007, *Conversations on Electric and Magnetic Fields in the Cosmos*, Princeton University Press, Princeton, NJ USA

Piddington, J. H.: 1956, "Solar atmospheric heating by hydromagnetic waves", *Mon. Not. R. Astron. Soc.* **116**, 314–323

Popper, K. R.: 1992, *The logic of scientific discovery*, London: Routledge

Pottasch, S. R.: 1964, "On the Interpretation of the Solar Ultraviolet Emission Line Spectrum", *Space Sci. Rev.* **3**, 816–855

Raymond, J. C. and Doyle, J. G.: 1981, "The Energy Balance in Coronal Holes and Average Quiet-Sun Regions", *Astrophys. J.* **247**, 686–691

Riley, K. F.: 1974, *Mathematical methods for the physical sciences*, Cambridge University Press, Cambridge, U. K.

Roberts, B. and Webb, A. R.: 1978, “Vertical motions in an intense magnetic flux tube”, *Solar Phys.* **56**, 5–35

Rosner, R., Tucker, W. H., and Vaiana, G. S.: 1978, “Dynamics of the quiescent solar corona”, *Astrophys. J.* **220**, 643

Schatzman, E.: 1949, “The heating of the solar corona and chromosphere”, *Annales d’Astrophysique* **12**, 203

Schlüter, A.: 1951, “Dynamik des Plasmas II. Plasma mit Neutralgas”, *Zeitschrift Naturforschung Teil A* **6**, 73

Schwarzschild, M.: 1948, “On noise arising from the solar granulation”, *Astrophys. J.* **107**, 1–5

Scudder, J. D.: 1992a, “On the causes of temperature change in inhogeneous low-density astrophysical plasmas”, *Astrophys. J.* **398**, 299–318

Scudder, J. D.: 1992b, “Why all stars should possess circumstellar temperature inversions”, *Astrophys. J.* **398**, 319–349

Scudder, J. D.: 1994, “Ion and electron suprathermal tail strengths in the transition region: Support for the velocity filtration model of the corona”, *Astrophys. J.* **427**, 446–452

Seaton, M. J.: 1964, “The spectrum of the solar corona”, *Planet. Space Sci.* **12**, 55–74

Shmeleva, O. P. and Syrovatskii, S. I.: 1973, “Distribution of Temperature and Emission Measure in a Steadily Heated Solar Atmosphere”, *Solar Phys.* **33**, 341–362

Spitzer, L.: 1965, *Physics of fully ionized gases*, Interscience Tracts on Physics and Astronomy, New York: Interscience Publication, 1965, 2nd rev. ed.

Spruit, H. C.: 1981, “Motion of magnetic flux tubes in the solar convection zone and chromosphere”, *Astron. Astrophys.* **98**, 155–160

Stepien, K. and Ulmschneider, P.: 1989, “X-ray emission from acoustically heated coronae”, *Astron. Astrophys.* **216**, 139–142

Thomas, J. H.: 1983, “Magneto-Atmospheric Waves”, *Annual Review of Fluid Mechanics* **15**, 321–343

Thomas, R. N. and Athay, R. G.: 1961, *Physics of the Solar Chromosphere*, Interscience, New York

Tu, C.-Y., Marsch, E., Wilhelm, K., and Curdt, W.: 1998, “Ion Temperatures in a Solar Polar Coronal Hole Observed by SUMER on SOHO”, *Astrophys. J.* **503**, 475

Ulmschneider, P.: 1976, “Is the solar 5 min oscillation an important heating mechanism for the chromosphere and the corona”, *Solar Phys.* **49**, 249–252

Ulrich, R. K.: 1970, “The five-minute oscillations on the solar surface”, *Astrophys. J.* **162**, 933–1002

Underwood, J. H., Bruner, M. E., Haisch, B. M., Brown, W. A., and Acton, L. W.: 1987, “X-ray photographs of a solar active region with a multilayer telescope at normal incidence”, *Science* **238**, 61–64

Van de Hulst, H. C.: 1953, “The chromosphere and the corona”, in G. P. Kuiper (Ed.), *The Sun*, Chicago University Press, Chicago, 207–321

Vernazza, J., Avrett, E., and Loeser, R.: 1981, “Structure of the solar chromosphere. III - Models of the EUV brightness components of the quiet-sun”, *Astrophys. J. Suppl. Ser.* **45**, 635

Walker, A. B. C., Lindblom, J. F., Barbee, T. W., and Hoover, R. B.: 1988, “Soft X-ray images of the solar corona with a normal-incidence Cassegrain multilayer telescope”, *Science* **241**, 1781–1787

Watko, J. A. and Klimchuk, J. A.: 2000, “Width variations along coronal loops observed by TRACE”, *Solar Phys.* **193**, 77–92

White, S. M.: 2000, "Radio vs. EUV/X-ray Observations of the solar atmosphere", *Solar Phys.* **190**, 309–330

Wikstøl, Ø., Judge, P. G., and Hansteen, V. H.: 1997, "Signatures of Acoustic and Magnetic Waves in Solar and Stellar Coronae", *Astrophys. J.* **483**, 972

Wilkinson, J. H.: 1965, *The Algebraic Eigenvalue Problem*, Clarendon Press, Oxford

Willson, R. C., Hudson, H. S., Frohlich, C., and Brusa, R. W.: 1986, "Long-term downward trend in total solar irradiance", *Science* **234**, 1114–1117

Withbroe, G. L.: 1988, "The temperature structure, mass and energy flow in the corona and inner solar wind", *Astrophys. J.* **325**, 442–467

Withbroe, G. L. and Noyes, R. W.: 1977, "Mass and energy flow in the solar chromosphere and corona", *Ann. Rev. Astron. Astrophys.* **15**, 363–387

Woltjer, L.: 1958, "A Theorem on Force-Free Magnetic Fields", *Proceedings of the National Academy of Science* **44**, 489–491

Woods, L. C.: 1987, *Principles of Magnetoplasma Dynamics*, Oxford University Press, Oxford

Woolley, R. D. V. R. and Allen, C. W.: 1948, "The Coronal Emission Spectrum", *Mon. Not. R. Astron. Soc.* **108**, 292–305

Young, C. A.: 1892, *The Sun*, Kegan Paul, Trench, Trübner & co. Ltd., London, 4th edition

Zirker, J. B.: 2003, *Sunquakes*, John Hopkins University Press

Glossary

C_a	collision term on rhs of Boltzmann transport equation	27
C_{ab}	collisional term on RHS of the Boltzmann equation for particle species a induced by collisions with particles b	27
F_M	average flux density radiated from the uppermost chromospheric scale height and above	20
F_W	energy flux density of acoustic waves	20
F_a	macroscopic force on each particle of species a	27
$G_i(T_e)$	contribution functions to line emission	5
I_P	ionization potential	4
L	characteristic coronal length scale	19
Q_a	heat generated in particle species a through collisions with all other particles b arising when $T_a \neq T_b$	28
T_e	electron temperature	4
Z_i	electric charge on ions in units of the charge on the electron	29
$\mathcal{Q}_a$	charge of particles of species a	27
ℓ	length scale for changes in plasma properties	38
ϵ_0	permittivity of free space	30
ϵ_M	magnetic component of the electromagnetic energy density	40
λ_a	mean free path for particles of species a	29
ω_a	gyro frequency of particles of species a	26
$\omega_a\tau_a$	magnetization of particles of species a	26
ω_e	electron gyro frequency	29
ω_i	ion gyro frequency	29
ρ	plasma mass density	20
ρ_a	mass density of particles of species a	27
τ_a	collision time of particles of species a	26
τ_{ab}	momentum-exchanging collision time for particles a colliding with particles b	29
$\mathbb{P}_a$	pressure tensor for particles of species a	28
$\mathbf{E}^\dagger$	effective electric field in Ohm's law	43
$\mathbf{R}_a$	frictional force on particles of species a	28

$\mathbf{b}$	unit vector directed along the local magnetic field $\mathbf{B}$	31
$\mathbf{g}$	local acceleration due to gravity	27
$\mathbf{j}$	electric current density	27
$\mathbf{q}_a$	heat flux density of particles of species a	28
$\mathbf{r}$	spatial coordinate	27
$\mathbf{v}$	total particle velocity	27
$\mathbf{v}'_a$	random component of velocity for particles of species a	28
$\boldsymbol{\pi}$	stress tensor (off diagonal parts of $\mathbb{P}$)	28
ξ	rms non-thermal linewidths	20
$\xi(T_e)$	differential emission measure	23
b	closest approach of particles impacting each other with energy ε_a and charge $\mathcal{Q}_a$	30
c_S	adiabatic sound speed	19
c_e	electron sound speed $\approx c_S\sqrt{m_p/m_e}$	42
e	electron charge	4
f_a	distribution function for particles of species a	27
f_n	neutral fraction	45
k_B	Boltzmann's constant	4, 19
$ln\ \Lambda$	Coulomb logarithm	30
m_a	mass of each particle of species a	27
m_e	electron mass	29
m_i	ion mass	29
m_p	proton mass	29
n_e	electron density	5
p_a	scalar pressure of particles of species a (lying on the diagonal of $\mathbb{P}_a$)	28
p_e	electron pressure	5
r_a	gyro radius for particles of species a	29
t_{cool}	coronal cooling time	19
$\frac{\mathrm{d}}{dt}_a$	total derivative for particles of species a moving with velocity $\mathbf{u}_a$	28

Index